

# Evaluation of Calculated and Measured Electron Inelastic Mean Free Paths Near Solid Surfaces

Cite as: Journal of Physical and Chemical Reference Data **28**, 19 (1999); <https://doi.org/10.1063/1.556035>  
Submitted: 21 September 1998 . Published Online: 25 March 1999

C. J. Powell, and A. Jablonski



View Online



Export Citation

## ARTICLES YOU MAY BE INTERESTED IN

[Electron mean free path in elemental metals](#)

Journal of Applied Physics **119**, 085101 (2016); <https://doi.org/10.1063/1.4942216>

[Optical Constants and Inelastic Electron-Scattering Data for 17 Elemental Metals](#)

Journal of Physical and Chemical Reference Data **38**, 1013 (2009); <https://doi.org/10.1063/1.3243762>

[Low-energy electron inelastic mean free path in materials](#)

Applied Physics Letters **108**, 172901 (2016); <https://doi.org/10.1063/1.4948248>



Where in the **world** is AIP Publishing?  
*Find out where we are exhibiting next*

# Evaluation of Calculated and Measured Electron Inelastic Mean Free Paths Near Solid Surfaces

C. J. Powell<sup>a)</sup>

Surface and Microanalysis Science Division, National Institute of Standards and Technology, Gaithersburg, Maryland 20899-8370

A. Jablonski<sup>b)</sup>

Institute of Physical Chemistry, Polish Academy of Sciences, ul. Kasprzaka 44/52, 01-224 Warsaw, Poland

Received September 21, 1998; revised manuscript received November 17, 1998

An analysis is given of the consistency of calculated and measured electron inelastic mean free paths (IMFPs) near solid surfaces for electron energies between 50 and  $10^4$  eV, the energy range of relevance for surface analysis by Auger electron spectroscopy and x-ray photoelectron spectroscopy. This evaluation is based on IMFPs calculated from experimental optical data and on IMFPs measured by elastic-peak electron spectroscopy (EPES). We describe the methods used for the calculations and measurements, and we identify the various sources of uncertainty. Most of our evaluation is based on IMFPs for seven elemental solids (Al, Si, Ni, Cu, Ge, Ag, and Au) for which there were at least two sources of IMFP calculations and at least two sources of IMFP measurements for each solid. Our comparison of the calculated IMFPs showed a high degree of consistency for Al, Ni, Cu, Ag, and Au. The comparison of measured IMFPs showed greater scatter than for the calculated IMFPs, but reasonable consistency was found for the measured IMFPs of Cu and Ag. The measured IMFPs for four elements (Ni, Cu, Ag, and Au) showed good consistency with the corresponding calculated IMFPs. It is recommended that IMFPs for these four elements (determined from fits of a simple analytic expression to the calculated IMFPs for each element) be used as reference values in future EPES experiments. More limited comparisons have been made of calculated and measured IMFPs for four additional elements (Fe, Mo, W, and Pt) and of calculated IMFPs for six compounds ( $\text{Al}_2\text{O}_3$ ,  $\text{SiO}_2$ , KCl, poly(butene-1-sulfone), polyethylene, and polystyrene). © 1999 American Institute of Physics and American Chemical Society. [S0047-2689(99)00201-9]

Key words: Auger electron spectroscopy; elastic-peak electron spectroscopy; electron inelastic mean free path; inelastic electron scattering; inelastic mean free path; solid surfaces; surface analysis; surface characterization; x-ray photoelectron spectroscopy.

## Contents

1. Introduction.....	21	Evaluation.....	29
2. Sources of IMFP Values.....	22	2.2.1. Overlayer-Film Method.....	29
2.1. Sources of Calculated IMFP Values for the Evaluation.....	22	2.2.2. Elastic-Peak Electron Spectroscopy Method.....	31
2.1.1. Overview of Theory of Inelastic Electron Scattering in Solids.....	22	2.2.3. Sources of Measured IMFP Values...	35
2.1.2. Methods for Calculating Electron IMFPs.....	22	2.2.4. Uncertainties of Measured IMFP Values.....	37
2.1.3. Sources of Calculated IMFP Values..	24	3. Evaluation of IMFP Values.....	41
2.1.4. Uncertainties of Calculated IMFP Values.....	28	3.1. Selection of Materials.....	41
2.2. Sources of Measured IMFP Values for the		3.2. Evaluation of Calculated IMFP Values.....	44
		3.2.1. Evaluation of Calculated IMFPs for Al, Si, Ni, Cu, Ge, Ag, and Au.....	44
		3.2.2. Evaluation of Calculated IMFPs for Selected Compounds.....	46
		3.3. Evaluation of Measured IMFP Values for Al, Si, Ni, Cu, Ge, Ag, and Au.....	46
		3.4. Consistency of Calculated and Measured	

<sup>a)</sup>Electronic mail: cedric.powell@nist.gov

<sup>b)</sup>Electronic mail: jablo@ichf.edu.pl

©1999 by the U.S. Secretary of Commerce on behalf of the United States. All rights reserved. This copyright is assigned to the American Institute of Physics and the American Chemical Society.

Reprints available from ACS; see Reprints List at back of issue.

IMFP Values.....	49
3.4.1. Evaluation of Calculated and Measured IMFPs for Al, Si, Ni, Cu, Ge, Ag, and Au.....	49
3.4.2. Evaluation of Calculated and Measured IMFPs for Fe, Mo, W, and Pt.....	55
3.5. Recommended Elemental IMFP Values....	55
4. Conclusions.....	59
5. Acknowledgments.....	60
6. References.....	60

### List of Tables

1. Values of $k_i$ and $p_i$ found in the fits of Eq. (7) with $n=2$ to the calculated IMFPs of Kwei <i>et al.</i> <sup>51</sup> and Chen <sup>51</sup> for the indicated elements and for electron energies between 100 and 2000 eV..	25
2. Values of $k_i$ and $p_i$ found in the fits of Eq. (7) with $n=3$ to the calculated IMFPs of Ding and Shimizu <sup>52</sup> for Cu and Au and for electron energies between 10 and 10 <sup>5</sup> eV.....	26
3. Values of $k_i$ and $p_i$ found in the fits of Eq. (7) with $n=2$ to the calculated IMFPs of Ashley <i>et al.</i> for the indicated elements and for electron energies between $E_{\min}$ and $E_{\max}$ .....	27
4. Sources of IMFP measurements made with the EPES method and in which multiple elastic-scattering events were simulated by Monte Carlo calculations.....	36
5. Elements for which IMFP values were determined by Beilschmidt <i>et al.</i> <sup>102</sup> from EPES measurements and an approximate analytical theory.....	37
6. Experimental procedures and configurations used for determining the IMFP values listed in Tables 4 and 5.....	38
7. Percentage differences between the differential elastic-scattering cross sections at 1000 eV from two databases for the indicated scattering angles and elements. <sup>126,127</sup> .....	39
8. Number of sources of IMFPs measured by EPES for solid elements (from Tables 4 and 5) and the total number $M$ of IMFP measurements for each element.....	42
9. Sources of calculated IMFPs for elements for which there are at least two sources of measured IMFPs (Table 8).....	42
10. Values of the parameters $k_j$ and $p_j$ found in the fits of Eq. (7) to the calculated IMFPs for each element and for electron energies between 50 and 10 <sup>4</sup> eV (as described in Sec. 3.2.1.).....	46
11. Values of the parameters $k$ and $p$ found in the fits of Eq. (24) to the measured IMFPs for each element and for electron energies between $E_{\min}$ and $E_{\max}$ (as described in Sec. 3.3.).....	51

12. The root-mean-square deviations $RMS$ from Eq. (30) and the mean percentage deviations $R$ from Eq. (31) of the measured IMFPs for each element from the function fitted to the calculated IMFP values (as described in Sec. 3.4.).....	55
13. Summary of criteria for evaluating calculated and measured IMFPs.....	58

### List of Figures

1. Ratios of IMFPs calculated from optical data with and without a correction for electron exchange by Ashley <sup>34</sup> for Al, Cu, Ag, and Au as a function of electron energy.....	26
2. Ratios of IMFPs calculated using the statistical model with and without a correction for electron exchange by Rendell and Penn <sup>59</sup> for Al and for Fe, Co, and Ni as a function of electron energy.....	26
3. Ratios of IMFPs calculated by Ashley <sup>34</sup> from optical data (without an exchange correction) for Al, Cu, Ag, and Au to the corresponding IMFPs obtained from the statistical model (without an exchange correction) by Ashley <i>et al.</i> <sup>36</sup> as a function of electron energy.....	27
4. Ratios of IMFPs calculated for Si from the statistical model with an exchange correction by Tung <i>et al.</i> <sup>39</sup> to those calculated from the same model without the exchange correction by Ashley <i>et al.</i> <sup>36</sup> as a function of electron energy...	27
5. Plots of effective attenuation lengths for silicon at two electron energies corresponding to photoemission from the Si 2 <i>p</i> shell by aluminum characteristic x rays ( $E=1387$ eV) and magnesium characteristic x rays ( $E=1157$ eV) as reported by ten investigators (Refs. 74–81, 85a, 85c).....	30
6. Plots of effective attenuation lengths for silicon dioxide at two electron energies corresponding to photoemission from the Si 2 <i>p</i> shell by aluminum characteristic x rays ( $E=1383$ eV) and magnesium characteristic x rays ( $E=1153$ eV) as reported by twelve investigators (Refs. 75, 76, 78, 79, and 81–85).....	31
7. IMFPs (open circles) for Al, Cu, Ag, and Au measured by Schmid <sup>88</sup> with the elastic-peak electron spectroscopy method and calculated IMFPs (solid line) from Tanuma <i>et al.</i> <sup>47</sup> .....	32
8. Illustrative calibration curves for measurement of IMFPs using the EPES method. <sup>128</sup> .....	34
9. Comparison of measured and calculated IMFPs for: (a) aluminum; (b) silicon; (c) nickel; (d) copper; (e) germanium; (f) silver; and (g) gold...	43
10. Percentage deviations $\delta_j$ of the calculated IMFPs from the mean value $\langle\lambda\rangle$ [Eqs. (25) and (26)] plotted as a function of energy for: (a) aluminum; (b) silicon; (c) nickel; (d) copper; (e) germanium; (f) silver; (g) gold.....	45

11. Percentage deviations $\Delta_i$ of the calculated IMFPs from the function fitted to all of the calculated IMFPs for a particular element as a function of energy for: (a) aluminum; (b) silicon; (c) nickel; (d) copper; (e) germanium; (f) silver; (g) gold. . . . .	47
12. Comparison of calculated IMFPs for aluminum oxide. . . . .	48
13. Comparison of calculated IMFPs for silicon dioxide. . . . .	48
14. Comparison of calculated IMFPs for potassium chloride. . . . .	48
15. Comparison of calculated IMFPs for poly(butene-1-sulfone). . . . .	48
16. Comparison of calculated IMFPs for polyethylene. . . . .	48
17. Comparison of calculated IMFPs for polystyrene. . . . .	48
18. Comparison of measured IMFPs and the fits of Eq. (24) to each set of elemental data for (a) aluminum, (b) silicon, (c) nickel, (d) copper, (e) germanium, (f) silver, and (g) gold. . . . .	50
19. Percentage deviations $\Delta_i$ of the measured IMFPs from the function fitted to each set of elemental IMFPs as a function of electron energy for: (a) aluminum, (b) silicon, (c) nickel, (d) copper, (e) germanium, (f) silver, and (g) gold. . . . .	52
20. Comparison of measured IMFPs with the fits of Eq. (7) to calculated IMFPs as a function of electron energy for (a) aluminum, (b) silicon, (c) nickel, (d) copper, (e) germanium, (f) silver, and (g) gold. . . . .	53
21. Percentage deviations of the IMFPs measured by Dolinski <i>et al.</i> <sup>113</sup> and Koch <sup>115</sup> from the function fitted to calculated IMFPs (solid lines in Fig. 20) as a function of electron energy for aluminum, silicon, nickel, copper, silver, and gold. . . . .	54
22. Percentage deviations $\Delta_i$ of the measured IMFPs from the fits of Eq. (7) to calculated IMFPs (solid lines in Fig. 20) as a function of electron energy for (a) aluminum, (b) silicon, (c) nickel, (d) copper, (e) germanium, (f) silver, and (g) gold. . . . .	56
23. Comparison of calculated IMFPs (lines) and measured IMFPs (symbols) for iron. . . . .	57
24. Comparison of calculated IMFPs (line) and measured IMFPs (symbols) for molybdenum. . . . .	57
25. Comparison of calculated IMFPs (line) and measured IMFPs (symbols) for tungsten. . . . .	57
26. Comparison of calculated IMFPs (line) and measured IMFPs (symbols) for platinum. . . . .	57
27. Values of <i>RMS</i> for Al, Si, Ni, Cu, Ge, Ag, and Au from Tables 10, 11, and 12. . . . .	59
28. Values of <i>R</i> for Al, Si, Ni, Cu, Ge, Ag, and Au from Tables 10, 11, and 12. . . . .	59

## 1. Introduction

The inelastic mean free path (IMFP) of electrons near solid surfaces is a key parameter in the widely used surface-analysis techniques of Auger electron spectroscopy (AES) and x-ray photoelectron spectroscopy (XPS). It is also relevant to other surface-characterization techniques in which electrons are incident on or emitted from a solid surface such as low-energy electron diffraction, ultraviolet photoelectron spectroscopy, appearance-potential spectroscopy, inverse photoemission, and ionization-loss spectroscopy, among others.<sup>1</sup> The favorable surface sensitivity of AES, XPS, and the other techniques arises largely from the fact that the IMFP is typically between 1 and 20 crystal-lattice spacings (about 3–50 Å) for electron energies between about 10 and 2,500 eV, the range of practical interest for these techniques; other factors that affect the surface sensitivity of AES and XPS (particularly the experimental configuration and elastic-electron scattering) are discussed elsewhere.<sup>2</sup> The IMFP is also needed for making so-called matrix corrections in quantitative surface analyses by AES and XPS<sup>3–6</sup> and in calculations of the transport of the signal electrons in AES and XPS for different purposes.<sup>7</sup>

IMFPs can be both calculated and measured but, for the reasons given in more detail below, it has been difficult to obtain reliable data. Briefly, a number of approximations have been made in the calculations but the magnitudes of the resulting systematic uncertainties have only been estimated. The experimental measurements are subject to other uncertainties that have also only been estimated. In addition, there has been a conceptual difficulty in that the IMFP has been defined and calculated for bulk solids, whereas the measurements have been made in the vicinity of surfaces. The IMFP has been defined<sup>8</sup> by Committee E-42 on Surface Analysis of the American Society for Testing and Materials as “the average of distances, measured along the trajectories, that particles with a given energy travel between inelastic collisions in a substance.” Some recent calculations, however, have indicated that the “effective” IMFP near surfaces can be different from the corresponding bulk IMFP.<sup>9,10</sup>

The purpose of the present review is to analyze the consistency of published IMFPs (both calculated and measured values) and to recommend data of the highest reliability. Information on sources of calculated and measured IMFPs is given in Sec. 2 together with information on possible uncertainties of the IMFP values. Our evaluations of the IMFPs are presented in Sec. 3 where we first select seven materials (all elemental solids) for which there are calculated IMFPs from at least two sources and measured IMFPs from at least two sources. We then give separate evaluations of the calculated and measured IMFPs for each solid and, finally, we compare the calculated and measured values, again for each element. On the basis of this analysis, we identify four elements that show the highest degree of consistency in their calculated and measured IMFPs. Recommended IMFP values for these four elements can be generated from an analytic expression. Some additional comparisons of calculated and

measured IMFPs are presented for an additional four elements and six compounds. Our conclusions are presented in Sec. 4.

## 2. Sources of IMFP Values

### 2.1. Sources of Calculated IMFP Values for the Evaluation

#### 2.1.1. Overview of Theory of Inelastic Electron Scattering in Solids

There is a voluminous literature concerned with the theory of inelastic scattering in solids, and we give here only a summary of information relevant to the present work. It is convenient to describe inelastic electron scattering in solids by a complex dielectric constant  $\epsilon(\omega, q)$  which is a function of frequency  $\omega$  and momentum transfer  $q$ .<sup>11-17</sup> For  $q=0$ , the dielectric constant is related to the index of refraction  $n$ , the extinction coefficient  $k$ , and the optical (often x-ray) absorption coefficient  $\mu_m$  by:

$$\epsilon(\omega, 0) = (n + ik)^2 = \epsilon_1 + i\epsilon_2, \quad (1a)$$

$$\epsilon_1 = n^2 - k^2, \quad (1b)$$

$$\epsilon_2 = 2nk = \rho c \mu_m / \omega, \quad (1c)$$

where  $\rho$  is the density of the solid and  $c$  is the velocity of light. The differential inelastic scattering cross section, per atom or molecule, for energy loss  $\Delta E = \hbar\omega$  and momentum transfer  $q$  in an infinite medium is

$$\frac{d^2\sigma_i}{d\omega dq} = \frac{2e^2}{\pi N \hbar v^2} \text{Im} \left( \frac{-1}{\epsilon(\omega, q)} \right) \frac{1}{q}, \quad (2)$$

where  $N$  is the atomic or molecular density (number of atoms or molecules per unit volume),  $e$  is the electronic charge, and  $v$  is the velocity of the incident electrons.<sup>11-18</sup> In the derivation of Eq. (2), the effects of electron exchange and correlation have been neglected although we will consider corrections for these effects below; the effects are expected to be important for electron energies less than about 200 eV. Another correction to Eq. (2) is required to account for surface excitations, such as surface plasmons,<sup>9,10,18</sup> the corresponding modification to "bulk" IMFPs will also be discussed below.

A total inelastic scattering cross section  $\sigma$  can be obtained from an integration of Eq. (2) over the kinematically allowed ranges of  $\Delta E$  and  $q$  for a particular incident electron energy  $E$ . The IMFP  $\lambda_i$  is then given simply by

$$\lambda_i = 1/(N\sigma_i). \quad (3)$$

The key material-dependent parameter in Eq. (2) is the electron energy-loss function

$$\text{Im}(-1/\epsilon) = \epsilon_2 / (\epsilon_1^2 + \epsilon_2^2). \quad (4)$$

This energy-loss function can be computed from an appropriate model or, more readily, can be obtained from experimental energy-loss spectra or compilations of optical data. We note here that the denominator in Eq. (4) is responsible

for the differences that can occur between the energy-loss function for a material and the corresponding optical absorption spectrum. For  $\Delta E$  less than about 100 eV (i.e., energy transfers predominantly due to valence–electron excitations),  $(\epsilon_1^2 + \epsilon_2^2)$  can be very different from unity and there is then a large difference between energy-loss and optical-absorption spectra.<sup>19</sup> In addition, the maximum in the energy-loss function often occurs for excitation energies between about 5 and 40 eV. The magnitude of the IMFP is thus largely associated with valence–electron excitations. For  $\Delta E \geq 100$  eV (i.e., energy transfers predominantly due to core–electron excitations), however,  $\epsilon_1 \approx 1$ ,  $\epsilon_2 \ll 1$ , and  $\text{Im}(-1/\epsilon) \approx \epsilon_2$ .<sup>19</sup> X-ray absorption data (whether for free atoms or for the corresponding solids) can therefore be useful in determining the contributions of core–electron excitations to the IMFP. The magnitude of these contributions will not depend significantly on chemical state and are small compared to the magnitude of the contributions associated with energy transfers of less than about 100 eV.

#### 2.1.2. Methods for Calculating Electron IMFPs

Early calculations<sup>20-25</sup> of electron IMFPs were based on the "jellium" model for a solid. According to this model, the valence electrons form an interacting electron gas that moves in the smeared-out background of positive charge which is a model of the ion cores. The inelastic scattering is due entirely to the production of bulk plasmons and to the excitation of electron–hole pairs. The only parameter in this model is the valence–electron density, often expressed in terms of the average interelectron spacing  $r_s$  where  $r_s = (3/4\pi n a_0^3)^{1/3}$ ,  $n$  is the valence–electron density, and  $a_0$  is the first Bohr radius (0.529 Å). Lundqvist<sup>21</sup> made a more detailed investigation of the interaction of an incident electron with a jellium solid and obtained expressions for the momentum dependence of the excitation energy, the damping rate, and the spectral weight for the elementary excitations produced by the interaction. Shelton<sup>24</sup> derived IMFPs for jellium with  $r_s = 1.5, 2.0, 3.0,$  and  $4.0$  that were based on Lundqvist's calculations. The Quinn<sup>20</sup> and Shelton IMFPs are expected to be reasonable estimates for the so-called free-electron-like solids (e.g., elemental solids that are not transition or noble metals) where the predominant form of inelastic scattering is plasmon excitation (volume or bulk plasmons in the bulk of the solid and surface plasmons near a bulk–vacuum interface<sup>13,16-18</sup>). It should also be noted that the Lundqvist–Shelton IMFPs were computed for relatively low electron energies (to a maximum energy of about 500 eV for  $r_s = 1.5$ ) and to smaller maximum energies for the larger values of  $r_s$ .<sup>24</sup>

Penn<sup>25</sup> investigated two corrections to IMFPs determined from the jellium model of Quinn.<sup>20</sup> First, he approximated the effects of electron exchange and correlation, and found that these increased the IMFP by between 10% and 20%. Second, he extended the Lundqvist–Shelton<sup>21,24</sup> calculations to higher electron energies (up to 4000 eV) and found that the resulting IMFPs were between 10% and 25% smaller than those obtained from the Quinn theory for electron ener-

gies greater than 200 eV. Penn then combined his treatment of correlation and exchange with the Lundqvist–Shelton theory; the resulting IMFPs were smaller than those obtained from the Quinn model by at most 10% and typically 5%. Finally, Penn added a correction to take account of the contributions to the IMFP of core–electron excitations since these are not considered in the jellium model. For example, the inner-shell contributions in the case of Al lead to a reduction in the IMFP of about 14% for an electron energy of 1000 eV.<sup>26</sup> IMFP values for 58 elemental solids were tabulated by Penn for electron energies between 200 and 2400 eV, and a prescription was given to calculate IMFPs in alloys and compounds.<sup>25</sup> The jellium model was applied to transition and noble metals even though it was not expected to be necessarily valid for these solids. As a result, the IMFPs were estimated to have uncertainties of up to 40% in these cases; for the free-electron-like solids, however, the uncertainty was estimated to be about 5%.<sup>25</sup>

We will discuss the use of sum rules for evaluating numerical data for the energy-loss function that have been derived from optical data or inelastic-electron-scattering experiments later in this section and in Sec. 2.1.4.<sup>27</sup> At this point, we note an implicit feature of the IMFP calculations with the jellium model, namely that the oscillator strength or *f*-sum rule for the energy-loss function,

$$(2/\pi E_a^2) \int_0^{\Delta E_{\max}} \Delta E \operatorname{Im}[-1/\epsilon(\Delta E)] d(\Delta E) = Z_{\text{eff}}, \quad (5)$$

is satisfied with  $Z_{\text{eff}}$  equal to the number  $N_v$  of valence electrons per atom or molecule rather than to the atomic number  $Z$  (as should be the case when  $\Delta E_{\max} = \infty$ ). In Eq. (5),  $E_a = (4\pi N_e e^2/m)^{1/2}$ ,  $N = N_a \rho/M$  is the density of atoms or molecules,  $N_a$  is Avogadro's number,  $M$  is the atomic or molecular weight,  $m$  is the electronic mass, and the upper limit  $\Delta E_{\max}$  is chosen to be slightly less than the binding energy of the shallowest core electrons. The fact that the integration of Eq. (5) for the jellium model gives  $N_v$  is expected because only valence–electron excitations are considered in this model. For real solids, however, there is no ‘‘partial’’ sum rule that would require integrations such as Eq. (5) to give  $N_v$ . General arguments have been made, based on the Pauli exclusion principle, that the integration of Eq. (5) would yield a value larger than  $N_v$ .<sup>28</sup> There is also the practical problem that the upper limit  $\Delta E_{\max}$  in the integration of Eq. (5) may not be large enough to include all of the oscillator strength associated with valence–electron excitations. That is, if the integration of Eq. (5) were performed with a upper limit larger than  $\Delta E_{\max}$ , there would then be contributions (of unknown magnitude) from core–electron excitations. The integration of Eq. (5) will converge to a known value ( $Z$ ) only when  $\Delta E_{\max}$  is chosen to be much larger than the binding energy of the deepest ( $K$ -shell) electrons.

For a relatively free-electron-like solid such as Al, evaluation of Eq. (5) with  $\Delta E_{\max} = 70$  eV (just below the binding energy of electrons in the Al  $L_3$  subshell) indicates that the ‘‘effective’’ number of valence electrons is 3.1 rather than 3, the actual number of valence electrons.<sup>29</sup> The 3% correction

in this case is small compared to the IMFP uncertainties estimated by Penn.<sup>25</sup> For transition and noble metals, however, evaluation of Eq. (5) leads to values of  $Z_{\text{eff}}$  that can be appreciably (up to a factor of 2) less than the corresponding values of  $N_v$ .<sup>30</sup> As a result, IMFPs calculated from the jellium model for nonfree-electron-like solids can be much smaller than those obtained from a more realistic model, described below, in which experimental optical data are used to determine  $\operatorname{Im}[-1/\epsilon(\omega, 0)]$ .

Ashley and co-workers have calculated IMFPs for many solids using several different models.<sup>31–35</sup> In a 1979 paper, Ashley *et al.*<sup>31</sup> calculated IMFPs for Al using an electron–gas (jellium) model which was modified to include the effects of damping, exchange and correlation, and ion–core polarizability. They, like earlier authors,<sup>20–22</sup> used the complex dielectric response function proposed by Lindhard.<sup>36</sup> Ashley *et al.* found that the Lindhard dielectric function with the damping modification provided a reasonable but approximate description of the excitations in free-electron-like solids for electron energies from a few to 10 000 eV. They also used generalized oscillator strengths for atoms to describe the excitations of inner-shell electrons.

Tung *et al.*<sup>32</sup> reported an electron–gas statistical model in 1979 for the calculation of IMFPs based on an approach developed by Lindhard *et al.*<sup>37</sup> The essence of this model is that the inelastic-electron scattering in a solid can be characterized by a space-varying density of electrons  $n(r)$  and that the contribution to the IMFP of electrons in a small volume element  $d^3r$  at  $r$  is the same as that of the same number of electrons in an electron gas of the same density.<sup>32</sup> The total IMFP (including the contributions of core–electron excitations) is found by averaging these functions of  $n(r)$  over the volume of the solid. IMFPs were calculated with this model for Al, Si, Ni, Cu, Ag, and Au.<sup>32,38</sup> In unpublished work, IMFPs were calculated using the statistical model for Si,<sup>39</sup> Ge,<sup>40</sup> and GaAs;<sup>40</sup> in these calculations, a correction for exchange effects was made.

The possibility of using experimental energy-loss or optical data (i.e., the energy-loss function) for calculating IMFPs was pointed out about 25 years ago.<sup>26,41</sup> Ashley *et al.*<sup>33</sup> developed a model–insulator dielectric function to describe the optical response of valence electrons. This dielectric function consists of a sum of terms to represent single-electron excitations, and the values of parameters in the dielectric function were obtained from fits to measured optical data. A total IMFP for a given electron energy was then obtained from an integration of the loss function computed from the model dielectric function for the valence–electron excitations (with various estimates for the dependence of the loss function on momentum transfer); atomic data were used to obtain the contributions of core–electron excitations to the IMFP. IMFP calculations of this type were made for  $\text{Al}_2\text{O}_3$ ,  $\text{SiO}_2$ , polystyrene, polyethylene, and other organic solids.<sup>33</sup>

Szajman and Leckey<sup>42</sup> developed a single-mode model to represent the excitations of valence electrons. Experimental optical and energy-loss data were analyzed to determine the centroid energy loss in the energy-loss function which in turn

was used in the model to determine the IMFP for valence–electron excitations; a correction for electron correlation and exchange was made and a separate estimate<sup>26</sup> was made of the contributions of core–electron excitations to the IMFP. The Szajman and Leckey model is applicable to semiconductors, insulators, and both free-electron-like and nonfree-electron-like metals.

In 1985, Powell<sup>43</sup> pointed out that IMFPs could be computed directly from experimental energy-loss functions of different materials without an often-times arbitrary separation of the contributions of valence electrons and core electrons to the loss function. He used a parameter  $c$  determined from the jellium model of Penn<sup>25</sup> to describe the dependence of the loss function on momentum transfer. This approach, which is applicable to any material, ensures that the various valence–electron and core–electron excitations of the solid are included in a consistent way. IMFPs were calculated for 100–2000 eV electrons in C, Mg, Al, Al<sub>2</sub>O<sub>3</sub>, Cu, Ag, Au, and Bi. A shortcoming of the model, however, was the assumption that the value of  $c$  for each material was appropriate for the entire loss spectrum. Model calculations, however, showed that the computed IMFPs were not sensitive functions of  $c$ ; variation of  $c$  by more than a factor of 4 led to changes in the computed IMFPs of less than  $\pm 50\%$  for  $E = 200$  eV, less than  $\pm 30\%$  for  $E = 1000$  eV, and less than  $\pm 25\%$  for  $E = 2000$  eV from the average IMFP values found for the extreme values of  $c$ .

A major advance occurred in 1987 when Penn<sup>44</sup> published an improved algorithm for obtaining IMFPs from experimental energy-loss functions. The Penn algorithm is based on a model dielectric function<sup>37</sup> in which the momentum dependence is determined using the statistical approximation. IMFP calculations with this approximation were first made by Tung *et al.*<sup>32</sup> who approximated the IMFP directly; Penn, however, approximated the dielectric function. The resulting energy-loss function at zero momentum transfer was equated with the measured loss function. In this way, the contributions of valence–electron and core–electron excitations to the IMFP for zero momentum transfer could be calculated consistently. The dependence of the energy-loss function on momentum transfer was assumed to be given in terms of the Lindhard dielectric function<sup>36,37</sup> for various values of the electron density. This dielectric function is believed to be a reasonable model for nonfree-electron-like solids because the differential inelastic-scattering cross section is peaked in the forward direction (i.e., zero scattering angle).<sup>45</sup> As a result, deviations from the momentum-transfer dependence determined from the Lindhard dielectric function should not greatly affect the calculated IMFPs. The use of the Lindhard function in describing the momentum-transfer dependence of core–electron excitations, however, is less likely to be correct although a more detailed calculation of the Al  $2p$  and Mo  $3d$  inner-shell cross sections showed good agreement with those found using the Lindhard function.<sup>46</sup>

The Penn algorithm has been employed by Tanuma *et al.*<sup>30,47–50</sup> to calculate IMFPs for 50–2000 eV electrons in 56 materials (comprising elements, inorganic compounds,

and organic compounds). The energy-loss function for each material was computed from measured optical constants for photon energies ranging from about 1 to 10 000 eV or more; in some cases, interpolations had to be made (generally between about 30 and 100 eV) using atomic photoabsorption data. The internal consistency of the computed energy-loss functions was assessed with two powerful sum rules, the  $f$ -sum rule [Eq. (5) with  $\Delta E_{\max}$  generally larger than the binding energy for the  $K$ -shell electrons] and another sum rule based on a limiting form of the Kramers–Kronig integral.<sup>27</sup> Tanuma *et al.* found that these sum rules were satisfied typically to an average root-mean-square (RMS) uncertainty of about 10% for the group of 27 elements, to about 18% for the group of 15 inorganic compounds, and to about 6% for the group of 14 organic compounds.<sup>49,50</sup> The RMS uncertainties for the elements and organic solids were considered to be acceptable for the IMFP calculations; for the inorganic compounds, it was suggested that IMFPs could be determined more reliably with an IMFP predictive formula based originally on the elemental IMFPs and later on the IMFPs for the groups of elements and organic compounds.<sup>48,50</sup>

Several other groups<sup>34,35,51–54</sup> have recently calculated IMFPs from optical data in a manner similar to that proposed by Penn<sup>44</sup> although there are differences in approach. For electron energies above 200 eV, Penn found empirically that the Lindhard expression for the energy-loss function could be replaced by the simpler single-pole or plasmon-pole approximation<sup>55</sup> with a resulting loss of accuracy in the IMFP of less than 3%. Penn then used a quartic dispersion relation between the square of the excitation energy and the momentum transfer. Other groups<sup>34,35,51–54</sup> have used the single-pole approximation for electron energies lower than 200 eV and a quadratic dispersion relation while Boutboul *et al.*<sup>53,54</sup> modified the dispersion relation to include the band gap energy for certain excitation energies in nonconductors. Kwei *et al.*<sup>51</sup> and Boutboul *et al.*<sup>53,54</sup> fitted Drude-like analytic functions to energy-loss functions computed from optical data; these groups also used atomic data to describe the contributions of core–electron excitations. Finally, Ashley included a correction for the effects of electron exchange which will be discussed below.

### 2.1.3. Sources of Calculated IMFP Values

We will mainly consider here calculations of IMFPs that are based on experimental optical data. These calculated IMFPs are expected to be more reliable than those based on other models (as described in Sec. 2.1.2.) because the electron energy-loss function for a given material [needed for evaluation of Eq. (2)] is “correct” for  $q = 0$ ; the degree of correctness in a specific case will, of course, depend on the accuracy of the available experimental optical data and can be evaluated using the two sum rules discussed above.<sup>27</sup> This approach avoids the use of oversimplified models (e.g., use of the jellium model for nonfree-electron-like solids). It can also ensure correct weighting of the contributions to the

IMFP of valence–electron and core–electron excitations, without any necessity to separate these contributions, although some groups<sup>52–54</sup> have chosen to make separate calculations for these excitations. For a few materials (Si, Ni, and Ge), however, we will also consider IMFPs calculated from the statistical model of Ashley *et al.*<sup>38–40</sup> Sources of uncertainty in the calculated IMFPs will be discussed further in Sec. 2.1.4.

Most of the calculated and measured IMFPs evaluated in this paper will be for solid elements (for the reasons discussed in Sec. 3.1.). We therefore identify the sources of calculated IMFPs here and the elements for which IMFPs have been computed. These calculated IMFPs from four groups have been reported for particular electron energies, and it was convenient for our evaluation to fit the IMFPs with selected analytic functions so that IMFPs could be obtained by interpolation at intermediate energies. We identify these functions here. We also identify a fifth group which has reported IMFP calculations for inorganic compounds.

(a) *IMFPs of Tanuma et al.*<sup>47</sup> These authors reported IMFPs for a group of 27 solid elements (C, Mg, Al, Si, Ti, V, Cr, Fe, Ni, Cu, Y, Zr, Nb, Mo, Ru, Rh, Pd, Ag, Hf, Ta, W, Re, Os, Ir, Pt, Au, and Bi) for electron energies between 50 and 2000 eV. They fitted their IMFPs to a modified form of the Bethe<sup>28</sup> equation for inelastic-electron scattering in matter:<sup>34,56</sup>

$$\lambda_i = \frac{E}{E_p^2 [\beta \ln(\gamma E) - (C/E) + (D/E^2)]}, \quad (6)$$

where  $E_p = 28.8 (N_v \rho / M)^{1/2}$  is the free-electron plasmon energy (in eV),  $N_v$  is the number of valence electrons per atom,  $M$  is the atomic weight,  $\rho$  is the density, and  $E$  is the electron energy. Values of the parameters  $\beta$ ,  $\gamma$ ,  $C$ , and  $D$  were obtained from fits to the computed IMFPs for each element and are available in the original paper.<sup>47</sup> The RMS deviations in the fits varied between 0.1% and 1%, while the maximum deviation at any one energy was 2.5%. Similar IMFP calculations have been made by Tanuma *et al.* for Ge and additional elements.<sup>47</sup>

IMFPs have also been computed by Tanuma *et al.* for 15 inorganic compounds<sup>48</sup> (Al<sub>2</sub>O<sub>3</sub>, GaAs, GaP, InAs, InP, InSb, KCl, LiF, NaCl, PbS, PbTe, SiC, Si<sub>3</sub>N<sub>4</sub>, SiO<sub>2</sub>, and ZnS) and 14 organic compounds<sup>50</sup> [26-n-paraffin, adenine,  $\beta$ -carotene, bovine plasma albumin, deoxyribonucleic acid, diphenylhexatriene, guanine, kapton, polyacetylene, poly(butene-1-sulfone), polyethylene, polymethylmethacrylate, polystyrene, and poly(2-vinylpyridine)]. We note here that Tanuma *et al.*<sup>50</sup> derived expressions for  $\beta$ ,  $\gamma$ ,  $C$ , and  $D$  so that IMFPs could be estimated from Eq. (6) for other materials.

(b) *IMFPs of Kwei et al. and Chen.*<sup>51</sup> IMFPs were initially calculated for Fe, Ni, Cu, Pd, Ag, and Au, and were published as plots of IMFP versus electron energy in the range 100–2000 eV. Numerical values of the IMFPs for these elements and also for Al were provided by one of the authors.<sup>51</sup> These IMFPs were fitted here with the following expression:

TABLE 1. Values of  $k_i$  and  $p_i$  found in the fits of Eq. (7) with  $n=2$  to the calculated IMFPs of Kwei *et al.*<sup>51</sup> and Chen<sup>51</sup> for the indicated elements and for electron energies between 100 and 2000 eV. The final column shows the root-mean-square deviation *RMS* in the fits

Element	$k_1$	$p_1$	$k_2$	$p_2$	<i>RMS</i> (Å)
Al	3.009	−0.010 05	0.047 09	0.8643	0.0350
Fe	34.48	−0.5477	0.052 32	0.8243	0.0337
Ni	112.3	−0.8521	0.052 06	0.8103	0.0484
Cu	18.82	−0.4353	0.044 30	0.8357	0.0625
Pd	207.4	−0.9863	0.065 00	0.8082	0.0464
Ag	706.2	−1.294	0.068 16	0.7803	0.0629
Au	5890.0	−1.751	0.1383	0.6715	0.143

$$\lambda_{\text{fit}} = \sum_{j=1}^n k_j E^{p_j}, \quad (7)$$

where  $k_j$  and  $p_j$  are fitting parameters,  $\lambda_{\text{fit}}$  is expressed in Å and  $E$  in eV, and  $n$  is an integer in the range  $1 \leq n \leq 3$ . Equation (3) cannot be linearized for  $n \geq 2$  and, for this reason, nonlinear regression methods must be applied to determine values of  $k_i$  and  $p_i$ . It was found that the best fits to the calculated IMFPs could be obtained by minimization of the sum of squared relative deviations

$$Q(k_1, k_2, \dots, k_n, p_1, p_2, \dots, p_n) = \sum_k \left( \frac{\lambda_k - \lambda_{\text{fit}}}{\lambda_k} \right)^2, \quad (8)$$

where the index  $k$  indicates summation over the available IMFPs. Due to the fact that only a limited number of IMFP values were available for each element, Eq. (7) with  $n=2$  was fitted to the IMFP data of Kwei *et al.* and Chen. The resulting values of the parameters  $k_i$  and  $p_i$  are listed in Table 1 together with values of the RMS deviation for each fit. This group has also computed IMFPs for MgO, Al<sub>2</sub>O<sub>3</sub>, and SiO<sub>2</sub>.<sup>51</sup>

It should be noted that there is no physical basis for the dependence of IMFP on energy given by Eq. (7). This expression, however, has been successfully used by other authors either with  $n=1$  or  $n=2$ .<sup>57,58</sup>

(c) *IMFPs of Ding and Shimizu.*<sup>52</sup> These authors published plots of the calculated IMFPs versus electron energy for Cu and Au for energies between 1 and 10<sup>4</sup> eV. One of the authors (ZJD) provided an extensive tabulation of the IMFP values for both elements in the energy range from 1 to 10<sup>5</sup> eV. Fits were made to the IMFPs between 10 and 10<sup>5</sup> eV using Eq. (7) with  $n=3$ , and the resulting parameter values are shown in Table 2.

(d) *IMFPs of Ashley et al.*<sup>35,38–40</sup> Ashley<sup>35</sup> reported IMFPs for electrons and positrons in C, Al, Cu, Ag, Au, and polystyrene for electron energies between 40 and 10<sup>4</sup> eV. The IMFPs for Al, Cu, Ag, and Au in Ref. 35 are believed to be more reliable than those given in an earlier report<sup>34</sup> because of the use of an additional restriction on momentum transfer.<sup>35</sup> For electron energies above 150 eV, the IMFPs

TABLE 2. Values of  $k_i$  and  $p_i$  found in the fits of Eq. (7) with  $n=3$  to the calculated IMFPs of Ding and Shimizu<sup>52</sup> for Cu and Au and for electron energies between 10 and 10<sup>5</sup> eV. The root-mean-square deviations *RMS* were calculated for the energy range from 50 to 10<sup>4</sup> eV, i.e., the range of most interest in the present analysis

Element	$k_1$	$p_1$	$k_2$	$p_2$	$k_3$	$p_3$	<i>RMS</i> (Å)
Cu	424.1	-1.408	2.047	0.067 33	0.029 86	0.8816	0.141
Au	162.3	-0.8889	-0.016 79	0.8254	0.060 13	0.8254	1.02

for Al, Cu, Ag, and Au from Refs. 34 and 35 agree within a few percent, but at lower energies there can be differences of up to 32% for Cu, Ag, and Au.

We now present comparisons of IMFPs obtained using different models by Ashley *et al.* because they will be helpful in assessing the magnitude of uncertainties in the calculated IMFPs and because they will enable us to use IMFPs obtained from the statistical model for Si, Ni, and Ge in our later evaluation. Specifically, we wish to identify the electron energy ranges over which the IMFPs computed from different models are in substantial agreement. Ashley's first paper<sup>34</sup> with IMFPs for Al, Cu, Ag, and Au computed from optical data contains IMFPs calculated both with and without corrections for electron exchange; we note that no correction for electron exchange was made in the IMFP calculations of Tanuma *et al.*,<sup>47</sup> Kwei *et al.*,<sup>51</sup> Chen,<sup>51</sup> and Ding and Shimizu.<sup>52</sup> Figure 1 shows a plot of the ratios of IMFPs calculated with the exchange correction to those without this correction for Al, Cu, Ag, and Au from Ashley's results.<sup>34</sup> This ratio is less than 10% for electron energies greater than 500 eV, but can be as much as 40% for Al at 40 eV. While the magnitude of the exchange correction gets larger at lower energies, as expected, there are clear differences in the magnitude and energy dependence of the correction for the four metals at energies below 500 eV. Another investigation of the effects of electron exchange on the IMFP was reported by Rendell and Penn.<sup>59</sup> Their IMFPs were computed using the statistical model of Ashley *et al.*<sup>32</sup> Values of the IMFP ratios computed with the exchange correction to those with-

out this correction are shown in Fig. 2 for Al and as a single curve representative of Fe, Co, and Ni. The two curves in Fig. 2 are of similar shape and magnitude, and indicate that the exchange correction is close to 10% for an electron energy of 100 eV and about 15% at 50 eV. The Rendell and Penn result is considered more reliable because these authors considered both energy transfer and momentum transfer in the exchange-scattering process whereas Ashley considered only energy transfer.

Figure 3 shows the ratios of IMFPs computed by Ashley<sup>34</sup> from optical data and without the exchange correction for Al, Cu, Ag, and Au to the corresponding IMFPs obtained from the statistical model (also without an exchange correction).<sup>36</sup> For Al, this ratio deviates from unity by less than 7% for electron energies between 40 and 10<sup>4</sup> eV. Thus, the statistical model appears to give reliable IMFPs for a free-electron-like metal such as Al. For Cu, Ag, and Au, however, the IMFP ratios are much larger, particularly for low electron energies. For copper, the deviation of the IMFP ratio from unity is less than 10% only for electron energies greater than 1000 eV, and the maximum deviation is about 47% at 60 eV. The deviations of the IMFP ratio from unity for Ag and Au are less than 10% for energies above 150 eV but can be very large at lower energies; the IMFP ratio is about 2 for both metals at 40 eV.

Figure 4 is a plot of the ratio of the IMFPs calculated for Si from the statistical model and with an exchange correction by Tung *et al.*<sup>39</sup> to IMFPs from the statistical model without the exchange correction by Ashley *et al.*<sup>36</sup> The exchange cor-

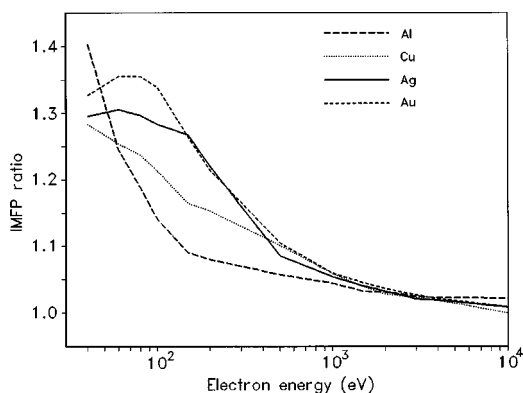


FIG. 1. Ratios of IMFPs calculated from optical data with and without a correction for electron exchange by Ashley<sup>34</sup> for Al, Cu, Ag, and Au as a function of electron energy. Lines have been drawn to connect the calculated data values.

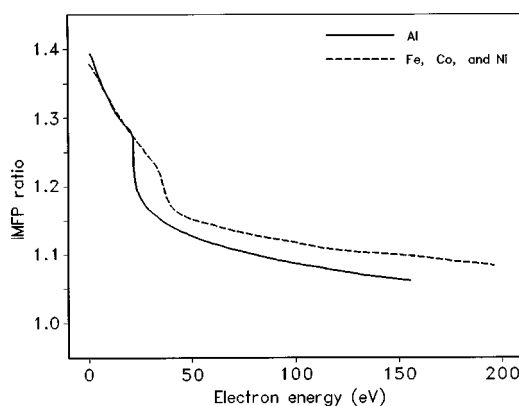


FIG. 2. Ratios of IMFPs calculated using the statistical model with and without a correction for electron exchange by Rendell and Penn<sup>59</sup> for Al and for Fe, Co, and Ni as a function of electron energy.

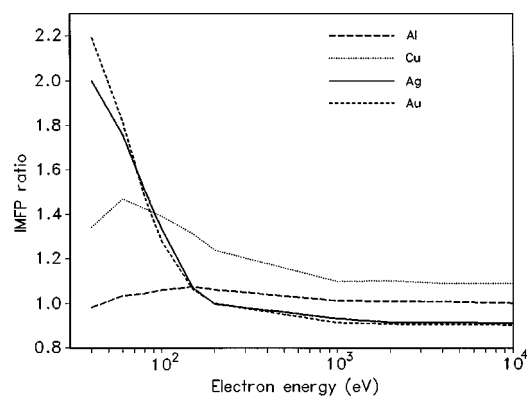


FIG. 3. Ratios of IMFPs calculated by Ashley<sup>34</sup> from optical data (without an exchange correction) for Al, Cu, Ag, and Au to the corresponding IMFPs obtained from the statistical model (without an exchange correction) by Ashley *et al.*<sup>36</sup> as a function of electron energy. Lines have been drawn to connect the calculated data values.

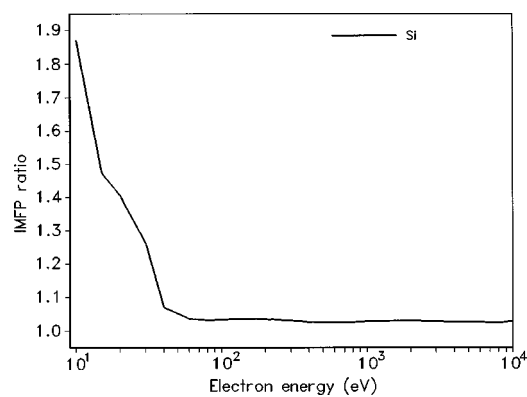


FIG. 4. Ratios of IMFPs calculated for Si from the statistical model with an exchange correction by Tung *et al.*<sup>39</sup> to those calculated from the same model without the exchange correction by Ashley *et al.*<sup>36</sup> as a function of electron energy. Lines have been drawn to connect the calculated data values.

rection for Si is less than 7% for electron energies of 40 eV or more. Since Si is a free-electron-like solid (the dominant energy loss is plasmon excitation, as for Al), the statistical model<sup>39</sup> should give reliable IMFPs for this element for energies of 40 eV and greater, as judged by the comparison for Al in Fig. 3. We thus do not consider further the surprisingly large exchange correction seen in Fig. 4 for lower electron energies. We similarly believe that IMFPs calculated for Ge (another free-electron-like solid) by Ashley *et al.*<sup>40</sup> using the statistical model and with the exchange correction should be reliable for electron energies of 40 eV and above.

We have chosen to include the calculated IMFPs for Ni of Ashley *et al.*<sup>38</sup> in our evaluation because nickel has been proposed as a reference material for IMFP measurements by the elastic-peak electron spectroscopy method described in Sec. 2.2.2. These Ni IMFP calculations were made with the statistical model and without any exchange correction.<sup>38</sup> The statistical model is unlikely to be reliable for a nonfree-electron-like solid such as Ni for electron energies lower than about 200 eV, as indicated by the plots in Fig. 3 for Cu, Ag, and Au. In addition, the calculated IMFPs for Ni could have an uncertainty of up to about 20% as judged by the IMFP ratio for Cu in Fig. 3.

We have fitted the calculated IMFPs of Ashley *et al.*<sup>35,38–40</sup> for Al, Si, Ni, Cu, Ge, Ag, and Au using Eq. (7)

with  $n=2$ , and the resulting parameter values are listed in Table 3. These fits were made for electron energies between 40 and  $10^4$  eV with the exception of Ni where the fit was made for energies between 200 and  $10^4$  eV for the reason just discussed. To make meaningful comparisons with the IMFP results of Tanuma *et al.*,<sup>47</sup> Kwei *et al.* and Chen,<sup>52</sup> and Ding and Shimizu<sup>51</sup> (where no exchange correction was made), we have chosen to make the evaluations of IMFPs calculated by Ashley *et al.* over restricted energy ranges. For Al, the exchange correction is less than 10% for electron energies of 200 eV and above (Figs. 1 and 2), and the evaluation of the Ashley Al IMFPs<sup>35</sup> was made between 200 and 2000 eV (where the upper limit here corresponds to that for the IMFPs calculated by the other groups). The exchange correction is larger for Cu, Ag, and Au (Fig. 1), and for these metals the evaluations of the Ashley IMFPs<sup>35</sup> were performed for electron energies between 500 and 2000 eV (for Ag) or  $10^4$  eV. For Si, the exchange correction appears to be small for electron energies greater than 40 eV (Fig. 4), and the evaluation of the Ashley *et al.* IMFPs<sup>39</sup> was made for energies between 50 and 2000 eV. It was decided to evaluate the Ashley *et al.* IMFPs<sup>40</sup> for Ge, a free-electron-like solid, over the 200 and  $10^4$  eV energy range (as for Al). Finally, the evaluation of the Ni IMFPs<sup>38</sup> was made over the 200– $10^4$  eV energy range although it was realized that the

TABLE 3. Values of  $k_i$  and  $p_i$  found in the fits of Eq. (7) with  $n=2$  to the calculated IMFPs of Ashley *et al.* for the indicated elements and for electron energies between  $E_{\min}$  and  $E_{\max}$ . The next-to-last column shows the root-mean-square deviation *RMS* for each fit

Element	$E_{\min}$	$E_{\max}$	$k_1$	$p_1$	$k_2$	$p_2$	<i>RMS</i> (Å)	Ref.
Al	40	10 000	13.36	−0.3787	0.070 89	0.8206	0.782	35
Si	40	10 000	6.192	−0.2871	0.062 88	0.8382	0.475	39
Ni	200	10 000	1.704	0.085 50	0.026 14	0.8793	0.0314	38
Cu	40	10 000	56.93	−0.5382	0.068 40	0.7950	0.585	35
Ge	40	10 000	163.6	−1.029	0.059 93	0.8126	0.745	40
Ag	40	10 000	453.3	−0.9380	0.063 69	0.7872	0.499	35
Au	40	10 000	1297	−1.168	0.075 24	0.7549	0.772	35

low-energy limit might have to be increased should there be evidence of appreciable uncertainty in the low-energy IMFPs for Ni from the statistical model (as indicated by the Cu curve in Fig. 3).

(e) *IMFPs of Boutboul et al.*<sup>53,54</sup> These authors reported IMFPs for a group of alkali halides (LiF, NaCl, KF, KCl, KBr, KI, and CsI) and a group of oxides (BeO, MgO, Al<sub>2</sub>O<sub>3</sub>, and SiO<sub>2</sub>) for electron energies between 50 and 10<sup>4</sup> eV.

#### 2.1.4. Uncertainties of Calculated IMFP Values

The uncertainties of the calculated IMFPs from the sources identified in Sec. 2.1.3. are of two general types: (a) uncertainties of the optical data for particular materials, and (b) uncertainties associated with the algorithms used to calculate the IMFPs by different groups. These sources of uncertainty will now be discussed in turn.

(a) *Uncertainties of the optical data.* Experimental optical data for many solids are available in two books edited by Palik<sup>60</sup> as well as in other compilations<sup>61</sup> and papers. Optical data may not be available over the entire photon-energy range of interest, particularly in the soft x-ray region. In such cases, interpolation may be necessary and atomic photoabsorption data can be used for this purpose.<sup>62</sup> The energy-loss function of a material for any photon energy can then be computed from the relevant optical constants [Eqs. (1) and (4)].

As indicated in Sec. 2.1.2., two sum rules were used by Tanuma *et al.*<sup>27</sup> to evaluate values of the energy-loss function computed from experimental optical data. These sum rules were satisfied typically to a RMS uncertainty of about 10% for the group of 27 elements analyzed by these authors.<sup>30</sup> This RMS uncertainty was considered acceptably small by Tanuma *et al.*<sup>30,47</sup> based on the expected reliability of the optical data and the fact that interpolations were needed for about half of the elements. Larger RMS uncertainties (18%) were found by Tanuma *et al.*<sup>48</sup> in their sum-rule analyses of energy-loss functions for the group of 15 inorganic compounds, and could be used to identify specific compounds for which the computed IMFPs were likely to be less reliable. The optical data for the group of 14 organic compounds analyzed by Tanuma *et al.*<sup>50</sup> satisfied the sum rules with a RMS uncertainty of about 5%.

It should be kept in mind, however, that the IMFP calculation is based on an integration of the energy-loss function [Eq. (2)] while the sum rules are based on an integration of the first-frequency moment of the energy-loss function [Eq. (5)] and an integration of the first-inverse-frequency moment of the energy-loss function.<sup>27</sup> The first of these sum rules emphasizes values of the energy-loss function for large excitation energies corresponding to inner-shell excitations and the second emphasizes values of the energy-loss function for small excitation energies (typically 1–100 eV). We believe that the average of the two sum-rule errors for a given material is a useful guide to the likely uncertainty, attributable to the optical data, in the computed IMFPs for that material. It is nevertheless conceivable that there might be greater un-

certainty in the energy-loss function (particularly for the frequency region over which the energy-loss function contains most of the “oscillator strength” for the calculated IMFPs) that was not detected in the sum-rule tests because of partial cancellations of errors in different frequency regions.

As noted in Sec. 2.1.2., two groups<sup>51,53,54</sup> have used experimental optical data to compute energy-loss functions for valence–electron excitations in their IMFP calculation and have used atomic data to describe the contributions of core–electron excitations. They have tested these computed energy-loss functions using Eq. (5) with  $\Delta E_{\max}$  less than the binding energy of the shallowest core electrons and  $Z_{\text{eff}}$  equal to the number of valence electrons per atom or molecule. Although such a test is a helpful guide, it is not exact.<sup>28</sup> In any case, the sum-rule errors were not specified in the original papers.<sup>51,53,54</sup>

(b) *Uncertainties associated with the IMFP algorithms.* Tanuma *et al.*<sup>49</sup> have discussed several sources of uncertainty associated with the Penn<sup>44</sup> algorithm for calculation of IMFPs. First, the Lindhard dielectric function<sup>36,37</sup> provides a physically plausible dependence of the energy-loss function on momentum transfer. This dependence is expected to be a reasonable approximation for free-electron-like solids but less reliable for other solids. While the resulting uncertainties are difficult to estimate, it has been suggested that they are about 10% for free-electron-like solids and energies above 200 eV.<sup>49</sup> Second, the effects of exchange and correlation are neglected and these are expected to be more significant at energies less than 200 eV (and lead to a larger IMFP). Figure 2 indicates that the exchange correction could be between about 10% and 15% for electron energies between 50 and 100 eV.

Finally, the IMFP calculations are for bulk solids whereas the detected electrons in AES and XPS originate close to the specimen surface and traverse the specimen–vacuum interface. It is known that the inelastic scattering modes near a surface are different from those for the corresponding bulk material and that surface plasmons can be excited in the surface region of free-electron-like solids.<sup>18,63</sup> In such solids, there is a rough cancellation of two effects: an increase in the total inelastic scattering cross section due to the excitation of surface plasmons and a decrease in this cross section due to a reduced rate of bulk plasmon excitation near the surface.<sup>18,63(a)</sup> The extent of this approximate cancellation, however, depends on the electron energy and the angle of electron incidence or emission.

Ding<sup>64</sup> has recently developed a formalism to describe bulk and surface inelastic-scattering cross sections near a surface as a function of electron energy, electron direction, and distance from the surface. With the use of a Drude–Lindhard model dielectric function, specific calculations were made for Mg, Si, Ag, and Au surfaces. Ding found that the assumption of a depth-independent IMFP is a reasonable approximation for Au at near-normal emission and for electron energies greater than 100 eV.

Two other recent studies<sup>65</sup> have shown that the assumption of a constant (bulk) IMFP in the surface region is a good

approximation for Si (for electron energies between 500 and 2000 eV), Ni (800 eV), Cu (800 eV), and Au (500–2000 eV) at zero angle of incidence or emission. In an analysis of electron energy-loss spectra (measured in a reflection-type geometry), Yubero *et al.*<sup>9</sup> found that the effective IMFPs (involving both bulk and surface excitations) for 300, 800, and 2000 eV electrons in Si and three different experimental configurations were less than the corresponding bulk IMFP values calculated by Tanuma *et al.*;<sup>47</sup> the decrease was greater for low-energy (300 eV) electrons and non-normal electron incidence or reflection, and could then be more than a factor of 2. In a similar analysis of Fe energy-loss spectra, Yubero *et al.*<sup>9</sup> found that the effective IMFPs were greater than the bulk values of Tanuma *et al.*<sup>47</sup> by as much as 30% for normal incidence and emission but less than the bulk values for most of the other configurations that were considered; the decrease could then be up to more than a factor of about 2 for 300 eV electrons and non-normal incidence or emission. For an electron energy of 800 eV at normal incidence and emission, the effective IMFP for Si was about 13% less than the bulk value of Tanuma *et al.*<sup>47</sup> while for Fe the effective IMFP was about 23% greater than the bulk value.

Chen<sup>10</sup> evaluated the effect of surface excitations on IMFPs measured by elastic-peak electron spectroscopy (EPES) measurements for Cu and Ag. In this analysis, he used IMFPs obtained from the early EPES experiments by Dolinski *et al.*<sup>66</sup> with a retarding-field analyzer having an acceptance angle of about 44°. Chen found that the IMFPs corrected for the effects of surface excitations were larger than the measured values by amounts ranging from about 12% at 1500 eV to about 40% at 250 eV. After this correction, the IMFPs measured by Dolinski *et al.*<sup>66</sup> were in much better agreement with the bulk IMFPs of Tanuma *et al.*<sup>47</sup> However, later measurements by Dolinski *et al.* for Cu and Ag (to be presented in Sec. 3) gave IMFPs that were larger than the previous values and which were in reasonable agreement with the bulk IMFPs of Tanuma *et al.* (without any correction for surface excitations). In general, the extent to which the IMFPs measured by EPES differ from the corresponding bulk values (on account of surface excitations) is expected to depend on the material, the surface roughness, the electron energy, and the incidence and emission angles for the experiments.<sup>18,63</sup> Further information on EPES for measuring IMFPs will be presented in Sec. 2.2.2.

It has been commonly believed for many years that the effects of surface excitations in electron energy loss (EEL) and EPES experiments should be greater than in AES and XPS experiments because the detected electrons traverse the specimen–vacuum interface twice in the former case and only once in the latter. Ding<sup>67</sup> has recently calculated the EEL spectrum of Au on the basis of different models and has found that the outgoing electron has a much greater probability of causing surface excitations than the incoming electron. He has also estimated that the effective IMFP for EEL and EPES experiments would be about 10% less than the corresponding bulk IMFP at 1 keV.<sup>67</sup>

With the exception of the IMFPs calculated for Si, Ni, and

Ge by Ashley,<sup>38–40</sup> all of the calculated IMFPs evaluated in Sec. 3.2.1. have been obtained using experimental optical data. While the calculational approaches used by different groups are very similar, there are some differences in the technical approach, as noted in Sec. 2.1.2. It is difficult to estimate the magnitude of the effects of these different approaches on the derived IMFPs. Instead, we will make comparisons of calculated IMFPs in Sec. 3.2. to determine the variability of IMFPs for the same material obtained by different groups.

## 2.2. Sources of Measured IMFP Values for the Evaluation

### 2.2.1. Overlayer-Film Method

In the early years of AES and XPS for surface analysis, many measurements of what was then believed to be the IMFP were made using the so-called overlayer method.<sup>68</sup> In these experiments, a film is deposited in layers of increasing thickness on a substrate, and measurements are made of the peak intensities of Auger electron or photoelectron features of the substrate ( $I_s$ ) or overlayer ( $I_l$ ) as a function of film thickness or emission angle. We have

$$I_l = I_l^\infty \left[ 1 - \exp\left(-\frac{d}{\lambda_l^i \cos \alpha}\right) \right] \quad (9a)$$

for the overlayer signal, and

$$I_s = I_s^\infty \exp\left(-\frac{d}{\lambda_s^i \cos \alpha}\right) \quad (9b)$$

for the substrate signal. In Eq. (9),  $d$  is the overlayer thickness,  $\alpha$  is the electron emission angle with respect to the surface normal,  $I_l^\infty$  is the intensity measured for the bulk overlayer material, and  $I_s^\infty$  is the intensity measured for the bulk substrate material. The terms  $\lambda_l^i$  and  $\lambda_s^i$  in Eq. (9) are the IMFPs in the overlayer material at the electron energies corresponding to the AES or XPS signals from the overlayer and substrate, respectively. These IMFP values are readily determined from the measured dependencies of the ratios  $I_l/I_l^\infty$  and  $I_s/I_s^\infty$  on overlayer thickness  $d$  or emission angle  $\alpha$ . Seah and Dench<sup>58</sup> reviewed IMFP measurements made by the overlayer method prior to 1979 and developed empirical formulas for the IMFPs in different classes of materials. Critiques of these and other predictive IMFP formulas have been published.<sup>69,70(b)</sup>

Two major types of scientific problems are associated with the overlayer method for determining IMFPs and in evaluating the results of measurements by this method; a possible third problem also exists. The first scientific problem with the overlayer method is experimental. Unfortunately, there are numerous sources of experimental uncertainty. These sources of uncertainty, which have been discussed in detail elsewhere,<sup>69,70</sup> include lack of film uniformity, the effects of surface excitations (e.g., surface plasmons), the effects of interferences between so-called intrinsic (or shake-up) excitations and extrinsic excitations occurring during electron

transport, atomic reconstruction at the surface and at the substrate/overlayer interface, intermixing at the substrate/overlayer interface, uncertainties in film-thickness measurement, and the effects of angular anisotropies in electron transport. It is very difficult to make reliable estimates of these effects on reported IMFPs (particularly in retrospect). Concerning the issue of film uniformity, it has only been possible with the advent of scanning tunneling microscopy and atomic force microscopy instruments to characterize overlayer-film morphologies in the early stages of film growth during the past 15 years. These investigations have shown that film growth is generally much more complex than was thought likely in the early overlayer experiments to measure IMFPs.<sup>70a</sup>

The second scientific problem with the overlayer method is conceptual. Equation (9) was derived on the implicit assumption that elastic-electron scattering was insignificant and, as a result, the electrons were considered to move on straight-line trajectories from their point of emission to the specimen surface. It is now well established, however, that elastic-electron scattering is often significant in AES and XPS;<sup>71,72</sup> as a result, the signal electrons have, on the average, longer trajectories than would be the case if elastic scattering were negligible. The effects of elastic scattering are particularly pronounced in XPS because the photoionization process is anisotropic.<sup>71,72</sup> The dependence of AES and XPS signal intensities on film thickness will, in general, not be exponential although for some common experimental conditions (particularly in AES) the dependence is at least approximately exponential. In these cases, the experimental parameters describing the dependence [ $\lambda_i^l$  and  $\lambda_i^s$  in Eq. (9)] are the effective attenuation lengths (EALs).<sup>6</sup> A separate term is needed to describe the electron attenuation because the IMFP can be larger than the corresponding EAL by up to about 30%.<sup>70(b)</sup>

Another consequence of the effects of elastic-electron scattering is that a measured EAL for a given overlayer material is not a well-defined parameter but instead depends on the atomic number of the particular substrate, the electron emission angle, and the acceptance solid angle of the electron energy analyzer, as shown by Jablonski and Ebel<sup>72</sup> and by Jablonski and Tougaard.<sup>73</sup> The latter authors investigated differences between the EAL and the IMFP based on simulations of XPS measurements with different experimental configurations for a silver overlayer film of different thicknesses on different substrates. They used a bulk IMFP of 13.0 Å in silver<sup>47</sup> (for photoelectrons excited from the Ag 3*d* subshell by Mg *K*  $\alpha$  x rays), and found that the corresponding EAL varied between 9.1 and 13.4 Å depending on the substrate, the range of Ag thicknesses, and the configuration. In principle, an analysis of the effects of elastic-electron scattering could be made for the particular materials and instrumental configurations used to obtain published EALs in order to derive corresponding IMFPs. In practice, such analyses would not be worthwhile because of the large computational effort involved and particularly because of the

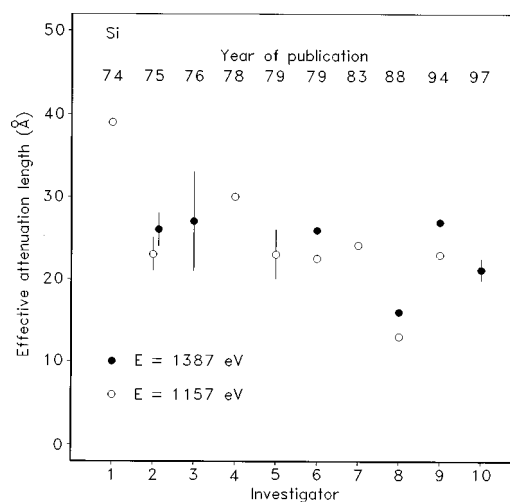


Fig. 5. Plots of effective attenuation lengths for silicon at two electron energies corresponding to photoemission from the Si 2*p* shell by aluminum characteristic x rays ( $E=1387$  eV) and magnesium characteristic x rays ( $E=1157$  eV) as reported by ten investigators (Refs. 74–81,85a,85c). The vertical lines represent the estimated one-standard-deviation uncertainties of the EAL values where these were given.

many sources of uncertainty in the experimental measurements that were identified above.

The possible third problem concerns the natural tendency of most scientists to report results that are consistent with the prevailing wisdom of the time. It was realized at an early stage in the use of the overlayer-film method that the films might not be deposited uniformly and that the AES or XPS signal intensities would then not vary exponentially with film thickness [as indicated by Eq. (9)]. It was therefore thought reasonable for experimentalists to discard data that did not show the expected exponential dependencies. Although raw data were often not published, we can reasonably assume that most of the reported EAL values were derived from measurements that were judged to be consistent with Eq. (9). Later work, which considered elastic-electron scattering,<sup>71</sup> showed that the AES or XPS signal intensities need not, in general, depend exponentially on film thickness because of the effects of elastic-electron scattering. It is therefore likely that at least some of the early published EAL values could be incorrect because they were based on the assumption, now known to be mistaken, that exponential signal variations were indicative of high-quality data. In actuality, some discarded data might have been more reliable (although analysis with consideration of elastic-electron scattering would not have been possible then). The fact that many published AES or XPS signal intensities show an essentially exponential dependence on film thickness should not necessarily lead to the conclusion that the overlayer films were uniform or that elastic-scattering effects were insignificant.

We finally examine the consistency of published EAL values obtained, with one exception, by use of the overlayer-film method.<sup>74–85</sup> Figures 5 and 6 show plots of replicate measurements of EALs for silicon and silicon dioxide, respectively, according to year of publication. In each figure,

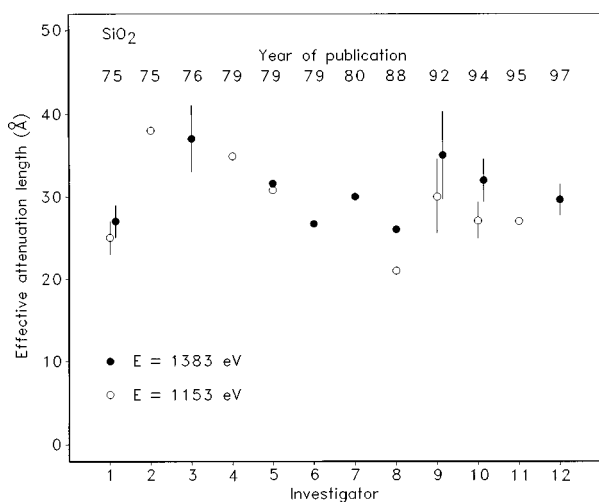


FIG. 6. Plots of effective attenuation lengths for silicon dioxide at two electron energies corresponding to photoemission from the Si 2*p* shell by aluminum characteristic x rays ( $E = 1383$  eV) and magnesium characteristic x rays ( $E = 1153$  eV) as reported by twelve investigators (Refs. 75, 76, 78, 79, and 81–85). The vertical lines represent the estimated one-standard-deviation uncertainties of the EAL values where these were given.

EAL values are given for two electron energies corresponding to XPS from the Si 2*p* shell with Al and Mg characteristic x rays. For those experiments where the uncertainties of the EAL measurements have been estimated (less than half of the published reports), the standard deviations were about 10%–15% in most cases. For Si, however, the ratio of the largest to the smallest EAL values (for  $E = 1157$  eV) is three. Although one might think of the extreme EAL values for Si as “outliers,” the smallest EAL values (published in 1988) seems to have been measured carefully; later EAL measurements, however, cluster close to the averages of earlier measurements. For SiO<sub>2</sub>, the ratio of the largest to smallest EAL values (for  $E = 1153$  eV) is 1.8. The range of measured EALs for both Si and SiO<sub>2</sub> is clearly much greater than would be expected from the uncertainties reported for some of the measurements. We can also examine the ratios of EALs reported in a single paper based on XPS measurements with Al and Mg x rays since these ratios should have much smaller uncertainties than the EAL values themselves. Nevertheless, these ratios range from 1.03 to 1.24 (while the corresponding IMFP ratios are close to 1.15).<sup>47,48</sup>

We believe that the large EAL ranges for each electron energy in Figs. 5 and 6 and the large range of EAL ratios for the two energies from individual papers are due to the experimental and conceptual problems discussed above. It is clearly critical that the experimental uncertainties be brought under control and reduced to a desirable level (e.g., 10% or less if possible). When this is done, it would be worthwhile to make a correction for the effects of elastic scattering on the EAL values so that meaningful comparisons could be made with the corresponding IMFP results.<sup>71,73</sup> At the present time, however, the uncertainties of measured EAL values are too large for meaningful comparisons to be made with calculated IMFPs, and we will not consider the EAL

values further in our evaluation of calculated and measured IMFPs. We also recommend that published EAL values be used with great caution because the uncertainties are not adequately documented.<sup>70,72</sup> In addition, we point out that the Seah and Dench predictive EAL formulas were derived before the experimental and conceptual problems with the overlayer method were fully appreciated. We recommend that these formulas be used now only as qualitative guides.

### 2.2.2. Elastic-Peak Electron Spectroscopy Method

IMFP values, in agreement with the ASTM definition,<sup>8</sup> can be determined from measurements of the intensity of electrons elastically backscattered from a given solid at various energies relative to the intensity of the incident beam. It is necessary, however, to make use of a model for describing elastic scattering of electrons into the acceptance solid angle of the electron energy analyzer. The present models of elastic scattering by the specimen material are based on the assumption that the solid is sufficiently amorphous or disordered for diffraction or channeling phenomena to be negligible. The solid is thus considered to consist of a random arrangement of atoms. While this assumption may appear to be a drastic simplification, it is nevertheless considered reasonable because the specimen surface is often cleaned by ion bombardment and this process generally leads to a disordered surface region. Clearly, the ion energy should be large enough so that the thickness of the disordered region is greater than the information depth in the measurement of the elastic-backscattering coefficient. In this section, we describe models used to account for elastic-electron scattering in the experiments and give details of the measurement and data-analysis procedures.

It has been shown that theoretical models of electron transport in solids describe the phenomenon of elastic-electron backscattering very well. Schilling and Webb<sup>86</sup> measured the angular distribution of electrons backscattered from liquid Hg. These authors proposed an analytical formalism expressing the elastically backscattered intensity in terms of the differential elastic-scattering cross section  $d\sigma_e/d\Omega$  and the total attenuation coefficient  $\mu_t$

$$\mu_t = \mu_i + N\sigma_e, \quad (10)$$

where  $\mu_i$  is the attenuation coefficient for inelastic scattering and  $\sigma_e$  is the total elastic-scattering cross section. Schilling and Webb<sup>86</sup> varied  $\mu_t$  to obtain best agreement of the theoretical predictions with the experimental data. They also listed the resulting values  $\mu_t$  as a function of energy in the range 100–500 eV. In this way, one can determine the inelastic-scattering contribution  $\mu_i$  if a value of  $\sigma_e$  is known or assumed. Schilling and Webb<sup>86</sup> found that the contribution of single-elastic scattering to the backscattered current was dominant although the contribution of multiply scattered electrons was not negligible.

From a very approximate analysis of elastic-electron backscattering, Gergely<sup>87</sup> found that the elastic-backscattered intensity was proportional to the IMFP. However, he did not

attempt to describe this relation quantitatively. The acronym EPES (for elastic-peak electron spectroscopy) appears to be used there for the first time to describe analytical applications based on the elastic-peak intensity in different materials. This acronym is now frequently used to indicate a useful method for determining IMFP from the elastic-peak intensity.

Schmid,<sup>88</sup> in his thesis, derived a relation between the backscattered intensity and the IMFP that was similar to the expression of Schilling and Webb [Eq. (10)].<sup>86</sup> For normal incidence of the primary beam, the elastically scattered intensity  $dI_1$ , within a solid angle  $d\Omega$  after one elastic scattering event is given by

$$\frac{dI_1}{d\Omega} = I_0 N \frac{d\sigma_e}{d\Omega} \int_0^\infty \exp(-\mu_i z) \exp(\mu_i z / \cos \theta) dz, \quad (11)$$

where  $I_0$  is the primary beam current,  $d\sigma_e/d\Omega$  is the differential elastic scattering cross section,  $z$  is the depth from the surface at which the elastic collision occurs, and  $\theta$  is the scattering angle. On integration, we obtain

$$\frac{dI_1}{d\Omega} = I_0 N \lambda_t \frac{d\sigma_e}{d\Omega} \frac{\cos \theta}{(\cos \theta - 1)}, \quad (12)$$

where  $\lambda_t$  is the total mean free path defined by

$$\lambda_t = 1/\mu_t = [N(\sigma_e + \sigma_i)]^{-1} = \left( \frac{1}{\lambda_e} + \frac{1}{\lambda_i} \right)^{-1}. \quad (13)$$

In this expression,  $\sigma_i$  is the inelastic scattering cross section,  $\lambda_e$  is the elastic mean free path, and  $\lambda_i$  is the IMFP. In a similar way, the elastically backscattered intensities were derived for electron trajectories having more than one elastic collision. These intensities were also related to the parameter  $\lambda_t$ . Schmid<sup>88</sup> was the first to propose that the IMFP could be determined by fitting a value of  $\lambda_t$  to the expression describing the backscattered intensity. The IMFP could then be calculated from the expression

$$\lambda_i = \lambda_e \lambda_t / (\lambda_e + \lambda_t). \quad (14)$$

In this way, IMFP values for some elemental solids were determined for electron energies between 150 and 1500 eV. Since these values have not been published (although Schmid *et al.*<sup>89</sup> described the use of elastically reflected electrons for surface characterization as suggested by Gergely<sup>87</sup>), we show the Schmid IMFPs for Al, Cu, Ag, and Au in Fig. 7 together with IMFPs calculated for these solids by Tanuma *et al.*<sup>47</sup>

A weak point in the formalism of Schmid<sup>88</sup> is the necessity to estimate the elastic mean free path of electrons for a given solid and electron energy. It has been pointed out<sup>72,90</sup> that the parameter  $\lambda_e$  is not well defined since elastic-scattering events occur mainly in the forward direction (that is, for near-zero scattering angles). These elastic collisions have a weak influence on the electron trajectory. Furthermore, the total elastic-scattering cross section depends strongly on the electron-atom interaction potential used in the calculations. For this reason, the parameter  $\lambda_e$  is not

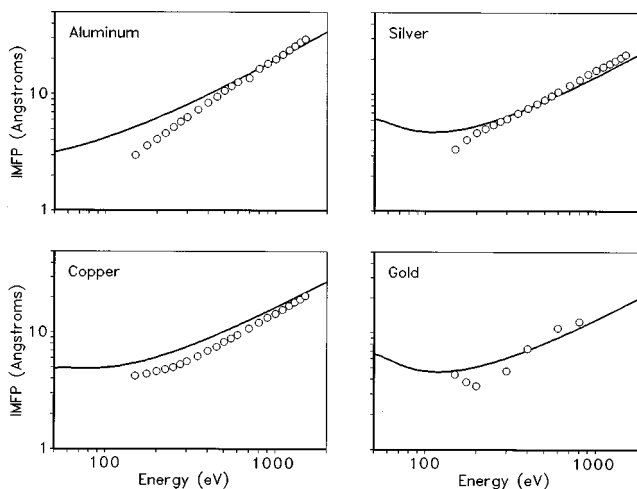


Fig. 7. IMFPs (open circles) for Al, Cu, Ag, and Au measured by Schmid<sup>88</sup> with the elastic-peak electron spectroscopy method and calculated IMFPs (solid line) from Tanuma *et al.*<sup>47</sup>

recommended for describing electron transport. Nevertheless, the Schmid IMFPs in Fig. 7 agree reasonably well with the calculated values although for two solids (Al and Ag) the measured dependence of the IMFP on energy is stronger than expected from the calculated IMFPs.

The first reports of investigations to determine the IMFP from measurement of the elastic backscattering probability were published by Jablonski *et al.*<sup>91,92</sup> Initially, a very simple model of elastic backscattering was introduced to circumvent the problem of estimating the elastic mean free path. This model was based on the assumption that an electron leaving the solid underwent only one large-angle scattering event (sufficient for backscattering into emission angles accepted by the analyzer). All other elastic scattering events were assumed to be small and were ignored. In this case, we obtain

$$\begin{aligned} \frac{dI}{d\Omega} &= I_0 N \frac{d\sigma_e}{d\Omega} \int_0^\infty \exp\left(-\frac{z}{\lambda_i} \frac{(\cos \theta - 1)}{\cos \theta}\right) dz \\ &= I_0 N \lambda_i \frac{d\sigma_e}{d\Omega} \frac{\cos \theta}{(\cos \theta - 1)}. \end{aligned} \quad (15)$$

Integration of Eq. (15) over the range of emission angles accepted by the analyzer gives

$$\eta_e = \lambda_i N \sigma_{\text{eff}}, \quad (16)$$

where  $\eta_e = I/I_0$  is the probability of elastic backscattering from a given surface into the analyzer, and

$$\sigma_{\text{eff}} = 2\pi \int_{\theta_1=\pi/2}^{\theta_2=\pi} \frac{d\sigma_e}{d\Omega} \frac{\cos \theta}{(\cos \theta - 1)} \sin \theta d\theta \quad (17)$$

is the effective total elastic-scattering cross section (here calculated for backscattering into all angles from the surface). Despite the considerable simplicity of this model, the single-large-angle-scattering formula was found to provide reasonable IMFP values for numerous materials. The good perfor-

mance of this formula was later discussed by Dwyer<sup>93</sup> who applied the transport approximation to describe elastic backscattering.

A major development in the theoretical description of elastic backscattering was the application of the Monte Carlo method to simulate the measurements.<sup>92</sup> This approach makes it possible to implement a theoretical model with realistic electron trajectories and especially to account properly for multiple elastic collisions. The Monte Carlo method has been used to derive most of the published IMFPs obtained with the EPES method.

The Monte Carlo algorithm is based on the following assumptions:

- (1) The scattering centers are randomly distributed in the solid, and are well approximated by the potentials of isolated atoms; the solid is thus assumed to be amorphous or polycrystalline.
- (2) The electron trajectory is considered as a "random walk" in which the electron direction is changed only by elastic scattering.
- (3) Multiple elastic-scattering events along the electron trajectory are described by the Poisson stochastic process.

The distribution  $W(\theta)$  of polar scattering angles is related to the differential elastic-scattering cross section by:

$$W(\theta) = 2\pi \frac{d\sigma_e/d\Omega}{\sigma_e} \sin\theta. \quad (18)$$

The azimuthal scattering angles  $\phi$  are assumed to be distributed uniformly in the angular range from 0 to  $\pi$ . From the second and third assumptions above, the distances between elastic collisions  $\Lambda$  are described by an exponential distribution

$$f(\Lambda) = (1/\lambda_e) \exp(-\Lambda/\lambda_e). \quad (19)$$

A Monte Carlo program is used to generate values of  $\theta$ ,  $\phi$ ,  $\Lambda$ , and the depth of photoelectron emission  $z$ , and thus to construct an electron trajectory in the solid. This trajectory is followed until either the electron leaves the solid or its length becomes too large for the trajectory to contribute significantly to the backscattered current.

The contribution to the elastic backscattered current corresponding to the  $k$ th trajectory is calculated from

$$\Delta I_k = \begin{cases} \exp(-x_k/\lambda_i) & \text{if an electron leaves the solid} \\ 0 & \text{otherwise} \end{cases}, \quad (20)$$

where  $x_k$  is the total trajectory length. The elastic backscattered current is calculated from

$$I = \frac{1}{n} \sum_{k=1}^n \Delta I_k, \quad (21)$$

where  $n$  is the number of generated trajectories. This number usually needs to exceed  $10^6$  to obtain reasonable precision. Simulations of the same type are repeated for different input values of the IMFP. The calculated dependence of the inten-

sity  $I$  on the IMFP is called a "calibration curve," and is used to determine the IMFP from a measured value of  $I$ . This process is facilitated by fitting the calculated calibration curve with an analytical expression. The following function has been found useful for this purpose<sup>92</sup>

$$I = N\sigma_{\text{eff}}\lambda_i + F\lambda_i^2, \quad (22)$$

where  $F$  is a fitting parameter.

The differential elastic-scattering cross sections used in the original report<sup>92</sup> describing the Monte Carlo algorithm for EPES were calculated using the first Born approximation (FBA). In general, the FBA tends to be more accurate for elements with low atomic numbers and for high electron energies. It is difficult, however, to define limits for the validity of the FBA. Ichimura *et al.*<sup>94</sup> found that screened Rutherford cross sections (the cross section calculated using the FBA with a screened Coulomb potential) often differ considerably from cross sections calculated with the more reliable partial-wave expansion method (PWEM). Differences of this type have been observed for electron energies up to 20 keV and a range of elements (Al, Cu, Ag, and Au). Only for Al at energies greater than 3 keV and scattering angles greater than  $15^\circ$  were the ratios of these two cross sections close to unity. Large differences in the two cross sections were found for Cu, Ag, and Au even at an energy of 20 keV. For example, the ratios of the cross sections for Cu at 3 keV and scattering angles between  $150^\circ$  and  $180^\circ$  were greater than 2. Similar results were obtained later by Jablonski<sup>95</sup> and Jablonski *et al.*<sup>96</sup> Thus, IMFP values derived from early EPES measurements and use of the Monte Carlo algorithm with differential cross sections calculated from the FBA may have significant systematic uncertainty. IMFP values resulting from Monte Carlo simulations with PWEM elastic-scattering cross sections were published later by Dolinski *et al.*<sup>97,98</sup>

The procedure described above was used in early measurements of the elastically backscattered current with a retarding-field analyzer (RFA) having a polar acceptance angle of about  $44^\circ$ .<sup>97,98</sup> To measure the primary beam current  $I_0$ , the incident beam was deflected to the RFA collector by applying a sufficiently negative voltage to the specimen in such a way that this beam produced a visible light spot of 5–10 mm diameter on the luminescent screen of the collector. The energy distribution of the primary beam was measured and the area under this distribution was used as a measure of the primary current. The current  $I$  of electrons elastically reflected from the specimen was measured with the RFA operated in its usual manner. The ratio  $\eta_e = I/I_0$  can then be compared with a calibration curve from Monte Carlo simulations [such as Eq. (22)] to derive an IMFP. The procedure of Dolinski *et al.*<sup>97,98</sup> gives absolute IMFP values and does not require separate absolute measurements of  $I_0$  (e.g., with a Faraday collector) and  $I$  (which would involve measurements of the transparency of the grids and the efficiency of the collector in the RFA).

Many workers have found it convenient to make EPES measurements with commonly available AES and XPS ana-

lyzers. To avoid the need for making absolute measurements of  $I_0$  and  $I$ , it is also convenient to measure the ratio  $I/I_s$  of elastic-peak intensities for two materials; here  $I$  is the elastic-peak intensity for the specimen of interest and  $I_s$  is the elastic-peak intensity for a reference or standard material for which IMFPs are known.<sup>92,99,100</sup> The measurements of  $I$  and  $I_s$  need to be made at the same electron energy and under the same experimental conditions (e.g., the same beam current  $I_0$  and the same analyzer settings). As before, Monte Carlo simulations are made for the specimen material using different input IMFP values; similar simulations are made separately for the standard material to obtain the value of  $I_s$ . The calibration curve in this case is a plot of the calculated ratio  $I/I_s$  versus input IMFP values for the specimen material. This procedure was suggested in 1985,<sup>92</sup> and the first applications were published several years later.<sup>99,100</sup> Presently, this is the most frequently used approach for IMFP measurements by EPES. The selection of a suitable standard material is discussed in Sec. 2.2.3.

Application of the EPES method with Monte Carlo simulations involves many computations. The elastic-backscattering probability is rather small and thus a large number of trajectories ( $10^6$  or more depending on the solid angle of the analyzer and the scattering properties of the solid) must be generated to obtain reasonable statistics. The simulations must be repeated for different assumed values of  $\lambda_i$ . Unfortunately, tabulation of the calibration curves in some universal form does not seem to be realistically possible because the curves depend on the experimental configuration (electron incidence angle, emission angle, analyzer acceptance angle), the solid, and the electron energy. Some calibration curves calculated for 500 eV electrons, a silicon specimen, and with nickel as a reference material are shown in Fig. 8 for different electron emission angles. As can be seen, the dependence of the ratio  $I/I_s$  on  $\lambda_i$  is monotonic but the value of  $I/I_s$  depends strongly on emission angle. A possible way to decrease the computational effort is to develop an analytical description of elastic-backscattering effects. It seems likely that an analytical expression, with reliability sufficient for EPES applications, could be derived from a solution of the kinetic Boltzmann equation within the so-called transport approximation.<sup>101,102</sup> This theoretical approach has been found to describe the transport of photoelectrons and Auger electrons in solids generally very well although the agreement between the two approaches is not as good for low-atomic-number elements such as Al.<sup>103,104</sup>

Beilschmidt *et al.*<sup>102</sup> derived an analytical formalism based on the transport approximation for EPES calculations. Details of the theoretical model were published separately by Werner *et al.*<sup>101</sup> These authors accurately described the first one or two elastic collisions of an electron entering a solid, and the angular distribution after these collisions was assumed to be the source function for the subsequent analysis using the transport approximation. Additional elastic collisions were treated using the transport approximation which is based on the following assumptions:

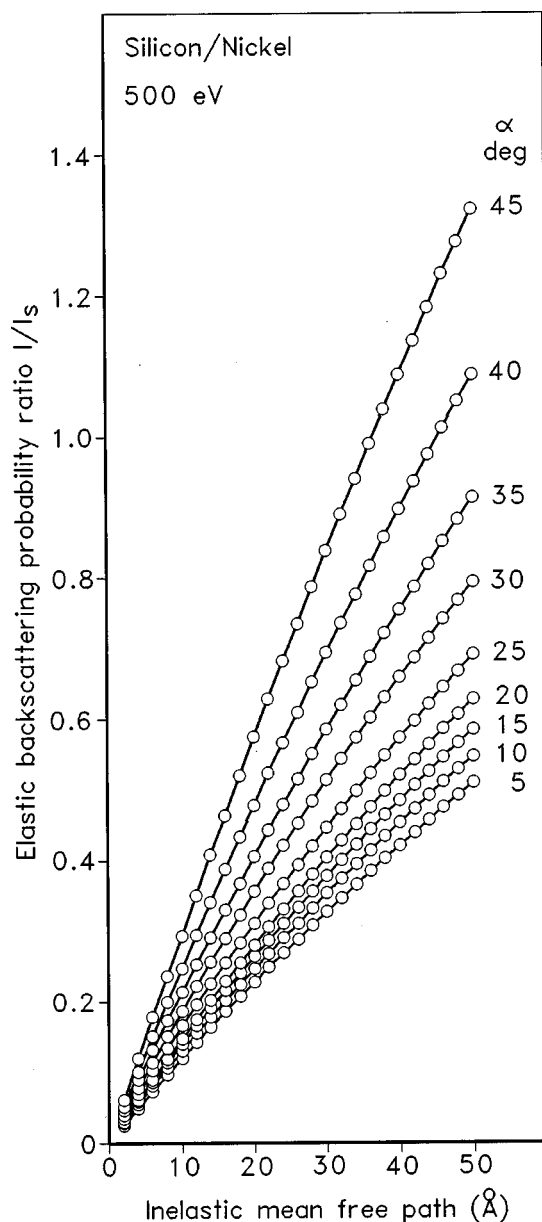


Fig. 8. Illustrative calibration curves for measurement of IMFPs using the EPES method.<sup>128</sup> These curves were calculated for 500 eV electrons, a silicon specimen, and with a nickel reference material for various values of the electron emission angle  $\alpha$ . The calibration curves here show ratios of the elastic-peak intensities for silicon and nickel as a function of the silicon IMFP value used in the Monte Carlo simulation.

- (1) the angular distribution of electrons after an elastic-scattering event is isotropic;
- (2) the characteristic length for elastic scattering is the transport mean free path  $\lambda_{tr}$ :

$$\lambda_{tr} = \left( 2\pi N \int_0^\pi (1 - \cos \theta) \frac{d\sigma_e}{d\Omega} \sin \theta d\theta \right)^{-1}. \quad (23)$$

This approach, however, requires knowledge of the elastic mean free path as an input parameter. Specifically, the back-scattered intensity derived from the single-scattering trans-

port approximation and the double-scattering transport approximation is expressed in terms of the parameter:

$$a = \frac{\lambda_e(\lambda_{tr} + \lambda_i)}{\lambda_{tr}(\lambda_i + \lambda_e)}$$

Some additional simplifying assumptions were made by Werner *et al.*<sup>101</sup> to facilitate the derivation. Nonetheless, the final expressions describing the elastically backscattered intensity are rather complex and this complexity may hinder their implementation by others.

Werner *et al.*<sup>101</sup> compared the angular distributions of backscattered electrons from their analytical model with results of Monte Carlo calculations and experimental data. The tests were made over a wide energy range (200–2000 eV) and for a wide range of atomic numbers (Al, Ni, Cu, Ta, Pt, and Au). Angular distributions calculated from the analytical model and the Monte Carlo simulations for Al, Cu, Ta, and Au agreed extremely well, within the thickness of the plotted lines in most cases. Comparisons of the angular distributions from the analytical model with experimental data were made after normalizing the measured intensities to the calculated intensities at a selected scattering angle (60° or 120°). Reasonable qualitative agreement was found in these comparisons, with the shapes of the distributions being similar in all cases (Al, Ni, Pt, and Au), especially the positions of maxima and minima. When using the analytical approach, however, one should be aware that the concept of a first elastic collision is related *via* the elastic mean free path to the elastic scattering cross section. On the other hand, the cross section (and consequently the source function) depends considerably on the interaction potential used in the calculations.<sup>6</sup> We expect that a change of the interaction potential will affect the source function and eventually the results from the transport approximation. In other words, for some elastic scattering cross sections (or interaction potentials), even two elastic collisions will not sufficiently randomize the electron directions of motion.

Measurement of IMFPs by the EPES method has many advantages. Measurements can be made with the electron spectrometers typically used for surface analysis. It is not necessary to prepare and characterize thin films of the type needed for the overlayer-film method (Sec. 2.2.1.). The EPES method is nondestructive and can be applied locally (e.g., to a given spot on the specimen material). In principle, an EPES measurement could accompany a quantitative analysis by AES or XPS (although some additional measurement time would then be needed). The EPES formalism can easily be extended to multicomponent solids. In early reports, the single large-angle scattering theory was generalized<sup>91,105</sup> and applied to an alloy.<sup>105</sup> In more recent studies, IMFP values were determined for alloys<sup>106,107</sup> and compounds<sup>108,109</sup> using a standard material and a Monte Carlo algorithm modified to describe multicomponent specimens.

### 2.2.3. Sources of Measured IMFP Values

We consider here sources of IMFP measurements made with the EPES method. As discussed in Sec. 2.2.2., the measured IMFPs are expected to be reliable when the following conditions for the EPES theoretical model are met:

- (1) proper account is taken of multiple elastic-scattering collision events; and
- (2) differential elastic-scattering cross sections are used from PWEM calculations.

IMFP values published in the early papers introducing the EPES method<sup>88,91,92</sup> do not satisfy these conditions, and therefore will not be considered further. The algorithm developed by Schmid<sup>88</sup> requires knowledge of the elastic mean free path which is not recommended as a characteristic length for description of electron transport in solids (as discussed in Sec. 2.2.2.). Furthermore, the theoretical treatment of multiple elastic scattering seems to be oversimplified. Jablonski *et al.*<sup>91,92</sup> used elastic-scattering cross sections based on the first Born approximation. Although these cross sections and the single large-angle scattering theory<sup>91,92</sup> give reasonable IMFP values (despite the simplicity of this approach), the backscattered intensities from this method deviate noticeably from the predictions of theories that use more accurate cross sections and that take account of multiple elastic-scattering events.

We decided to include IMFPs from the theoretical model of Werner *et al.*<sup>101,102</sup> in our evaluation despite the fact that this model requires the elastic mean free path as an input parameter. These authors performed extensive tests which indicate that their theoretical model gives results in good agreement with Monte Carlo simulations and experimental data. Furthermore, as mentioned earlier, the transport approximation was found in other studies<sup>103,104</sup> to describe multiple elastic collisions of Auger electrons and photoelectrons in solids reasonably well, especially in cases where the source function did not change substantially with direction (i.e., when the anisotropy of photoelectron emission is small). Nevertheless, the IMFPs of Beilschmidt *et al.*<sup>102</sup> will be clearly distinguished in the following sections from IMFPs resulting from Monte Carlo calculations.

Most of the published IMFP values for elemental solids<sup>97–100,107,109–118</sup> from the EPES method were obtained from Monte Carlo calculations based on PWEM elastic-scattering cross sections. Table 4 lists these sources of measured IMFPs (from papers published prior to June, 1998) together with the range of electron energies in the measurements. Plots of measured IMFPs versus energy for a given material and source (to be presented in Sec. 3) often show considerable scatter. It was convenient for our evaluation of the measured IMFPs to fit these values with the simple expression:<sup>99,100,102,107,117</sup>

$$\lambda_i = kE^p, \quad (24)$$

where  $k$  and  $p$  are fitting parameters [that is, Eq. (7) with  $n = 1$ ]. Systematic deviations from this simple exponential

TABLE 4. Sources of IMFP measurements made with the EPES method and in which multiple elastic-scattering events were simulated by Monte Carlo calculations. We show the minimum ( $E_{\min}$ ) and maximum ( $E_{\max}$ ) electron energies for which IMFPs were measured, give values of the parameters  $k$  and  $p$  found from fits of Eq. (24) to the measured IMFPs, and show values of the root-mean-square deviation  $RMS$  for each fit

Element	$E_{\min}$ (eV)	$E_{\max}$ (eV)	$k$	$p$	$RMS$ (Å)	Ref.
Carbon (glassy) <sup>a</sup>	270	2350	0.267	0.696	3.59	99
Carbon (graphite) <sup>a</sup>	270	2350	0.118	0.751	4.77	99
Magnesium <sup>b</sup>	700	2000	0.0452	0.919	0.886	115
Aluminum <sup>b</sup>	50	2500	0.1183	0.763	3.49	112
Aluminum <sup>b</sup>	600	2100	0.0636	0.828	0.978	115
Silicon <sup>c</sup>	500	3000	0.0650	0.867	2.12	110
Silicon <sup>b</sup>	100	5000	0.1129	0.797	3.74	111
Silicon <sup>b</sup>	100	1500	0.1599	0.745	1.47	112
Silicon <sup>b</sup>	600	2200	0.0635	0.859	0.494	115
Chromium <sup>c</sup>	500	3000	0.1515	0.665	1.02	110
Iron <sup>b</sup>	50	3000	0.204	0.640	4.56	112
Iron <sup>b</sup>	600	2000	0.0567	0.791	0.529	115
Cobalt <sup>d</sup>	200	1000	0.490	0.436	0.799	107
Cobalt <sup>a</sup>	200	1000	0.358	0.553	1.82	107
Nickel <sup>d</sup>	270	2350	0.210	0.592	2.43	99
Nickel <sup>b</sup>	600	2200	0.0409	0.834	0.552	115
Copper <sup>d</sup>	250	1500	0.0266	0.879	0.381	97
Copper <sup>d</sup>	250	1500	0.0475	0.794	0.743	98
Copper <sup>c</sup>	150	2000	0.0493	0.830	2.40	113
Copper <sup>c</sup>	500	3000	0.1242	0.700	1.22	114
Copper <sup>b</sup>	600	2100	0.0393	0.854	0.530	115
Copper <sup>b</sup>	400	1600	0.1442	0.694	0.331	109
Gallium <sup>b</sup>	500	2200	0.0240	0.946	0.761	115
Germanium <sup>c</sup>	500	3000	0.234	0.660	1.25	110
Germanium <sup>b</sup>	100	5000	0.250	0.640	5.82	111
Germanium <sup>b</sup>	100	1500	0.319	0.604	1.19	112
Germanium <sup>b</sup>	500	2100	0.0814	0.811	0.898	115
Molybdenum <sup>c</sup>	500	3000	0.0635	0.767	2.15	110
Molybdenum <sup>b</sup>	50	2000	0.842	0.425	2.75	112
Palladium <sup>a</sup>	200	1000	0.878	0.383	0.295	107
Silver <sup>a</sup>	500	3000	0.0900	0.699	0.725	100
Silver <sup>d</sup>	250	1500	0.0939	0.704	0.600	97
Silver <sup>d</sup>	250	1500	0.0922	0.697	0.781	98
Silver <sup>c</sup>	250	1700	0.211	0.620	0.747	113
Silver <sup>b</sup>	600	2000	0.0944	0.718	0.799	115
Indium <sup>b</sup>	100	1400	0.1702	0.661	1.15	116
Antimony <sup>b</sup>	600	2200	0.0676	0.815	2.24	115
Tellurium <sup>b</sup>	600	2200	0.0827	0.800	1.26	115
Tantalum <sup>a</sup>	500	3000	0.084	0.669	1.21	117
Tungsten <sup>a</sup>	500	3000	0.112	0.623	0.717	117
Tungsten <sup>d</sup>	250	1500	0.0727	0.742	0.671	118
Platinum <sup>a</sup>	270	2350	0.431	0.451	1.70	99
Gold <sup>a</sup>	500	3000	0.178	0.587	2.52	117
Gold <sup>c</sup>	150	2000	0.0244	0.911	0.794	113
Gold <sup>b</sup>	600	2000	0.1058	0.675	0.251	115
Thallium <sup>b</sup>	600	2000	0.0508	0.817	0.959	115
Lead <sup>b</sup>	600	2000	0.1545	0.716	0.512	115
Bismuth <sup>b</sup>	600	2200	0.0776	0.792	0.608	115

<sup>a</sup>Published parameters  $k$  and  $p$ .

<sup>b</sup>Exponential dependence fitted to original numerical values provided by the authors.

<sup>c</sup>Exponential dependence fitted to values taken from a published plot.

<sup>d</sup>Exponential dependence fitted to the published numerical data.

dependence did occur, particularly for low electron energies, but these were smaller than the scatter of the experimental values about the fitted curve. Similar fits with a larger number of parameters therefore did not seem to be useful. Table 4 contains values of  $k$  and  $p$  for each material and source together with the root-mean-square deviation for each fit.

Acceptable IMFP values may also be obtained from the approximate analytical model based on the transport approximation.<sup>101,102</sup> Nevertheless, as discussed in Sec. 2.2.1., differences from the IMFPs based on Monte Carlo calculations can, in general, occur. Values of the parameters  $k$  and  $p$  obtained from fits of Eq. (24) to the Beilschmidt

TABLE 5. Elements for which IMFP values were determined by Beilschmidt *et al.*<sup>102</sup> from EPES measurements and an approximate analytical theory. We show the minimum ( $E_{\min}$ ) and maximum ( $E_{\max}$ ) electron energies for which IMFPs were measured and give values of the parameters  $k$  and  $p$  found from fits of Eq. (24) to the measured IMFPs

Element	$E_{\min}$ (eV)	$E_{\max}$ (eV)	$k$	$p$	RMS (Å)
Aluminum <sup>a</sup>	250	1500	0.282	0.655	1.88
Aluminum <sup>b</sup>	250	1500	0.1839	0.721	1.65
Aluminum <sup>c</sup>	250	1500	0.0589	0.896	2.33
Nickel <sup>a</sup>	250	1500	0.943	0.379	1.77
Nickel <sup>b</sup>	250	1500	0.597	0.450	1.81
Nickel <sup>d</sup>	250	1500	0.374	0.462	1.07
Platinum <sup>a</sup>	250	1500	0.1890	0.609	0.827
Platinum <sup>c</sup>	250	1500	0.0577	0.793	1.50
Platinum <sup>d</sup>	250	1500	0.0959	0.665	0.655
Gold <sup>b</sup>	250	1500	0.1051	0.700	0.905
Gold <sup>c</sup>	250	1500	0.0456	0.831	1.35
Gold <sup>d</sup>	250	1500	0.0713	0.711	0.796

<sup>a</sup>Gold reference.

<sup>b</sup>Platinum reference.

<sup>c</sup>Nickel reference.

<sup>d</sup>Aluminum reference.

*et al.* IMFPs are listed in Table 5 with the corresponding root-mean-square deviations. For each of the four elements, the parameter values depend on which of the other three elements was selected as the standard material.

We now consider the procedures and experimental configurations used to make the IMFP measurements listed in Tables 4 and 5. Details of these experiments are shown in Table 6. As can be seen, most of the EPES measurements were made with a reference material (because these measurements are simpler), and nickel was most frequently used for this purpose. The EPES measurements were made in a number of different experimental configurations. Although the angle of incidence for the primary-electron beam was usually zero (with two exceptions), the emission angles varied considerably. The experimental configurations can be divided into two groups according to the range of emission angles investigated:

- (1) Experiments with a wide range of emission angles (from 5° to 44°) accepted by a retarding-field analyzer or with EPES measurements made over a wide range of emission angles (from 20° to 70°) using a rotatable analyzer. For these experiments, a standard material was not used.
- (2) Experiments with narrow range of emission angles (up to 6°) accepted by the analyzer. In these cases, the emission angles in different experiments varied between 34° and 48°, and a standard material was used in the EPES measurements.

We also note from Tables 4 and 5 that EPES measurements were made for incident electron energies ranging from 50 to 5000 eV, although most experiments were performed over smaller ranges.

Table 7 summarizes the number of sources of IMFP measurements by EPES and the total number of experimental IMFP values for the elements listed in Tables 4 and 5. The

total number of IMFPs for Si and Ge reported in the original papers has been reduced slightly to eliminate the same values that were included in duplicate reports from the same group.<sup>111,112</sup> It was also decided to remove the early IMFP measurements of Dolinski *et al.*<sup>97,98</sup> for Cu and Ag because they have been superseded by later work with improved experimental procedures (better vacuum, better surface cleaning, and better measurement of the elastically scattered electron intensity).<sup>113</sup>

#### 2.2.4. Uncertainties of Measured IMFP Values

We consider here sources of uncertainty in IMFP measurements with the EPES method. We also indicate whether each uncertainty component leads to random or systematic contributions to the total uncertainty for a measured IMFP. It is also necessary to point out that there have been few investigations of the uncertainties in IMFP measurements by EPES, and that most IMFP publications do not contain estimates of the uncertainties in the reported IMFPs. Our comparison in Sec. 3.3. of measured IMFPs from different laboratories is thus useful in providing a means for assessing the degree of consistency of independent measurements for particular elements.

(a) *Validity of the theoretical model providing the elastic backscattering probability (systematic).* As shown in Sec. 2.2.2, the elastic backscattering probability  $\eta_e$  or the backscattered current  $I$  has to be known to determine IMFPs using the analytical formalism [e.g., Eqs. (16) and (17)] or the Monte Carlo algorithm [Eq. (22)] for the particular mean electron emission angle and analyzer acceptance angle of an experiment. Previous investigations of the dependence of the elastic backscattering probability on electron energy and of the angular distribution of elastically backscattered electrons have shown generally good qualitative agreement between results of Monte Carlo simulations and experiment.<sup>96,101,119–124</sup> Pronounced differences between the simulations and the experimental data were observed only for relatively low energies. The calculated angular distribution of electrons elastically backscattered from Au deviated distinctly from the experimental distribution at energies below 200 eV.<sup>119</sup> The calculated and measured energy dependencies of the elastically backscattered intensity from gold within the solid angle of a retarding-field analyzer are noticeably different at energies below 100–300 eV depending on the potential used in the calculations.<sup>119</sup> Similar effects were observed for other elements.<sup>101,121</sup> For Al and Ag, the calculated dependencies of backscattered intensity on energy deviated sharply from the measured dependencies below 200 eV.<sup>121</sup> For carbon, the difference was not so pronounced but was found to increase with decreasing energy.<sup>121</sup> In more recent work, Werner *et al.*<sup>101</sup> compared measured angular distributions of electrons elastically backscattered from Al, Ni, Pt, and Au at energies varying from 300 to 1000 eV with predictions from the transport approximation. The largest deviations were observed at 300 eV (Al, Ni, and Au). Agree-

TABLE 6. Experimental procedures and configurations used for determining the IMFP values listed in Tables 4 and 5.<sup>a</sup> The abbreviations CMA, HSA, and RFA refer to a cylindrical-mirror analyzer, a hemispherical-sector analyzer, and a retarding-field analyzer, respectively

Element	Standard	Incidence angle (deg)	Emission angle (deg)	Analyzer	Ref.
Carbon (glassy)	Al	0	42±6	PHI <sup>c</sup> double-pass CMA	99
Carbon (graphite)	Al	0	42±6	PHI <sup>c</sup> double-pass CMA	99
Magnesium	—	0	20–70	Home made rotatable analyzer	115
Aluminum	Ni	0	42±6	PHI <sup>c</sup> double-pass CMA	112
	Ni	0	42±3.5	Riber CMA	112
Aluminum	—	0	20–70	Home made rotatable analyzer	115
Aluminum	Ni	0	35±1	Home-made HSA	102
	Pt	0	35±1	Home-made HSA	102
	Au	0	35±1	Home-made HSA	102
Silicon	Ni	0	42±3.5	Riber CMA	110
Silicon	Ni	0	42±3.5	Riber CMA	111
	Ni	0	42±6	PHI <sup>c</sup> double-pass CMA	111
	Ni	50	0 <sup>b</sup>	Home-made HSA	111
Silicon	Ni	0	42±6	PHI <sup>c</sup> double-pass CMA	112
Silicon	—	0	20–70	Home-made rotatable analyzer	115
Chromium	Ni	0	42±3.5	Riber CMA	110
Iron	Ni	0	42±6	PHI <sup>c</sup> double-pass CMA	112
	Ni	0	42±3.5	Riber CMA	112
Iron	—	0	20–70	Home-made rotatable analyzer	115
Cobalt	Al	0	42±6	PHI <sup>c</sup> double-pass CMA	107
Cobalt	Pd	0	42±6	PHI <sup>c</sup> double-pass CMA	107
Nickel	Al	0	42±6	PHI <sup>c</sup> double-pass CMA	99
Nickel	—	0	20–70	Home-made rotatable analyzer	115
Nickel	Al	0	35±1	Home-made HSA	102
	Pt	0	35±1	Home-made HSA	102
	Au	0	35±1	Home-made HSA	102
Copper	—	0	5–44	Home-made RFA	97
Copper	—	0	5–44	Home-made RFA	98
Copper	—	0	5–44	Home-made RFA	113
Copper	Ni	0	42±3.5	Riber CMA	114
Copper	—	0	20–70	Home-made rotatable analyzer	115
Copper	Ni	0	35±4.1	VG <sup>d</sup> HSA	109
Gallium	—	0	20–70	Home-made rotatable analyzer	115
Germanium	Ni	0	42±3.5	Riber CMA	110
Germanium	Ni	0	42±3.5	Riber CMA	111
	Ni	0	42±6	PHI <sup>c</sup> double-pass CMA	111
	Ni	50	0 <sup>b</sup>	Home-made HSA	111
Germanium	Ni	0	42±6	PHI <sup>c</sup> double-pass CMA	112
Germanium	—	0	20–70	Home-made rotatable analyzer	115
Molybdenum	Ni	0	42±3.5	Riber CMA	110
Molybdenum	Ni	0	42±6	PHI <sup>c</sup> double-pass CMA	112
	Ni	0	42±3.5	Riber CMA	112
Palladium	Al	0	42±6	PHI <sup>c</sup> double-pass CMA	107
Silver	Al	0	42±3.5	Riber CMA	100
Silver	—	0	5–44	Home-made RFA	97
Silver	—	0	5–44	Home-made RFA	98
Silver	—	0	5–44	Home-made RFA	113
Silver	—	0	20–70	Home-made rotatable analyzer	115
Indium	—	0	5–55	Riber RFA	116
Antimony	—	0	20–70	Home-made rotatable analyzer	115
Tellurium	—	0	20–70	Home-made rotatable analyzer	115
Tantalum	Al	0	42±3.5	Riber CMA	117
Tungsten	Al	0	42±3.5	Riber CMA	117
Tungsten	—	0	5–44	RFA	118
Platinum	Al	0	42±6	PHI <sup>c</sup> double-pass CMA	99
Platinum	Al	0	35±1	Home-made HSA	102
	Ni	0	35±1	Home-made HSA	102
	Au	0	35±1	Home-made HSA	102
Gold	Al	0	42±3.5	Riber CMA	117
Gold	—	0	5–44	Home-made RFA	113
Gold	—	0	20–70	Home-made rotatable analyzer	115

TABLE 6. Experimental procedures and configurations used for determining the IMFP values listed in Tables 4 and 5.<sup>a</sup> The abbreviations CMA, HSA, and RFA refer to a cylindrical-mirror analyzer, a hemispherical-sector analyzer, and a retarding-field analyzer, respectively—Continued

Element	Standard	Incidence angle (deg)	Emission angle (deg)	Analyzer	Ref.
Gold	Al	0	35 ± 1	Home-made HSA	102
	Ni	0	35 ± 1	Home-made HSA	102
	Pt	0	35 ± 1	Home-made HSA	102
Thallium	—	0	20–70	Home-made rotatable analyzer	115
Lead	—	0	20–70	Home-made rotatable analyzer	115
Bismuth	—	0	20–70	Home-made rotatable analyzer	115

<sup>a</sup>Certain commercial instruments are identified here to specify the experimental conditions. Such identification is not intended to imply recommendation or endorsement by the National Institute of Standards and Technology, nor is it intended to imply that the equipment identified is necessarily the best available for the purpose.

<sup>b</sup>The solid acceptance angle was not conical. The emission angle varied from 0° to a maximum of 5.3°.

<sup>c</sup>Physical Electronics.

<sup>d</sup>Vacuum Generators.

ment at the higher energies was very good for all of the studied elements.

The differences between the calculated and measured elastic-backscattering probabilities at low energies can be ascribed to several different factors. One reason for the deviations may be the growing influence of surface contamination. Furthermore, the contribution of surface excitations, not considered in most of the theoretical models, is expected to be larger at low energies, as discussed in Sec. 2.1.4. Werner *et al.*<sup>101</sup> have shown that the angular distribution of electrons backscattered from Au at 300 eV, after correction for surface excitations, is in much better agreement with the theoretical prediction. Nevertheless, the effects of surface excitations (discussed further below) on IMFP measurements by EPES are only expected to be significant if the EPES measurements are made *without* the use of a standard material. It is believed that the major reason for differences between calculated and measured elastic-backscattering probabilities at low energies is probably associated with the uncertainties of the electron-scattering cross sections, particularly the dependencies of the differential cross section  $d\sigma_e/d\Omega$  on scattering angle and primary-electron energy.<sup>119,120,124</sup>

Values of the differential cross section depend on the atomic potential used to calculate them. While the potential of an atomic scattering center in a solid is different from the

potential for the corresponding isolated atom, theoretical models based on cross sections derived from atomic potentials describe the phenomenon of elastic backscattering at sufficiently high energies quite well, as shown above. This result seems to be evidence for a more general rule, namely that the relative difference in cross sections due to a difference in the interaction potentials decreases with increasing energy. For example, it has been found that the difference between cross sections calculated with the Thomas–Fermi–Dirac (TFD) and Dirac–Hartree–Fock (DHF) potentials also decreases with increasing energy.<sup>119,125</sup> For Au, good agreement was observed for energies exceeding 200 eV.<sup>119</sup> The same effect was noticed when different analytical approximations of the TFD potential for Au were used in calculations of elastic-scattering cross sections.<sup>126</sup>

The differences between elastic-scattering cross sections in various publications have been recently analyzed in detail.<sup>127</sup> As an example, Table 7 shows the percentage differences found between the differential cross sections from two databases<sup>127,128</sup> for scattering of 1000 eV electrons by C, Al, Fe, Ag, and Au at selected scattering angles. It was found that the differences between cross sections calculated using the TFD and DHF potentials was usually less than 10% for scattering angles between 30° and 180°. The largest difference, exceeding 130%, was found for a scattering angle of 1°; while this difference is large, it should not have a profound effect on the results of Monte Carlo simulations since small scattering angles only slightly influence the electron trajectories.

It seems that the reliability of theoretical models for describing elastic-electron backscattering cannot be readily correlated with the atomic number of a solid. As mentioned above, large differences between calculated and measured results for the energy dependence of the absolute elastic backscattering probability were observed below 200 eV for low- and medium-atomic-number elements, i.e., for C, Al, and Ag.<sup>121</sup> On the other hand, in a more recent study, comparisons of theoretical and experimental backscattered intensities (in arbitrary units) showed good agreement for Pt and

TABLE 7. Percentage differences between the differential elastic-scattering cross sections at 1000 eV from two databases for the indicated scattering angles and elements<sup>126,127</sup>

Scattering angle (deg)	Percentage Difference				
	C	Al	Fe	Ag	Au
1	23.27	132.78	25.89	−20.44	−33.71
30	4.83	−7.31	−4.51	−1.25	−12.24
60	−3.10	−1.52	12.81	8.45	−8.09
90	−0.73	4.06	6.22	2.16	−17.21
120	1.05	2.88	1.55	−15.28	−3.49
150	3.00	−0.10	−2.63	−1.98	−6.76
180	4.50	−1.63	−4.46	−3.78	−10.13

Au for electron energies as low as 50 eV although similar comparisons made for Al and Cu showed poorer agreement.<sup>123</sup> On consideration of these observations, a lower limit of 200 eV for validity of the theoretical model used in EPES calculations appears to be reasonable.

A recent analysis of many measured intensities of elastically backscattered electrons for electron energies from 50 to 500 eV and emission angles from 5° to 45° indicates that most of the scatter in the resulting IMFP values is due to a systematic variation of these IMFPs with emission angle.<sup>129</sup> This result has been ascribed partly to possible instrumental uncertainties (e.g., deflection of electrons by stray electrostatic fields in the vicinity of the electron gun) and partly to systematic uncertainties associated with the theoretical model.<sup>129</sup> It was found that the dependence of the IMFPs on emission angle became less pronounced for emission angles between 20° and 45°. This range of emission angles was therefore recommended for EPES measurements. Furthermore, the analysis confirmed that the lower energy limit for satisfactory modeling of EPES experiments was 200 eV.<sup>129</sup>

(b) *Technique for measuring the elastic peak intensity (systematic and random).* The peak of elastically scattered electrons generally overlaps with intensity due to inelastically scattered electrons. If the absolute energy resolution  $\Delta E$  of the EPES instrument is sufficient, this overlap may not be a problem but, in other cases and for some materials, the overlap can be severe (particularly for larger electron energies on instruments for which the relative energy resolution  $E/\Delta E$  is constant).<sup>99</sup> One approach has been to measure the area of the high-energy-side half of the elastic peak, i.e., the side which is much less affected by the inelastic background. If  $\Delta E$  is sufficiently small so that there is negligible overlap of the inelastic intensity with the elastic peak, the entire area of the elastic peak can be measured.<sup>102</sup> A more sophisticated approach involves fitting a measured spectrum with a linear background and appropriate functions to represent the elastic peak and other peaks in the energy-loss spectrum.<sup>99</sup> The latter procedure is believed to give a more accurate measure of the elastic-peak intensity. There will also be a random component of uncertainty associated with measurement statistics for the elastic-peak measurement.

(c) *IMFP values for the standard material (systematic).* If a standard (or reference) material is used in the EPES measurements, the IMFPs at different electron energies for the specimen material will clearly depend on the accuracy of the IMFPs for the standard. Nickel has been employed as the standard material in most of the EPES experiments that utilized a standard (Table 6), and the calculated IMFPs of Tanuma *et al.*<sup>47</sup> were frequently used as reference values in these experiments.

The uncertainties of the calculated IMFPs have been discussed in Sec. 2.1.4. The average of the sum-rule errors in the evaluation of the Ni optical data for the Tanuma *et al.*<sup>47</sup> IMFP calculation was about 3%.<sup>30</sup> The uncertainty in the calculated IMFPs for bulk Ni (a nonfree-electron-like solid) due to uncertainties of the IMFP algorithm is probably more

than 10% (but cannot be estimated with confidence).

(d) *Surface excitations (systematic).* The effects of surface excitations (Sec. 2.1.4.) need to be considered in EPES measurements of IMFPs. The magnitude of these effects on EPES measurements depends on the inelastic-scattering properties of the material of interest, the surface roughness, the electron energy, and the angles of electron incidence and emission in the experiment.<sup>18,63</sup> Their effect on a derived IMFP depends on whether or not a standard material is used in the EPES experiments.

If a standard material is employed, it is believed that the effects of surface excitations are likely to be small, probably negligible, if the specimen material and the standard have similar inelastic-scattering properties (e.g., if they are both free-electron-like metals, nonfree-electron-like metals, semiconductors, or insulators).<sup>51,102</sup> Since IMFPs are determined from ratios of elastically backscattered intensities for the specimen and the standard, the ratios of corrections to bulk IMFPs (to take account of surface excitations) for the two materials is likely to be close to unity if these materials have similar energy-loss functions (Sec. 2.1.1.). Aluminum was used as a standard material in some EPES experiments (Table 6), but the strong dependence of the surface-plasmon excitation probability on surface roughness and scattering angle in electron energy-loss experiments<sup>63(b)</sup> makes Al an unsuitable choice for a standard (unless EPES measurements are to be made on another free-electron-like material with similar surface roughness).

If a standard material is not used in the EPES experiments, surface excitations will lead to a measured "effective" IMFP being smaller than the corresponding bulk IMFP. Chen<sup>10</sup> has shown that surface excitations in Cu and Ag (with surfaces assumed to be smooth) lead to differences between effective and bulk IMFPs varying from about 40% at 250 eV to about 12% at 1500 eV. Ding's<sup>67</sup> calculations for Au, however, indicate that these differences could be about 10%. Experiments are needed to determine the magnitudes of surface corrections to bulk IMFPs for application in areas such as AES and XPS.

(e) *Surface roughness (systematic and random).* An increase in surface roughness is expected to decrease the elastic backscattering probability due to the possibility that emitted electrons will be "recaptured" by geometrical protrusions. It would then be expected from Eq. (16) that the resulting IMFP would be underestimated. Surface roughness would also reduce the probability of surface excitations over that expected for smooth surfaces;<sup>63(b)</sup> as a result, an IMFP measured by EPES could be closer to the bulk value (Sec. 2.1.4.). Variations in surface roughness of the same material in different EPES experiments would clearly lead to random uncertainties in the IMFP measurements. Experimental tests are needed to determine the extent to which surface roughness affects elastic-peak intensities and derived IMFPs for different types of materials and for different experimental configurations.

The systematic effects of surface roughness depend on whether or not a standard material is used in the EPES mea-

surements. If a standard material is not used, it is likely that surface roughness will have a greater effect on a resulting IMFP. If a standard material is used in the EPES experiments, the effects of surface roughness will be minimized if both the specimen and the standard materials have similar roughnesses. It is recommended that the specimen and standard materials be carefully polished and that any subsequent surface cleaning (e.g., by ion sputtering) be as mild as possible to avoid increasing the surface roughness. Ion bombardment will often lead to increased surface roughness and possibly to complex topographical changes (such as the production of etch pits, pyramids, cones, whiskers, ripples, recrystallization, and swelling) as described in recent reviews.<sup>130,131</sup>

(f) *Surface composition (systematic)*. The elastic-peak intensity is sensitive to surface contamination because the backscattered electrons pass the surface region twice. A contamination layer (e.g., carbonaceous residues) will generally have scattering properties that are completely different from those of the underlying specimen material. The effects of any contamination will be particularly severe at low electron energies (50–100 eV) when the IMFP is close to its minimum value. It is recommended that the surface cleanliness of specimen and standard materials be checked *in situ* by AES or XPS (not only after any surface cleaning but also after the EPES measurements have been completed).

For EPES measurements with alloys or compounds, it is important but often difficult to ensure that the surface composition of the specimen over the EPES probing depth is uniform and preferably not significantly different from the bulk composition. If ion bombardment is used for surface cleaning of alloys or compounds, this will generally lead to changes in surface composition, variations of composition with depth, and to other surface changes.<sup>130,131</sup>

(g) *Specimen crystallinity (systematic)*. As indicated in Sec. 2.2.2., an assumption in the analysis of EPES measurements using Monte Carlo simulations is that the scattering centers are randomly distributed in the solids. Most EPES measurements have been made with polycrystalline specimen materials and the surfaces had been cleaned by ion bombardment prior to data acquisition. It is well known that ion bombardment disorders initially crystalline solids but the net effect of specimen crystallinity on EPES measurements depends on the relative magnitudes of the depth of the disordered region (which depends on the specimen material and on the ion species and energy)<sup>130,131</sup> and the information depth for EPES (which depends on the material and the electron energy). The information depth has been defined by ASTM Committee E-42 on Surface Analysis as the maximum depth, normal to the specimen surface, from which useful signal information is obtained,<sup>8</sup> and can be identified with the specimen thickness from which a specified percentage (e.g., 95% or 99%) of the detected signal originates. For EPES, the information depth will depend in part on the IMFP and in part on the effects of elastic-electron scattering for the particular measurement configuration. If the incidence and emission angles were less than about 20° and if the effects of

elastic scattering on trajectory lengths were assumed to be negligible, it would be expected that about 98% of the detected elastic-peak signal would come from a depth of about twice the IMFP. This estimate is roughly consistent with the results of Monte Carlo simulations by Robert *et al.*<sup>132</sup> for EPES measurements with a retarding-field analyzer having an acceptance angle of between 2° and 55°. Their simulations with 200 eV electrons incident on Si, Ni, Ag, and Au showed that most of the elastically reflected electrons penetrated less than 2 monolayers. With 1000 eV electrons, most of the elastically reflected electrons penetrated less than about 10 monolayers.

If EPES measurements are made with crystalline specimens, strong angular anisotropies in electron transport are expected due to forward focusing and diffraction effects.<sup>133</sup> Modulations of up to about 50% have been observed in Auger electron yields, for example, as a function of electron emission angle or of incidence angle of the primary beam on single-crystal specimens or when the primary beam was incident on a single grain of a polycrystalline solid.<sup>134</sup> In EPES experiments, Goto *et al.*<sup>135</sup> found that the intensities of elastically scattered 1000 eV electrons measured with a cylindrical-mirror analyzer varied by up to about 50% for different single-crystal surfaces of copper. Similar results have been found by Gergely *et al.*<sup>136</sup> with crystalline InSb and GaSb. It is therefore important that tests be made to demonstrate that crystallinity effects are small in EPES experiments. While ion bombardment is convenient for surface cleaning and for disordering crystalline solids, it can also lead to unwanted compositional and topographical changes in alloys and compounds;<sup>130,131</sup> the effects of these changes on IMFP measurements need to be investigated and shown to be small.

(h) *Stability of the primary-beam current (systematic or random)*. The primary-beam current should be stable during the sequence of EPES measurements. If this current drifts or varies randomly during the experiments, the derived IMFP values will be directly affected.

### 3. Evaluation of IMFP Values

#### 3.1. Selection of Materials

We have selected materials for the IMFP evaluation based on the following criteria. First, we selected materials for which the IMFPs were measured by elastic-peak electron spectroscopy (for the reasons discussed in Secs. 2.2.1. and 2.2.2.). Second, we selected materials (all solid elements) for which IMFP measurements had been made in at least two different laboratories. Table 8 indicates that the following elements should be considered: Al, Si, Fe, Ni, Cu, Ge, Mo, Ag, W, Pt and Au. We then selected elements for which independent IMFP calculations had been reported by at least two groups (Table 9). The elements Al, Si, Fe, Ni, Cu, Ge, Ag, and Au satisfy the above criteria. We have chosen, however, to exclude Fe from our detailed evaluation mainly because we wished to make comparisons among the elements over similar ranges of electron energy and over as wide an

TABLE 8. Number of sources of IMFPs measured by EPES for solid elements (from Tables 4 and 5) and the total number  $M$  of IMFP measurements for each element

Element	Number of sources of IMFP measurements	Total number of IMFP measurements $M$
Carbon (glassy)	1	10
Carbon (graphite)	1	15
Magnesium	1	14
Aluminum	3	61
Silicon	4	41
Chromium	1	6
Iron	2	21
Cobalt	1	12
Nickel	3	56
Copper	5	49
Gallium	1	18
Germanium	4	33
Molybdenum	2	16
Palladium	1	6
Silver	5	21
Indium	1	9
Antimony	1	9
Tellurium	1	9
Tantalum	1	5
Tungsten	2	9
Platinum	2	50
Gold	4	57
Thallium	1	8
Lead	1	8
Bismuth	1	9

energy range as possible. For Fe, the two sets of calculated IMFPs have maximum electron energies of 2000 eV while, for the other seven elements, there is at least one set of calculated IMFPs extending to  $10^4$  eV. We also wished to identify one or more elements in our evaluation that showed superior agreement in comparisons of calculated and measured IMFPs over a wide energy range so that these elements

TABLE 9. Sources of calculated IMFPs for elements for which there are at least two sources of measured IMFPs (Table 8)

Element	Tanuma <i>et al.</i> <sup>a</sup>	Ashley <i>et al.</i> <sup>b</sup>	Kwei, Chen <i>et al.</i> <sup>c</sup>	Ding and Shimizu <sup>d</sup>
Aluminum	+	+	+	
Silicon	+	+		
Iron	+		+	
Nickel	+	+	+	
Copper	+	+	+	+
Germanium	+	+		
Molybdenum	+			
Silver	+	+	+	
Tungsten	+			
Platinum	+			
Gold	+	+	+	+

<sup>a</sup>Reference 47.

<sup>b</sup>References 35, 38–40.

<sup>c</sup>Reference 51.

<sup>d</sup>Reference 52.

could be used as standard materials in future EPES measurements (Sec. 2.2.2.). Our evaluation is based on papers that had been published prior to June, 1998.

Figure 9 shows calculated and measured IMFPs for Al, Si, Ni, Cu, Ge, Ag, and Au (from the sources identified in Tables 4, 5 and 9). Separate curves are shown for each source of calculated IMFPs for each element, and different symbols are used to indicate the measured IMFPs from each source. Measured EALs for silicon are shown in Fig. 9(b) (squares) from the data in Fig. 5. The scatter in the EAL values is greater than for the IMFP measurements but it does appear that the IMFP values at  $\sim 1270$  eV are greater than the average EAL values, as expected from the discussion of Sec. 2.2.1.

The IMFPs in Fig. 9 will be analyzed in the following sections. First, we will examine differences between the calculated IMFPs (Sec. 3.2.1.). Second, we will review differences between the measured IMFPs (Sec. 3.3.). Third, we will compare the calculated and measured IMFPs (Sec. 3.4.1.). Since the number of materials for which IMFP calculations and measurements have been made is rather small, we will make some additional comparisons of calculated IMFPs in Sec. 3.2.2. (for selected compounds) and of calculated and measured IMFPs in Sec. 3.4.2. (for Fe, Mo, W, and Pt). Finally, we will discuss criteria for the selection of recommended IMFP values in Sec. 3.5. and identify elements that have a high degree of consistency in the calculated IMFPs from different sources, in the measured IMFPs from different sources, and in the calculated and measured IMFPs.

We note here that most IMFP measurements by EPES have been made for elemental solids. Very recently, the EPES method has been used to measure IMFPs for Au–Pd alloys,<sup>106</sup> Pd–Co alloys,<sup>107</sup> GaAs,<sup>108(a),108(b),108(c)</sup> InP,<sup>108(a),108(b)</sup> CuO,<sup>109</sup> Cu<sub>2</sub>O,<sup>109</sup> GaSb,<sup>108(d)</sup> InSb,<sup>108(d)</sup> polyacetylene,<sup>108(e)</sup> and Pd-doped polyacetylene.<sup>108(e)</sup> A potentially large source of uncertainty in EPES measurements with compounds is the extent to which the surface composition of the specimen materials is uniform (over the volume probed by EPES) and possibly different from the bulk stoichiometry after surface cleaning [Sec. 2.2.4.(e)]. IMFP calculations have been reported by Tanuma *et al.*<sup>48,50</sup> for some of these compounds (GaAs, GaP, InP, InSb, and polyacetylene) but the optical data for some of the inorganic compounds (particularly those for GaAs and InSb) were of poorer consistency than for most of the materials for which IMFP calculations have been made.<sup>47,48,50</sup> We did not make any comparison of IMFP calculations and measurements for compounds here because of the small number of materials for which replicate IMFP measurements have been made (GaAs, InP, GaSb, and InSb), the difficulty of assessing the composition and the compositional uniformity in the surface region probed by EPES (particularly if the surface had been cleaned by ion bombardment), the greater uncertainty in the calculated IMFPs of Tanuma *et al.* for GaAs and InSb, and the fact that the most recent results for GaSb and InSb were not available by the time our analysis was completed.

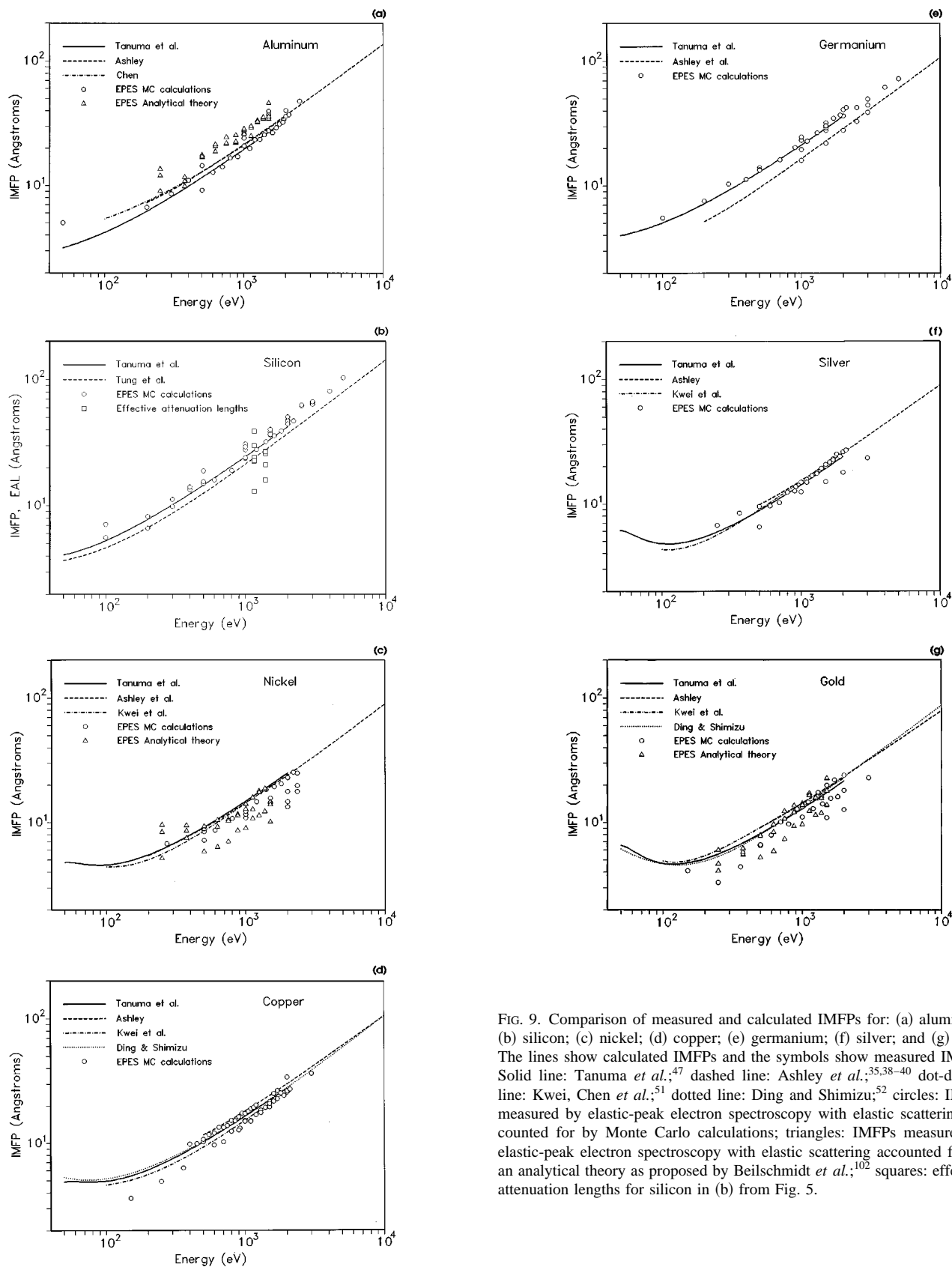


FIG. 9. Comparison of measured and calculated IMFPs for: (a) aluminum; (b) silicon; (c) nickel; (d) copper; (e) germanium; (f) silver; and (g) gold. The lines show calculated IMFPs and the symbols show measured IMFPs. Solid line: Tanuma *et al.*;<sup>47</sup> dashed line: Ashley *et al.*;<sup>35,38-40</sup> dot-dashed line: Kwei, Chen *et al.*;<sup>51</sup> dotted line: Ding and Shimizu;<sup>52</sup> circles: IMFPs measured by elastic-peak electron spectroscopy with elastic scattering accounted for by Monte Carlo calculations; triangles: IMFPs measured by elastic-peak electron spectroscopy with elastic scattering accounted for by an analytical theory as proposed by Beilschmidt *et al.*;<sup>102</sup> squares: effective attenuation lengths for silicon in (b) from Fig. 5.

## 3.2. Evaluation of Calculated IMFP Values

### 3.2.1. Evaluation of Calculated IMFPs for Al, Si, Ni, Cu, Ge, Ag, and Au

The IMFPs were calculated over different energy ranges by the different authors and, as can be seen in Fig. 9, these ranges for a given element only partially overlap. In addition, there are some energy ranges for which there is only one source of calculated IMFPs. To estimate the degree of consistency in the calculated IMFPs from different sources, we have followed the following procedure:

(1) IMFPs were calculated for fixed energy values in the total energy range for which IMFPs were available from a given source (as indicated in Table 9). These calculations were made using the analytic functions described in Sec. 2.1.3. [Eqs. (6) and (7) and the parameters in Tables 1–3]. The fixed energy values for these calculations were chosen as follows within the energy range for which IMFPs had been reported by each source:

- steps of 1 eV in the range from 50 to 99 eV;
- steps of 10 eV in the range from 100 to 990 eV; and
- steps of 100 eV in the range from 1000 to 10000 eV.

(2) If at least two IMFP values were available at a given energy, the mean IMFP at that energy was calculated from:

$$\langle \lambda \rangle = \frac{1}{m} \sum_{j=1}^m \lambda_j, \quad (25)$$

where  $\lambda_j$  denotes the IMFP value found from the  $j$ th source at a particular electron energy, and  $m$  is the number of available sources for that energy. For simplicity, we have deleted the subscript  $i$  on the IMFP  $\lambda$  in Eq. (25) and in the following equations.

(3) For each source, the percentage deviation from the mean IMFP at each energy was calculated from:

$$\delta_j = 100(\lambda_j - \langle \lambda \rangle) / \langle \lambda \rangle. \quad (26)$$

This procedure ensures that IMFPs at any energy from different sources receive the same weight in our analysis of consistency.

The dependencies of the deviations  $\delta_j$  on energy in the overlapping energy ranges are shown in Fig. 10 for each element. As can be seen, the deviations from the mean  $\delta_j$  are less than 15% for six of the elements and less than 20% for Ge. Note that the steps at certain energies in Fig. 10 [e.g., at 100, 500, and 2000 eV in Fig. 10(d)] are due to the number of IMFP sources for the mean  $m$ , changing at these energies; as a result, there is a sudden change in the mean IMFP. Inspection of Fig. 10 leads to the following conclusions:

(1) The smallest deviations from the mean are observed for Si, Ni, Ag, and Au. For Si, there are only two sources of calculated IMFPs, and the overlapping energy range is from 200 to 2000 eV. The deviations in this range vary from  $-7\%$  to  $7\%$ . For Ni, there are three sources, the overlapping energy range extends from 100 to 2000 eV (although the range of one source is 200–2000 eV), and the deviations vary between  $-5.9\%$  and  $4.4\%$ . For Ag, there are three

sources, the overlapping energy range extends from 100 to 2000 eV (although the range of IMFPs calculated by Ashley<sup>35</sup> has been restricted to energies from 500 to 2000 eV for the reasons discussed in Sec. 2.1.3.), and the deviations vary from  $-5.3\%$  to  $6.9\%$ . For Au, four sources with overlapping energy ranges between 50 and  $10^4$  eV have deviations varying between  $-7\%$  and  $8.4\%$ .

(2) The deviations from the mean for the other three elements (Al, Cu, and Ge) occur over much larger ranges than for Si, Ni, Ag, and Au. The largest deviations [from  $-16.5\%$  to  $16.5\%$ , note the change of the scale in Fig. 10(e)] are found for Ge. In this case, only two sources are available for a relatively small overlapping energy range (200–2000 eV).

We have found a function that represents the dependence of the calculated IMFPs from all available sources for each of the seven elements (Table 9) on electron energy. For this purpose, the IMFP values were again calculated for fixed energies using the procedure described above, i.e., steps of 1 eV in the range from 50 to 99 eV, steps of 10 eV in the range from 100 to 990 eV, and steps of 100 eV in the range from 1000 to 10000 eV using Eqs. (6) and (7) and the parameters in Tables 1–3. Equation (7) was fitted to all of the IMFP values calculated at the specified energies for a given element (within the energy ranges for which IMFPs had been reported in the original publications). These fits were obtained by minimization of Eq. (8), as described in Sec. 2.1.3. It was decided to set the number of components  $n$  in Eq. (7) equal to two since there were problems with convergence if  $n$  were larger. Three parameters were selected to describe the quality of each fit:

- (1) Root-mean-square deviation *RMS*:

$$RMS = \sqrt{\frac{1}{r} \sum_{j=1}^r (\lambda_j - \lambda_{\text{fit}})^2}, \quad (27)$$

where  $\lambda_j$  is a computed IMFP for a given element, source, and energy,  $\lambda_{\text{fit}}$  is the IMFP obtained from the fit at a particular energy, and  $r$  is the total number of computed IMFPs (for all sources and energies for a particular element).

- (2) Mean percentage deviation *R* from the fitted function:

$$R = 100 \frac{1}{r} \sum_{j=1}^r \left| \frac{\lambda_j - \lambda_{\text{fit}}}{\lambda_{\text{fit}}} \right|. \quad (28)$$

- (3) Percentage deviation  $\Delta_j$  from the fitted function:

$$\Delta_j = 100(\lambda_j - \lambda_{\text{fit}}) / \lambda_{\text{fit}}. \quad (29)$$

Values for the fitting parameters  $k_j$  and  $p_j$  in Eq. (7) found in the fits for each element are shown in Table 10 together with the corresponding values of *RMS* and *R*. The percentage deviations  $\Delta_j$  for each element are plotted in Fig. 11. From Table 10, the smallest values of *RMS* are found for Ag, Ni, Al, and Cu; the values of *RMS* for these elements are less than the average value of *RMS* for the seven elements and also less than 1 Å. If values of the mean percentage deviation *R* are considered, the smallest values are found for Ag, Ni, Cu, Au, and Al; the *R* values for these elements are less than

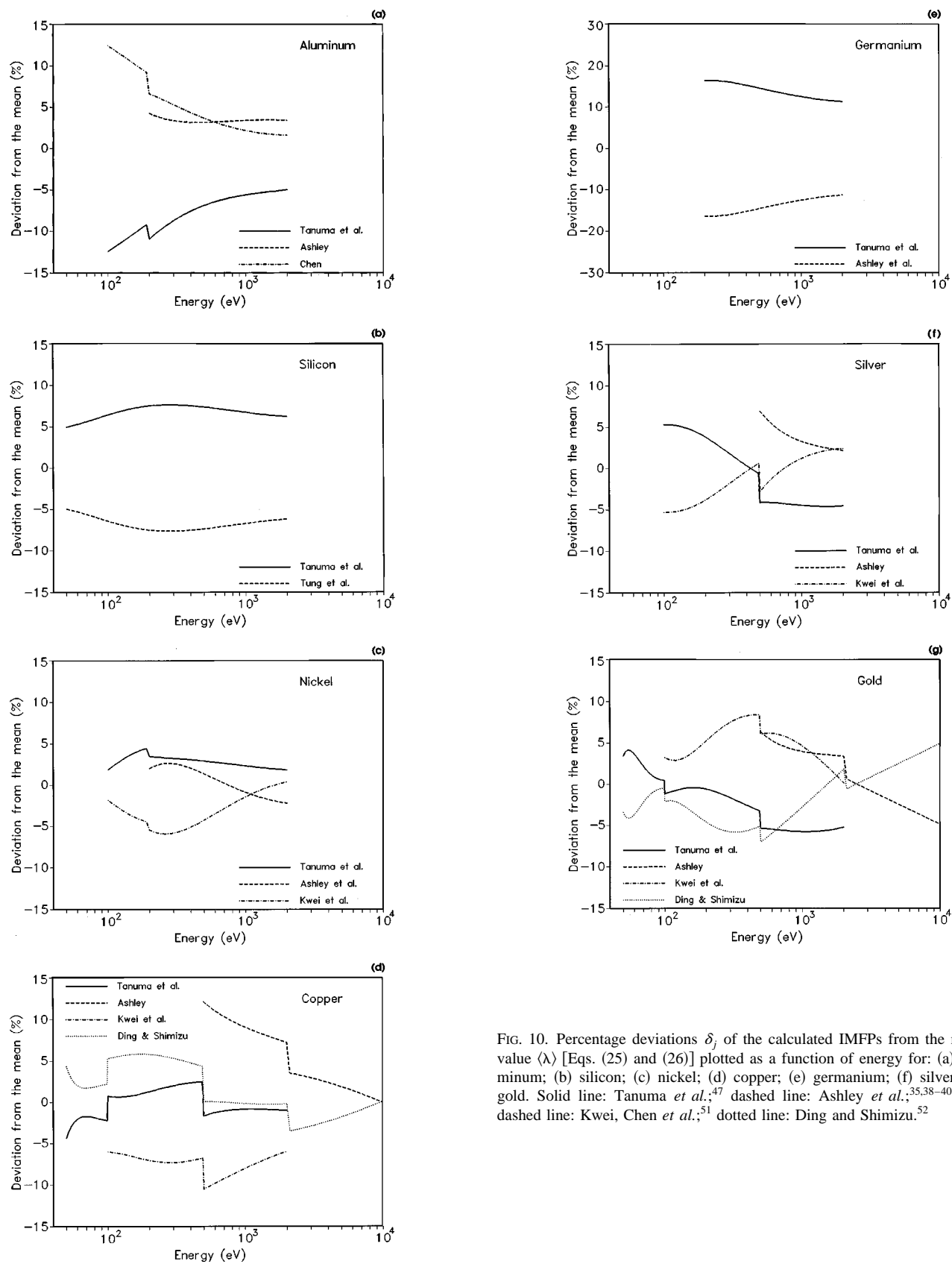


FIG. 10. Percentage deviations  $\delta_j$  of the calculated IMFPs from the mean value  $\langle \lambda \rangle$  [Eqs. (25) and (26)] plotted as a function of energy for: (a) aluminum; (b) silicon; (c) nickel; (d) copper; (e) germanium; (f) silver; (g) gold. Solid line: Tanuma *et al.*;<sup>47</sup> dashed line: Ashley *et al.*;<sup>35,38-40</sup> dot-dashed line: Kwei, Chen *et al.*;<sup>51</sup> dotted line: Ding and Shimizu.<sup>52</sup>

TABLE 10. Values of the parameters  $k_j$  and  $p_j$  found in the fits of Eq. (7) to the calculated IMFPs for each element and for electron energies between 50 and  $10^4$  eV (as described in Sec. 3.2.1.). Values of  $RMS$  and  $R$  from Eqs. (27) and (28) are shown for each fit. The last line of the table shows the average values of  $RMS$  and  $R$ . See Secs. 3.2.1. and 3.4.1. for a discussion of the IMFP data of Ge

Element	$k_1$	$p_1$	$k_2$	$p_2$	$RMS$ (Å)	$R$ (%)
Al	0.6210	0.2921	0.031 64	0.9028	0.757	4.08
Si	7.938	-0.3689	0.085 68	0.8032	1.04	5.57
Ni	48.58	-0.6648	0.058 06	0.7949	0.419	2.11
Cu	32.34	-0.5464	0.054 78	0.8193	0.784	3.67
Ge	12.53	-0.3978	0.071 25	0.7929	1.67	9.27
Ag	442.1	-1.145	0.066 19	0.7828	0.361	2.10
Au	252.0	-1.002	0.060 83	0.7824	1.21	3.80
Average values:					0.89	4.4

the average value of  $R$ . Figure 11 shows that the smallest percentage deviations occur for Ni (for which the deviations vary between  $-5.8\%$  and  $4.0\%$ ).

A relatively large range of deviations is found for Cu [ $-7.9\%$ – $15.8\%$  in Fig. 11(d)]. These large positive deviations are associated with the IMFPs computed by Ashley,<sup>35</sup> one reason for the positive deviations of the Ashley data for Al, Cu, Ag, and Au in Fig. 11 is the exchange correction shown in Fig. 1 and discussed in Sec. 2.1.3. The largest positive deviations for Cu in Fig. 11(d) occur for a relatively small electron energy range (500–1000 eV), and these deviations do not greatly affect the magnitudes of  $RMS$  and  $R$ . The percentage deviations for the other three IMFP sources in Fig. 11(d) range from  $-7.9\%$  to  $6.8\%$ .

The largest values of  $RMS$  and  $R$  in Table 10 are found for Ge; the percentage deviations for Ge in Fig. 11(e) vary between  $-18.1\%$  and  $20.4\%$ . These relatively large values of  $RMS$  and  $R$  are mainly due to different choices and treatments of the optical data used in the two IMFP calculations.<sup>40,47</sup> From Fig. 9(e), it can be seen that most of the measured IMFPs for Ge lie close to the IMFP calculations of Tanuma *et al.*,<sup>47</sup> and we therefore believe that the calculated IMFPs from this source should be preferred.

The average values of  $RMS$  and  $R$  in Table 10 are 0.89 Å and 4.4%, respectively. These values provide a measure of the extent to which the calculated IMFPs from different sources for the seven selected elements differ from curves [Eq. (7)] fitted to the calculated IMFPs for those elements. The average values of  $RMS$  and  $R$  are considered acceptably small considering the differences in the technical approaches for calculating IMFPs by different groups (described in Secs. 2.1.2. and 2.1.3.) and possible differences in choices of experimental optical data. Further information on the uncertainties of the calculated IMFPs is given in Sec. 2.2.4.

### 3.2.2. Evaluation of Calculated IMFPs for Selected Compounds

Figures 12–17 show comparisons of calculated IMFPs for six compounds: aluminum oxide, silicon dioxide, potassium chloride, poly(butene-1-sulfone), polyethylene, and polystyrene. For each compound, there were at least two indepen-

dent sources for the IMFP values. The data of Akkerman *et al.*<sup>54</sup> in Figs. 12–14 show apparent discontinuities at 100 eV due to the fact that IMFPs were computed at a limited number of electron energies; in addition, there is an apparent maximum at 5000 eV which is unexpected but which is also apparent in the original publication.

In general, Figs. 12–17 show a degree of consistency similar to that found for the calculated IMFPs for the seven elements in Fig. 9. The computed IMFPs of Akkerman *et al.*,<sup>54</sup> however, are consistently larger at 50 eV than those of Tanuma *et al.*,<sup>50</sup> this difference is largely due to explicit consideration of the band gap in modifying the accessible range of momentum transfers for insulators.<sup>54</sup> We also point out a difference in the IMFPs calculated by Tanuma *et al.*<sup>50</sup> and Ashley<sup>33(f)</sup> for poly(butene-1-sulfone) at energies less than 200 eV in Fig. 15; no differences of this type are seen in the comparisons of similar data in Figs. 12–14, 16, and 17 for which the same IMFP algorithms were employed.

Figure 16 also shows measurements of EALs for SiO<sub>2</sub> at two energies from Fig. 6. The calculated IMFPs are greater than the averages of the EALs at each energy, as expected from the effects of elastic-electron scattering (Sec. 2.2.1.), but the spread in measured EALs is too large to make a reliable determination of the magnitude of these effects (let alone any assessment of the calculated IMFPs from different sources).

### 3.3. Evaluation of Measured IMFP Values for Al, Si, Ni, Cu, Ge, Ag, and Au

Figures 9(a)–9(g) show considerable scatter in the IMFPs measured by elastic-peak electron spectroscopy. This scatter is due in part to scatter in the data from a particular source (Tables 4 and 5) and in part to differences in data from different sources for the same element. To analyze the degree of consistency of the measured IMFPs as was done with the calculated IMFPs in Sec. 3.2.1., we decided to fit the measured IMFPs with Eq. (24). Equation (24) is not expected to be the most appropriate function for this purpose,<sup>137</sup> but we found this equation useful in fitting the measured IMFPs from each source (Tables 4 and 5), and the scatter of the measured IMFPs in Fig. 9 made it difficult to consider other possible functions. Figure 18 shows the measured IMFPs for each element and the fits to these values with Eq. (24); the fit parameters are shown in Table 11.

Use of Eq. (24) for fitting the measured IMFPs leads, as expected,<sup>133</sup> to systematic deviations for electron energies less than about 200 eV. These deviations, however, are generally less than the scatter in the measured IMFPs. If we consider the energy range from 50 to 150 eV, Figs. 18(a), 18(b), 18(d), 18(e) and 18(g) indicate that the measured IMFPs tend to be systematically larger than the fitted values. However, there is only one clear outlier in this energy range [the IMFP for Al at 50 eV in Fig. 18(a)]. While Eq. (24) is not expected to be correct in detail for describing the IMFP energy dependence over a wide energy range, the large scatter in the measured IMFPs and the limited number of mea-

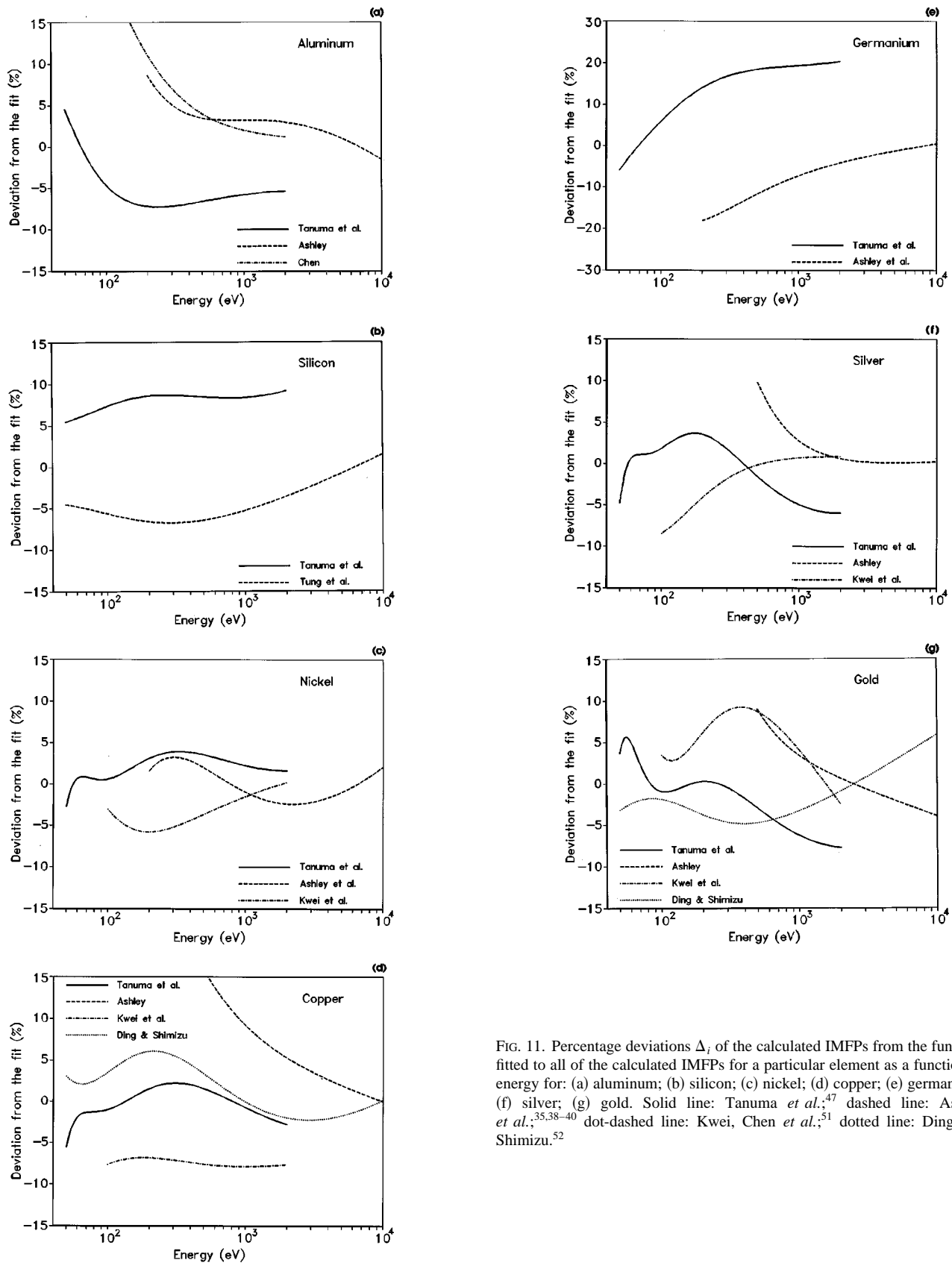


FIG. 11. Percentage deviations  $\Delta_i$  of the calculated IMFPs from the function fitted to all of the calculated IMFPs for a particular element as a function of energy for: (a) aluminum; (b) silicon; (c) nickel; (d) copper; (e) germanium; (f) silver; (g) gold. Solid line: Tanuma *et al.*;<sup>47</sup> dashed line: Ashley *et al.*;<sup>35,38-40</sup> dot-dashed line: Kwei, Chen *et al.*;<sup>51</sup> dotted line: Ding and Shimizu.<sup>52</sup>

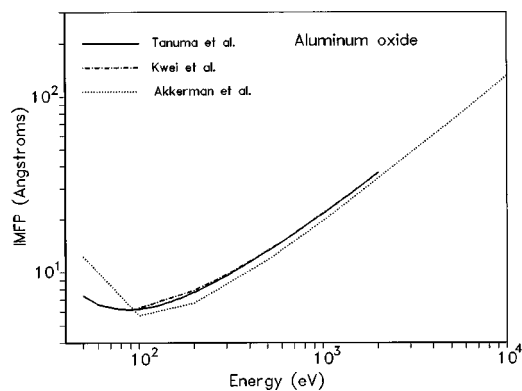


FIG. 12. Comparison of calculated IMFPs for aluminum oxide. Solid line: Tanuma *et al.*;<sup>48</sup> dot-dashed line: Kwei, Chen *et al.*;<sup>51</sup> dotted line: Akkerman *et al.*<sup>54</sup>

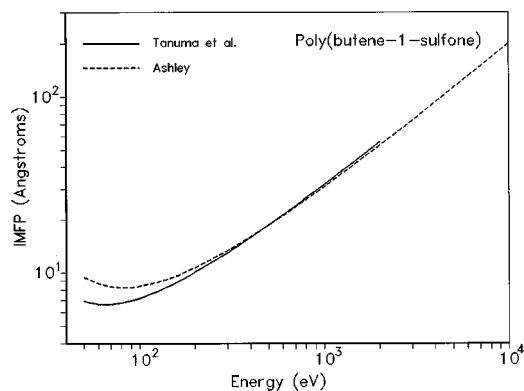


FIG. 15. Comparison of calculated IMFPs for poly(butene-1-sulfone). Solid line: Tanuma *et al.*;<sup>50</sup> dashed line: Ashley.<sup>33(f)</sup>

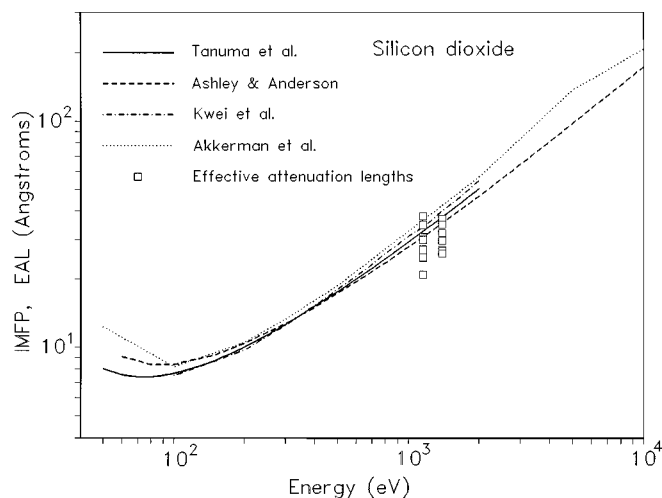


FIG. 13. Comparison of calculated IMFPs for silicon dioxide. Solid line: Tanuma *et al.*;<sup>48</sup> dashed line: Ashley and Anderson;<sup>33(d)</sup> dot-dashed line: Kwei, Chen *et al.*;<sup>51</sup> dotted line: Akkerman *et al.*<sup>54</sup> The open squares show values of the effective attenuation length from Fig. 6.

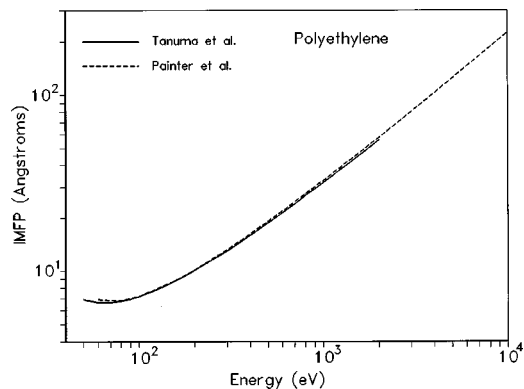


FIG. 16. Comparison of calculated IMFPs for polyethylene. Solid line: Tanuma *et al.*;<sup>50</sup> dashed line: Painter *et al.*<sup>33(c)</sup>

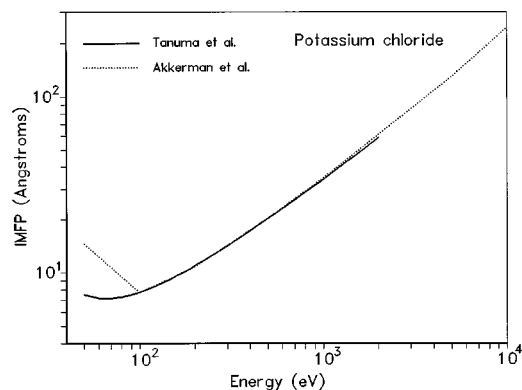


FIG. 14. Comparison of calculated IMFPs for potassium chloride. Solid line: Tanuma *et al.*;<sup>48</sup> dotted line: Akkerman *et al.*<sup>54</sup>

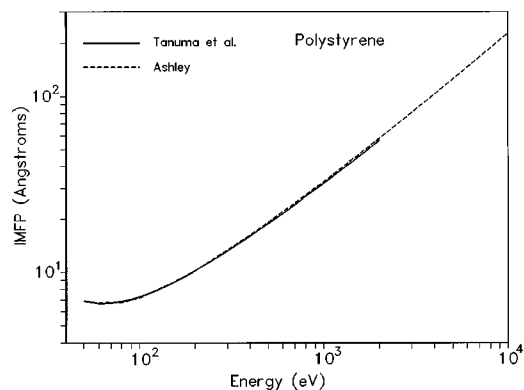


FIG. 17. Comparison of calculated IMFPs for polystyrene. Solid line: Tanuma *et al.*;<sup>50</sup> dashed line: Ashley *et al.*<sup>33(b)</sup>

measurements made it undesirable to consider alternative expressions [e.g., Eqs. (6) or (7)] with a larger number of parameters. We also note that the fitted lines in Fig. 18 are generally consistent with the energy dependence of the IMFPs measured in different laboratories (even though there were differences in the IMFP magnitudes at various energies).

We analyzed the measured IMFPs in the same way as for the calculated IMFPs. For each of the fits shown in Fig. 18, we determined the root-mean-square deviation  $RMS$ , the mean percentage deviation  $R$ , and the percentage deviations  $\Delta_j$  from the fitted function using Eqs. (27)–(29) (where  $r$  is now the number of IMFP measurements  $M$  in Table 8). The fit parameters are listed in Table 11 together with values of  $RMS$  and  $R$ , and the values of  $\Delta_j$  are shown in Fig. 19. The plots of the percentage deviations in Fig. 19 show much greater scatter than the corresponding plots for the calculated IMFPs in Fig. 11. The largest deviations can reach or exceed 50%, e.g., for Al at 50 eV and Si at 100 eV. Even for the elements with the smaller ranges of deviations, most of the deviations occur over rather large ranges, e.g., from  $-20\%$  to  $25\%$  for Si, from  $-20\%$  to  $30\%$  for Cu, and from  $-25\%$  to  $20\%$  for Ge. The values of  $RMS$  and  $R$  in Table 11 are much greater than the corresponding values in Table 10. Four elements (Ni, Cu, Ag, and Au) had values of  $RMS$  less than the average value for the seven elements. Examination of the values of  $R$  in Table 11 showed that four elements (Si, Cu, Ge, and Ag) had essentially identical values of  $R$  (between  $9\%$  and  $11\%$ ); these values were also less than the average value of  $R$  for the seven elements.

We comment now on similarities and differences of the IMFP measurements in Fig. 19 from EPES experiments with elastic scattering accounted for by Monte Carlo simulations and the results of Beilschmidt *et al.*<sup>102</sup> where an analytical theory based on the transport approximation was used for this purpose (as described in Secs. 2.2.2. and 2.2.3.). Inspection of the deviations for the sets of data in Fig. 19 shows that the deviations for the two approaches are not clearly distinguishable for Ni and Au. For Al, however, the deviations for the Beilschmidt *et al.* IMFPs are generally larger (and more positive) than those for Ni and Au. One possible reason for the difference found for Al, proposed by Beilschmidt *et al.*, could be the greater strength of surface excitations (Secs. 2.1.4. and 2.2.4.) in this metal compared to Ni and Au. A more likely explanation in our opinion is that the transport approximation used by Beilschmidt *et al.* may be less reliable for low-atomic-number elements such as Al. For such elements, the elastic-scattering cross sections are smaller than for elements with higher atomic numbers, and the electrons have a smaller chance of becoming randomized. Comparisons of trajectory-length distributions calculated using an analytic formalism based on the transport approximation with those calculated from Monte Carlo simulations showed noticeable deviations for Al while better agreement was found for Cu and Au.<sup>103</sup> In addition, mean electron escape depths calculated for Al from the analytical formalism of the transport approximation showed poorer

agreement with those from Monte Carlo calculations than was the case for Ag and Au.<sup>104</sup>

The average values of  $R$  and  $RMS$  in Table 11 are  $3.00 \text{ \AA}$  and  $13.2\%$ , respectively. These values give an indication of the overall uncertainties in IMFP measurements by EPES. Sources of systematic and random uncertainty were discussed in Sec. 2.2.4. Although it is difficult to quantify the systematic uncertainties from each source, we believe it likely that the sources with the largest contributions to the overall uncertainty are associated with the theoretical model, the effects of surface excitations, possible instrumental effects associated with the recently observed dependence of the derived IMFP on emission angle,<sup>129</sup> variations of surface roughness, and variations of specimen crystallinity. We also note that the average values of  $R$  and  $RMS$  in Table 11 are approximately a factor of three greater than the corresponding values for the calculated IMFPs in Table 10.

### 3.4. Consistency of Calculated and Measured IMFP Values

#### 3.4.1. Evaluation of Calculated and Measured IMFPs for Al, Si, Ni, Cu, Ge, Ag, and Au

We now compare the calculated IMFPs for Al, Si, Ni, Cu, Ge, Ag, and Au with the corresponding measured IMFPs. If the logic used for the comparisons of calculated IMFPs in Sec. 3.2.1. and for the comparisons of measured IMFPs in Sec. 3.3. were followed, a combined fit should be made to calculated and measured IMFPs for each element and then the deviations from the fitted curve should be analyzed. There are, however, several difficulties which render this approach impractical:

- (1) For some elements, there were computational problems with the nonlinear regression [minimization of Eq. (8)] when Eq. (7) with  $n > 1$  is fitted to the calculated and measured IMFPs. This situation is due to the relatively large scatter of the measured IMFPs.
- (2) The calculated IMFPs can be conveniently expressed by functions while the measured IMFPs were reported for fixed electron energies. We could, for example, determine IMFPs from the functions fitted to the calculated elemental IMFPs at the energies selected in the analysis of Sec. 3.2.1., but measured IMFPs would not then be available for most of these energies. Alternatively, we could calculate IMFPs from the functions at the energies at which IMFP measurements were made. These energies, however, would be different for each element. In addition, the results of the combined fits (if they were successful) would depend on the number of measured (and calculated) IMFPs for each element and on the specific electron energies at which the IMFP measurements were made.
- (3) As discussed in Secs. 2.1.4. and 2.2.4., IMFPs measured by EPES could be different from the corresponding calculated IMFPs because the former values are for a surface region while the latter values are for a bulk solid. A common fit to measured and calculated IMFPs would

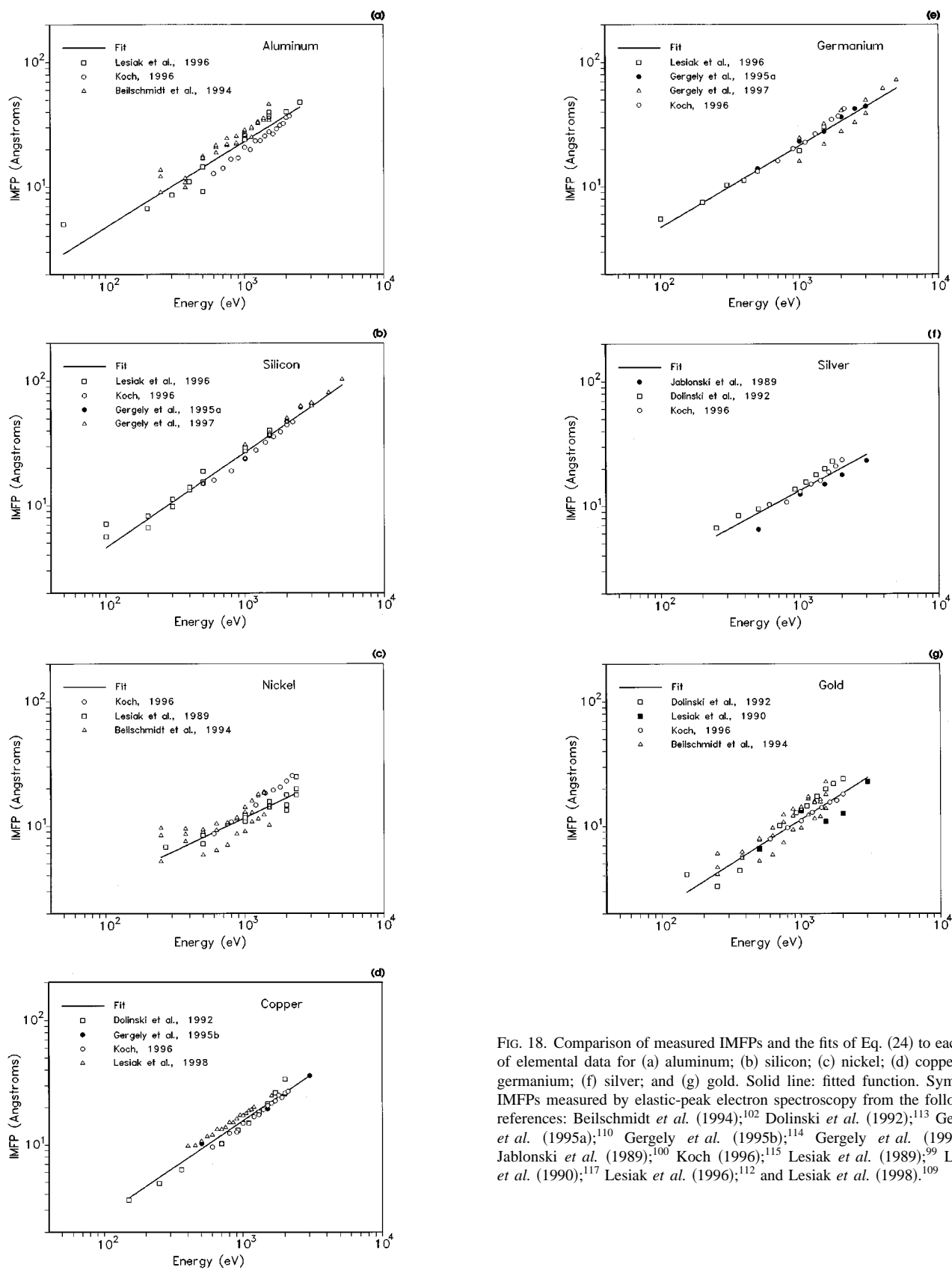


FIG. 18. Comparison of measured IMFPs and the fits of Eq. (24) to each set of elemental data for (a) aluminum; (b) silicon; (c) nickel; (d) copper; (e) germanium; (f) silver; and (g) gold. Solid line: fitted function. Symbols: IMFPs measured by elastic-peak electron spectroscopy from the following references: Beilschmidt *et al.* (1994);<sup>102</sup> Dolinski *et al.* (1992);<sup>113</sup> Gergely *et al.* (1995a);<sup>110</sup> Gergely *et al.* (1995b);<sup>114</sup> Gergely *et al.* (1997);<sup>111</sup> Jablonski *et al.* (1989);<sup>100</sup> Koch (1996);<sup>115</sup> Lesiak *et al.* (1989);<sup>99</sup> Lesiak *et al.* (1990);<sup>117</sup> Lesiak *et al.* (1996);<sup>112</sup> and Lesiak *et al.* (1998).<sup>109</sup>

TABLE 11. Values of the parameters  $k$  and  $p$  found in the fits of Eq. (24) to the measured IMFPs for each element and for electron energies between  $E_{\min}$  and  $E_{\max}$  (as described in Sec. 3.3.). Values of  $RMS$  and  $R$  from Eqs. (27) and (28) are shown for each fit. The last line of the table shows the average values of  $RMS$  and  $R$

Element	$E_{\min}$ (eV)	$E_{\max}$ (eV)	$k$	$p$	$RMS$ (Å)	$R$ (%)
Al	50	2500	0.1927	0.6936	4.41	17.7
Si	100	5000	0.1323	0.7692	3.32	8.96
Ni	250	2350	0.3005	0.5296	2.80	17.9
Cu	150	3000	0.083 77	0.7573	1.78	9.64
Ge	100	5000	0.2252	0.6597	4.19	9.90
Ag	250	3000	0.2049	0.6053	1.94	10.9
Au	150	3000	0.084 62	0.7087	2.57	17.1
Average values:					3.00	13.2

thus be inappropriate; in addition, such a fit would mask any deviations or trends due, for example, to surface excitations.

It was therefore decided to compare the measured IMFPs for each element to the function fitted to the calculated IMFPs for that element [Eq. (7) with  $n=2$  and with the parameter values listed in Table 10]. This approach was considered reasonable because of the generally close agreement found between the calculated IMFPs for each element from each source (Sec. 3.2.1.). The measured IMFPs and the fitted function for each element are plotted in Fig. 20.

We first consider whether there is any evidence for a systematic difference between the measured and calculated IMFPs that could be attributed to the effects of surface excitations and/or to the effects of electron exchange; both of these effects were ignored in the IMFP calculations shown in Fig. 9. Chen<sup>10</sup> has recently shown that IMFPs measured by EPES for Cu and Ag should be lower, because of surface excitations, than the calculated IMFPs for the bulk solids (as discussed in Sec. 2.1.4.); the decrease was found to be about 40% at 250 eV and about 12% at 1500 eV for Ag. Similar work by Ding<sup>67</sup> indicates that the correction for Au at 1000 eV was about 10%. Figure 2 indicates that consideration of electron exchange would increase the calculated IMFPs by about 15% for an electron energy of 50 eV and by smaller amounts for higher energies (Sec. 2.1.3.).

The effects of surface excitations and electron exchange are expected to be noticeable only for IMFPs from EPES measurements made *without* a standard material (Sec. 2.2.4.). We therefore need to examine the IMFP measurements of Dolinski *et al.*<sup>113</sup> and Koch from Table 6.<sup>115</sup> Inspection of Fig. 20 shows that the measured IMFPs of Dolinski *et al.* and Koch are generally close to the function fitted to the calculated IMFPs (the solid lines) or are slightly lower in magnitude. The only exceptions to this observation are for Si and Ge. For Ge, the Koch IMFPs are above the fitted curve in Fig. 20(e) but we believe that this result is probably misleading because of the large differences in the calculated IMFPs of Ashley *et al.*<sup>40</sup> and Tanuma *et al.*<sup>47</sup> in Fig. 9(e). As noted in Sec. 3.2.1., the IMFPs from these sources were cal-

culated with different choices and treatments of optical data. Since the optical data used by Tanuma *et al.* satisfied the sum-rule tests (Sec. 2.1.4.) within about 3%, the IMFPs from these authors are believed to be more reliable. If this is the case, the IMFPs measured by Koch for Ge [identified in Fig. 20(e)] should be compared with the IMFPs calculated by Tanuma *et al.* in Fig. 9(e). This comparison indicates that the Koch IMFPs are then very close to the calculated IMFPs of Tanuma *et al.*

The IMFPs measured by Dolinski *et al.* and Koch for Al, Ni, Cu, Ge, Ag, and Au thus appear to be similar in magnitude or slightly smaller than the calculated IMFPs. This observation could have three explanations. First, there might be a common experimental reason for the measured IMFPs tending to be smaller than the corresponding calculated values. For example, the measured elastic-backscattered intensities for specimen materials with finite surface roughness (after the ion bombardment used for surface cleaning) would be smaller than if the surfaces were atomically smooth (as assumed in the Monte Carlo simulations). As a result, the measured IMFPs would be underestimated (Sec. 2.2.4.). Second, any systematic difference between calculated and measured IMFPs could be due to approximations made in the IMFP calculations (Sec. 2.1.4.). A difference of this type would probably not be apparent in comparisons of IMFPs measured *with* a standard material and the corresponding calculated IMFPs unless the specimen and standard materials had different inelastic-scattering properties [such as those for free-electron-like and nonfree-electron-like solids (Sec. 2.1.2.)]. Finally, the differences could be due to the effects of surface excitations and electron exchange. If these effects predominated, we would expect that the differences would increase with decreasing electron energy. There is no clear evidence for any such increase although we should keep in mind two possible reasons for the expected trend not being observed. One reason is that the expected increase might be masked by an unsuspected energy-dependent error in the elastic-scattering cross sections used in the Monte Carlo simulations (Sec. 2.1.4.). The second reason is that surface excitations would probably be weaker on surfaces roughened by sputtering than for the atomically smooth surfaces considered in the calculations.<sup>63(b)</sup>

Figure 21 shows a plot of the percentage deviations between the IMFPs measured by Dolinski *et al.*<sup>113</sup> and Koch<sup>115</sup> for Al, Si, Ni, Cu, Ag, and Au and the functions fitted to the calculated IMFPs for these elements (the solid lines in Fig. 20). Data for Ge have not been included in Fig. 21 because of the substantial uncertainty in the calculated IMFPs for this element as just discussed in Sec. 3.2.1. Figure 21 indicates that most of the IMFPs measured *without* a standard are systematically smaller than the corresponding calculated values. The average deviation is  $-7.7\%$ . Figure 21 also shows that there is no clear dependence of the deviations on electron energy. Although the deviations for Cu and Au become more negative with decreasing electron energy and the deviations for Ag become positive, these apparent trends are based on a small number of measurements. More experimental tests are

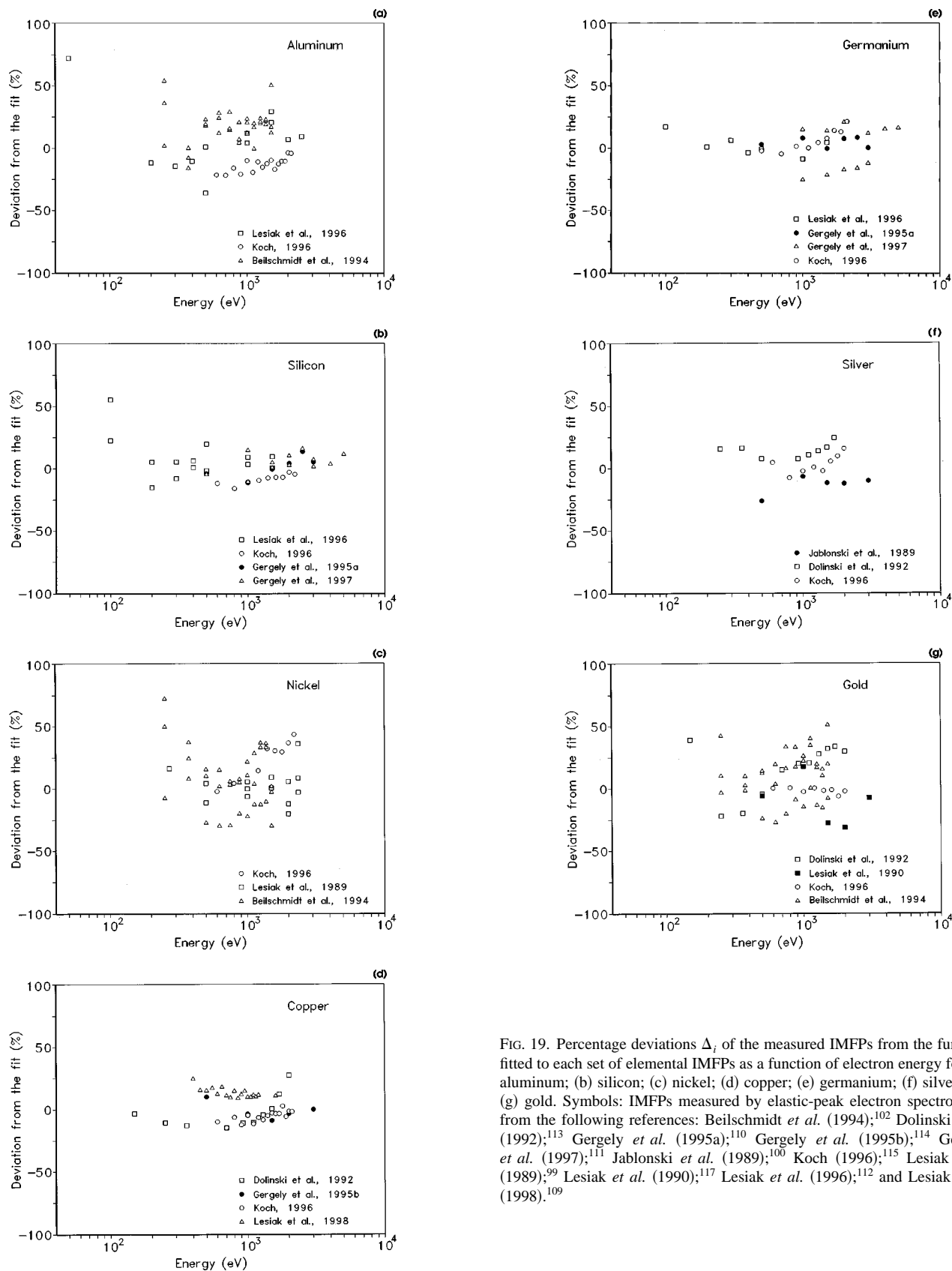


FIG. 19. Percentage deviations  $\Delta_i$  of the measured IMFPs from the function fitted to each set of elemental IMFPs as a function of electron energy for: (a) aluminum; (b) silicon; (c) nickel; (d) copper; (e) germanium; (f) silver; and (g) gold. Symbols: IMFPs measured by elastic-peak electron spectroscopy from the following references: Beilschmidt *et al.* (1994);<sup>102</sup> Dolinski *et al.* (1992);<sup>113</sup> Gergely *et al.* (1995a);<sup>110</sup> Gergely *et al.* (1995b);<sup>114</sup> Gergely *et al.* (1997);<sup>111</sup> Jablonski *et al.* (1989);<sup>100</sup> Koch (1996);<sup>115</sup> Lesiak *et al.* (1989);<sup>99</sup> Lesiak *et al.* (1990);<sup>117</sup> Lesiak *et al.* (1996);<sup>112</sup> and Lesiak *et al.* (1998).<sup>109</sup>

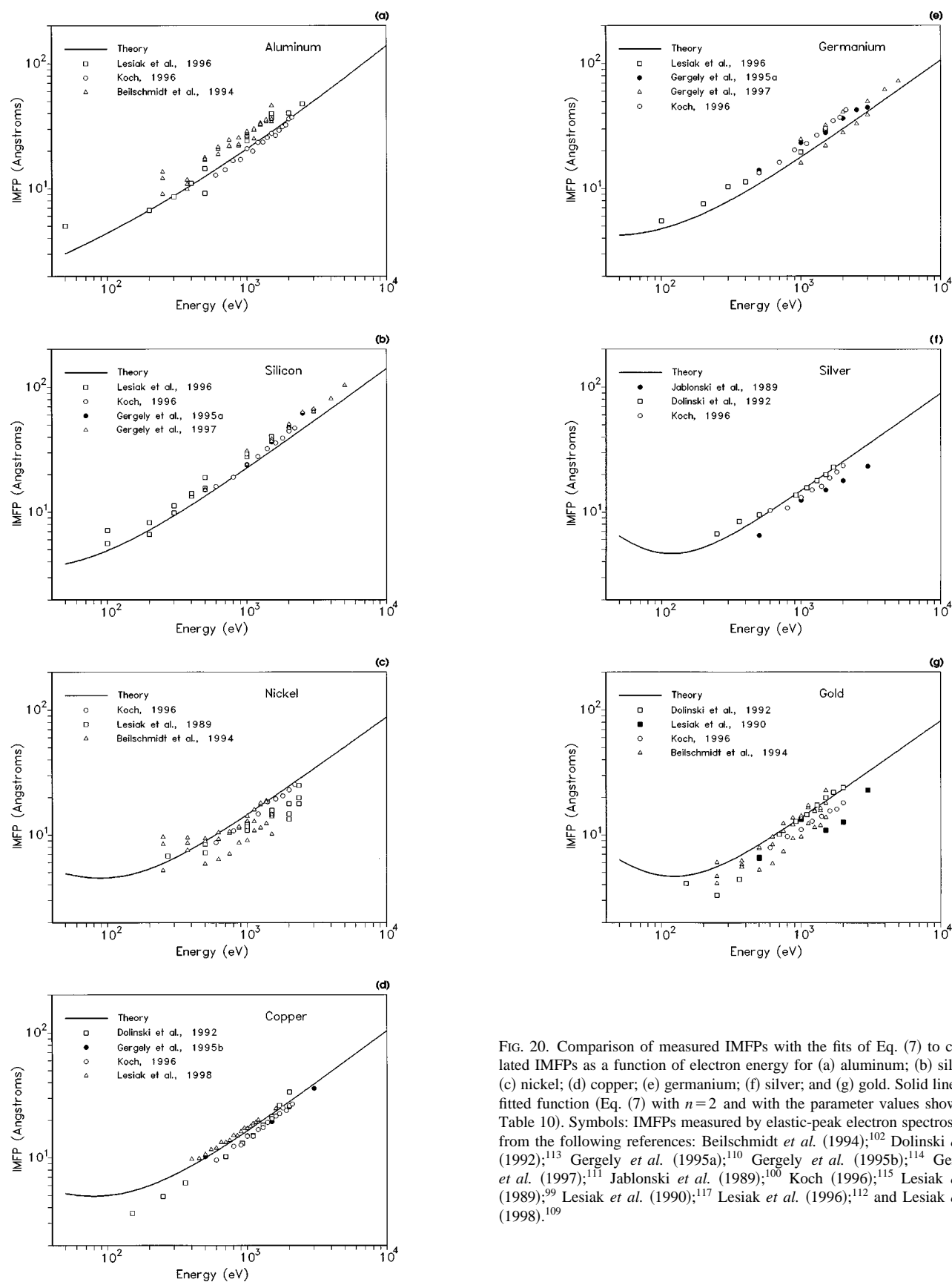


FIG. 20. Comparison of measured IMFPs with the fits of Eq. (7) to calculated IMFPs as a function of electron energy for (a) aluminum; (b) silicon; (c) nickel; (d) copper; (e) germanium; (f) silver; and (g) gold. Solid line: the fitted function (Eq. (7) with  $n=2$  and with the parameter values shown in Table 10). Symbols: IMFPs measured by elastic-peak electron spectroscopy from the following references: Beilschmidt *et al.* (1994);<sup>102</sup> Dolinski *et al.* (1992);<sup>113</sup> Gergely *et al.* (1995a);<sup>110</sup> Gergely *et al.* (1995b);<sup>114</sup> Gergely *et al.* (1997);<sup>111</sup> Jablonski *et al.* (1989);<sup>100</sup> Koch (1996);<sup>115</sup> Lesiak *et al.* (1989);<sup>99</sup> Lesiak *et al.* (1990);<sup>117</sup> Lesiak *et al.* (1996);<sup>112</sup> and Lesiak *et al.* (1998).<sup>109</sup>

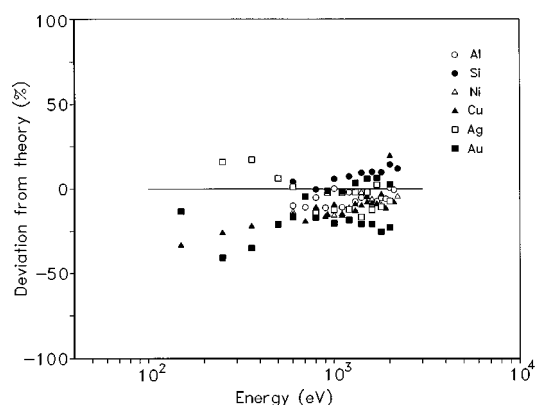


FIG. 21. Percentage deviations of the IMFPs measured by Dolinski *et al.*<sup>113</sup> and Koch<sup>115</sup> from the function fitted to calculated IMFPs (solid lines in Fig. 20) as a function of electron energy for aluminum, silicon, nickel, copper, silver, and gold. The solid line indicates zero deviation.

needed to identify the effects of surface roughness and of surface excitations on calculated IMFPs for bulk solids (e.g., from measurements for a range of angles of incidence and emission in EPES<sup>129</sup>). When the magnitudes of corrections to bulk IMFPs for surface roughness and surface excitations have been determined, it should then be possible to make a more detailed comparison of measured IMFPs (*without* use of a standard) and calculated IMFPs. Such a comparison is needed to determine the magnitude of effects due to electron exchange (expected to be about 15% for an electron energy of 50 eV) and to other approximations made in the IMFP calculations.

We now begin an overall comparison of the measured IMFPs in Fig. 20 with the calculated IMFPs (represented by the solid lines). For Ni, Ag, and Au, most of the measured IMFPs are smaller than the calculated values in Fig. 20; on the other hand, most of the measured IMFPs are larger than the calculated IMFPs for Al, Si, and Ge (although the measured IMFPs for Ge agree well with the preferred IMFPs calculated by Tanuma *et al.*<sup>47</sup> as just discussed). Most of the measured IMFPs shown in Fig. 20 were measured *with* use of a reference material (Table 6), and we note that the IMFPs for the reference materials were generally calculated values for the bulk solids; that is, no correction was made for surface excitations. As discussed in Sec. 2.2.4., the effects of surface excitations are expected to be small if the specimen and reference materials had similar inelastic-scattering properties. Many transition and noble metals have very similar bulk energy-loss functions [given by Eq. (4)],<sup>138</sup> and the surface energy-loss functions for these solids (given by  $\text{Im}[-1/(1 + \epsilon)]$ ) will also be similar. It would therefore not be surprising for the effects of surface excitations to be similar for Ni, Cu, Ag, and Au, and to be different from the corresponding effects for the free-electron-like elements Al, Si, and Ge. The magnitude of the correction to a measured IMFP for surface excitations will depend, however, on the particular specimen and reference materials, the surface roughness of each material, the electron energy, and the incidence and emission angles in the experiment.<sup>18,63</sup> Further

calculations like those of Chen<sup>10</sup> and Ding<sup>67</sup> are needed to determine the magnitudes of the corrections to IMFPs measured by EPES for specific pairs of materials.

The positive deviations found between the measured IMFPs and the solid lines for Al at 50 eV in Fig. 20(a) and for Si at 100 eV in Fig. 20(b) might be due in part to exchange effects and in part to surface excitations. Unfortunately, the large scatter of the deviation plots in Figs. 19(a) and 19(b) and the correspondingly large values of *RMS* and *R* in Table 11 prevent us from making a clear experimental identification of the effects of exchange or surface excitations. Additional measurements, particularly for electron energies between 50 and 200 eV, are needed for Al, Si, and other solids to define the dependence of measured IMFPs on energy more clearly and the extent of deviations from calculated IMFPs for which the effects of exchange and surface excitations have been ignored.

We next examined the extent to which the measured IMFPs in Fig. 20 for each element deviated from the curve fitted to the calculated IMFPs for that element. As in Secs. 3.2.1. and 3.3., we consider the root-mean-square deviation *RMS*, the mean percentage deviation *R*, and the percentage deviation  $\Delta_j$  from the fitted function. Equations (27)–(29) for these quantities need to be modified slightly as follows:

$$RMS = \sqrt{\frac{1}{r} \sum_{j=1}^r (\lambda_j - \lambda_{\text{fit,calc}})^2}, \quad (30)$$

$$R = 100 \frac{1}{r} \sum_{j=1}^r \left| \frac{\lambda_j - \lambda_{\text{fit,calc}}}{\lambda_{\text{fit,calc}}} \right|, \quad (31)$$

$$\Delta_j = 100(\lambda_j - \lambda_{\text{fit,calc}})/\lambda_{\text{fit,calc}}, \quad (32)$$

where *r* is again the number of IMFP measurements *M* in Table 8 and  $\lambda_{\text{fit,calc}}$  is the IMFP (at the energy for each IMFP measurement) found from the fit to the calculated IMFPs. Values of *RMS* and *R* for each element are shown in Table 12 and values of  $\Delta_j$  are plotted in Fig. 22.

The values of *RMS* and *R* for each element in Table 12 are generally greater than the corresponding values in Table 11 (the sole exception is for the value of *R* for Au). Similarly, the average values of *RMS* and *R* in Table 12 are 53% and 29% greater, respectively, than the corresponding values in Table 11. The increases in *RMS* and *R* are expected because the function fitted to the measured IMFPs will be generally different from the function fitted to the calculated IMFPs. The smallest value of *RMS* in Table 12 is found for Cu (1.96 Å); this value is only slightly larger than the *RMS* value for Cu in Table 11 (1.78 Å). The values of *RMS* for Ni, Ag, and Au in Table 12 are less than the average value of *RMS* for the seven elements. The smallest values of *R* in Table 12 are for Cu (10.4%), Ag (12.8%), and Au (16.6%); these values are also less than the average value of *R* for the seven elements.

The values of *R* and *RMS* for Ge in Table 12 are based on deviations of the measured IMFPs from a curve fitted to the IMFPs calculated by Ashley *et al.*<sup>40</sup> and Tanuma *et al.*<sup>47</sup> which were based on different choices and treatments of op-

TABLE 12. Values of the root-mean-square deviations  $RMS$  from Eq. (30) and the mean percentage deviations  $R$  from Eq. (31) of the measured IMFPs for each element from the function fitted to the calculated IMFP values (as described in Sec. 3.4.). The last line of the table shows the average values of  $RMS$  and  $R$

Element	$RMS$ (Å)	$R$ (%)
Al	5.46	22.9
Si	7.75	18.8
Ni	4.14	19.2
Cu	1.96	10.4
Ge	5.79	21.0
Ag	3.59	12.8
Au	3.21	16.6
Average values:	4.56	17.4

tical data, as discussed in Sec. 3.2.1. The measured IMFPs for Ge agree much better with the IMFPs calculated by Tanuma *et al.* [Fig. 9(e)]. If deviations of the measured Ge IMFPs were computed from the IMFP curve of Tanuma *et al.*, the resulting values of  $R$  and  $RMS$  would be much smaller than those shown for Ge in Table 12.

The average values of  $RMS$  and  $R$  in Table 12 are 4.56 Å and 17.4%, respectively, and are about four times larger than the corresponding values in Table 10. It is therefore not possible to identify experimentally the principal sources of uncertainty in the IMFP calculations (Sec. 2.1.4. and Table 10) until the uncertainties in the IMFP measurements (Sec. 2.2.4. and Table 11) can be substantially reduced. Nevertheless, Fig. 20 shows that the precision of IMFP measurement in a particular laboratory is generally sufficient to show that the energy dependence of the measured IMFPs is close to that expected from the IMFP calculations. Figure 20 also indicates that the measured IMFPs (at the level of measurement uncertainty indicated by Table 11) are consistent with the calculated IMFPs. It therefore appears that the uncertainties in the calculated IMFPs (Sec. 2.1.4.) are less than the typical uncertainties of the IMFP measurements (Table 11).

As expected, the deviation plots in Fig. 22 are generally similar to the corresponding plots in Fig. 19. These plots will differ in detail because the function fitted to the measured IMFPs for each element (Fig. 18) is different from the function fitted to the calculated IMFPs (Fig. 20). The scatter of the deviations, however, is similar in the corresponding plots of Figs. 19 and 22. For Cu, Ag, and Au, most of the deviations in Fig. 22 are between  $-34\%$  and  $13\%$ , between  $-33\%$  and  $17\%$ , and between  $-41\%$  and  $21\%$ , respectively.

#### 3.4.2. Evaluation of Calculated and Measured IMFPs for Fe, Mo, W, and Pt

Figures 23–26 show comparisons of calculated and measured IMFPs for Fe, Mo, W, and Pt, respectively. There are two sources of calculated IMFPs for Fe,<sup>47,51</sup> and these agree as closely as the calculated IMFPs from different sources for each element in Fig. 9. We also point out that the IMFPs measured by Koch<sup>115</sup> for Fe *without* a standard material in Fig. 23 are smaller than the calculated IMFPs of Tanuma

*et al.*<sup>47</sup> and Kwei *et al.*;<sup>51</sup> the average deviation of  $-17\%$  (with respect to the Tanuma *et al.* IMFPs) is consistent with the deviations shown in Fig. 21.

The measured IMFPs for Fe and Mo in Figs. 23 and 24 agree reasonably well with the calculated IMFPs. Although the measured IMFPs for W and Pt in Figs. 25 and 26 are generally smaller than the calculated values, the differences are similar to those found for Ni and Au in Fig. 20. The scatter of the measured IMFPs in Figs. 23–26 is also comparable to the scatter of the measured IMFPs in Figs. 9 and 20. The energy dependence of the measured IMFPs for Fe, Mo, and W from each source is similar to that of the calculated IMFPs.

### 3.5. Recommended Elemental IMFP Values

It is necessary to consider appropriate criteria for evaluation of calculated and measured IMFPs in order to recommend IMFP values for the elements considered in the previous subsections. We list the criteria we have used in Table 13 and will proceed to discuss each criterion in turn. We also identify the particular solid elements in Table 13 that ranked highest on each criterion using information from the source shown in the final column. We then select the elements and the recommended IMFP values based on our criteria.

(a) *Quantity of IMFP data.* It is clearly desirable to have a sufficient number of independent IMFP calculations and measurements to give confidence in the results (e.g., that there were no unsuspected mistakes or systematic uncertainties) and to indicate clearly the dependence of the IMFP on electron energy. Table 8 shows that there were five independent sources of IMFP measurements for two elements (Cu and Ag), four sources of IMFP measurements for three elements (Si, Ge, and Au), and three sources of IMFP measurements for two elements (Al and Ni). Somewhat arbitrarily, we have chosen to identify the two elements (Cu and Ag) in Table 13(a) which had the largest number of sources of IMFP measurements.

Table 8 also shows the three elements (Al, Ni, and Au) which had the largest number of IMFP measurements; the number of measurements was slightly smaller for three elements (Al, Ni, and Pt). We have highlighted the first three elements in Table 13(a) with the + symbol.

Table 9 shows the sources of calculated IMFPs for those elements for which there were at least two sources of IMFP measurements (Table 8). There were two elements which had four independent sources of IMFP calculations (Cu and Au), and these have been identified with the + symbol in Table 13(a). There were three elements (Al, Ni, and Ag) which had three sources of calculated IMFPs.

(b) *Comparison of calculated IMFPs (Sec. 3.2.1.).* Figure 10 shows that four elements (Si, Ni, Ag, and Au) had the smallest ranges of deviations of the calculated IMFPs from the mean values of the calculated IMFPs. The deviations were between  $-7\%$  and  $8.4\%$  for these four elements which are indicated by the + symbol in Table 13(b).

Four elements (Al, Ni, Cu, and Ag) had values of  $RMS$

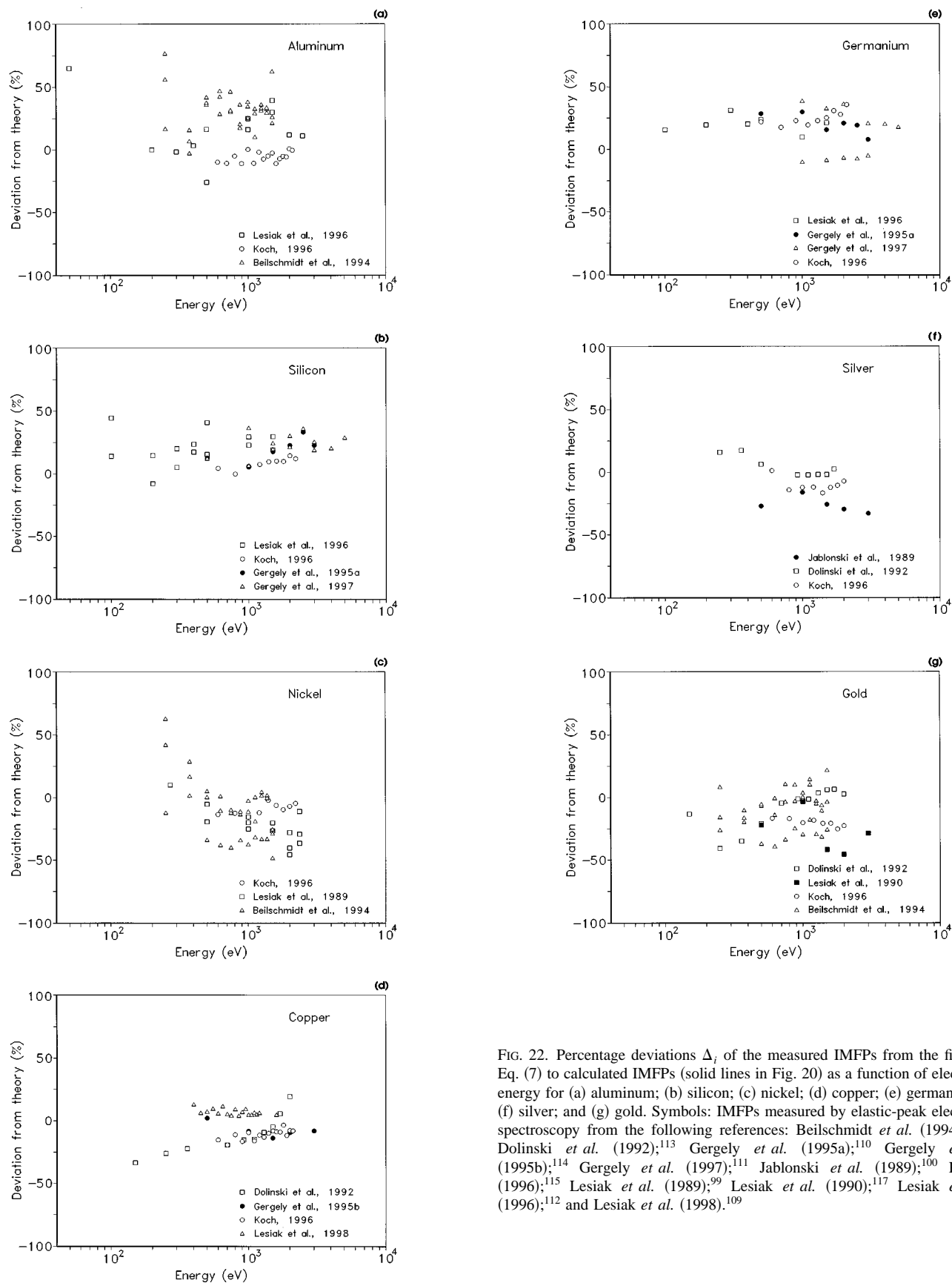


FIG. 22. Percentage deviations  $\Delta_i$  of the measured IMFPs from the fits to Eq. (7) to calculated IMFPs (solid lines in Fig. 20) as a function of electron energy for (a) aluminum; (b) silicon; (c) nickel; (d) copper; (e) germanium; (f) silver; and (g) gold. Symbols: IMFPs measured by elastic-peak electron spectroscopy from the following references: Beilschmidt *et al.* (1994);<sup>102</sup> Dolinski *et al.* (1992);<sup>113</sup> Gergely *et al.* (1995a);<sup>110</sup> Gergely *et al.* (1995b);<sup>114</sup> Gergely *et al.* (1997);<sup>111</sup> Jablonski *et al.* (1989);<sup>100</sup> Koch (1996);<sup>115</sup> Lesiak *et al.* (1989);<sup>99</sup> Lesiak *et al.* (1990);<sup>117</sup> Lesiak *et al.* (1996);<sup>112</sup> and Lesiak *et al.* (1998).<sup>109</sup>

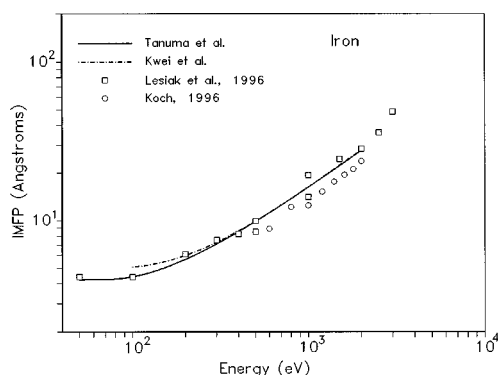


FIG. 23. Comparison of calculated IMFPs (lines) and measured IMFPs (symbols) for iron. Solid line: Tanuma *et al.*<sup>47</sup> Dot-dashed line: Kwei, Chen *et al.*<sup>51</sup> Symbols: IMFPs measured by elastic-peak electron spectroscopy from the following references: Koch (1996);<sup>115</sup> and Lesiak *et al.* (1996).<sup>112</sup>

from Eq. (27) for the root-mean-square deviation of the calculated IMFPs from the function fitted to all of the calculated IMFPs for each element of less than 1 Å; as indicated in Table 10, these values of *RMS* were also less than the average value of *RMS* for the seven elements. The four elements have been selected for emphasis in Table 13(b).

Table 10 shows five elements (Al, Ni, Cu, Ag, and Au) that had values of *R* from Eq. (28) for the mean percentage deviation of the calculated IMFPs from the function fitted to all of the calculated IMFPs for each element which were less than the average value for the seven elements. These five elements are indicated in Table 13(b).

From Table 10, the average values of *RMS* and *R* are 0.89 Å and 4.4%, respectively. These values indicate the current degree of consistency found in the calculated IMFPs by different groups for each of the seven elements.

Two elements (Ni and Ag) were highlighted with the + symbol on each of the three criteria listed in Table 13(b), and three elements (Al, Cu, and Au) were highlighted on two of the criteria. The calculated IMFPs from different sources for these five elements thus show a high degree of consistency. We recommend that calculated IMFPs for these elements be

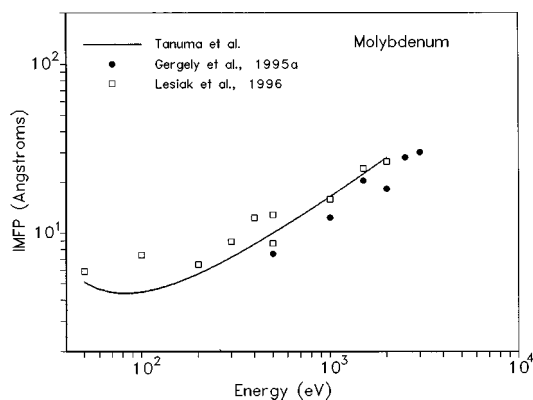


FIG. 24. Comparison of calculated IMFPs (line) and measured IMFPs (symbols) for molybdenum. Solid line: Tanuma *et al.*<sup>47</sup> Symbols: IMFPs measured by elastic-peak electron spectroscopy from the following references: Gergely *et al.* (1995a);<sup>110</sup> and Lesiak *et al.* (1996).<sup>112</sup>

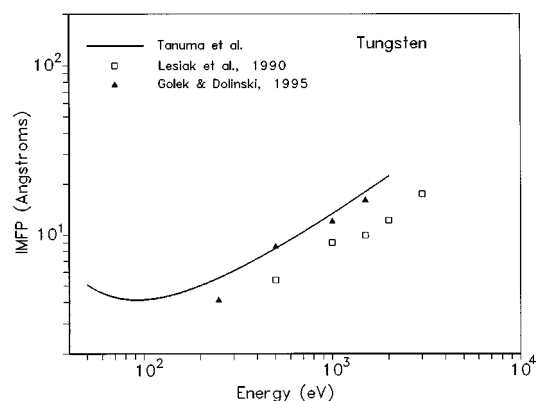


FIG. 25. Comparison of calculated IMFPs (line) and measured IMFPs (symbols) for tungsten. Solid line: Tanuma *et al.*<sup>47</sup> Symbols: IMFPs measured by elastic-peak electron spectroscopy from the following references: Golek and Dolinski (1995);<sup>118</sup> and Lesiak *et al.* (1990).<sup>117</sup>

obtained from the individual sources identified in Table 9 or by use of Eq. (7) with the parameters listed in Table 10. These recommended IMFPs can be calculated for electron energies between 50 and 10<sup>4</sup> eV. We note here that the average of the sum-rule errors (Sec. 2.1.2.) of the energy-loss functions for Al, Ni, Cu, Ag, and Au computed from the optical data used by Tanuma *et al.*<sup>30,47</sup> were 12%, 3%, 1%, 5%, and 7%, respectively; these average errors are smaller than the corresponding values of *R* for the mean percentage deviations of the measured IMFPs from the function fitted to all of the measured IMFPs for each element in Table 11.

(c) *Comparison of measured IMFPs (Sec. 3.3.)* Table 11 shows that four elements (Ni, Cu, Ag, and Au) had values of *RMS* from Eq. (27) for the root-mean-square deviation of the measured IMFPs from the function fitted to all of the measured IMFPs for each element that were less than the average value of *RMS* for the seven elements. These four elements have been indicated with the + symbol in Table 13(c).

There are four elements (Si, Cu, Ge, and Ag) in Table 11 that have values of *R* from Eq. (28) (for the mean percentage deviation of the measured IMFPs from the function fitted to all of the measured IMFPs for each element) less than the

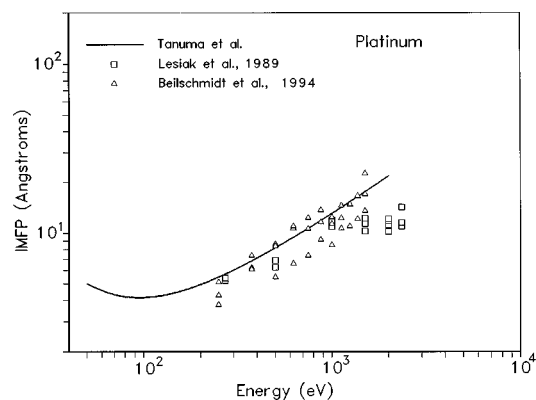


FIG. 26. Comparison of calculated IMFPs (line) and measured IMFPs (symbols) for platinum. Solid line: Tanuma *et al.*<sup>47</sup> Symbols: IMFPs measured by elastic-peak electron spectroscopy from the following references: Beilschmidt *et al.* (1994);<sup>102</sup> and Lesiak *et al.* (1989).<sup>99</sup>

TABLE 13. Summary of criteria for evaluating calculated and measured IMFPs. The elements which ranked highest on each criterion are identified with the + symbol using information from the source indicated in the final column

Criterion	Al	Si	Ni	Cu	Ge	Ag	Au	Source
<i>(a) Quantity of IMFP Data</i>								
Largest number of sources of measured IMFPs				+		+		Table 8
Largest number of measured IMFPs	+		+				+	Table 8
Largest number of calculated IMFPs				+			+	Table 9
<i>(b) Comparison of Calculated IMFPs</i>								
Smallest deviations of the calculated IMFPs from the mean values		+	+			+	+	Fig. 10
Smallest RMS deviations of the calculated IMFPs from the function fitted to the calculated IMFPs	+		+	+		+		Table 10
Smallest mean percentage deviations of the calculated IMFPs from the function fitted to the calculated IMFPs	+		+	+		+	+	Table 10 Fig. 11
<i>(c) Comparison of Measured IMFPs</i>								
Smallest RMS deviations of the measured IMFPs from the function fitted to the measured IMFPs			+	+		+	+	Table 11
Smallest mean percentage deviations of the measured IMFPs from the function fitted to the measured IMFPs		+		+	+	+		Table 11 Fig. 19
<i>(d) Comparison of Measured and Calculated IMFPs</i>								
Smallest RMS deviations of the measured IMFPs from the function fitted to the calculated IMFPs			+	+		+	+	Table 12
Smallest mean percentage deviations of the measured IMFPs from the function fitted to the calculated IMFPs				+		+	+	Table 12 Fig. 22
Totals	3	2	6	8	1	8	7	

average value of  $R$  for the seven elements. These elements have been identified with the + symbol in Table 13(c).

The average values of  $RMS$  and  $R$  in Table 11 are 3.00 Å and 13.2%, respectively. These values illustrate the current degree of consistency found in IMFP measurements for the seven elements in different laboratories. The values of  $RMS$  and  $R$  are substantially larger than the corresponding values for the calculated IMFPs in Table 10.

Two elements (Cu and Ag) were identified on both criteria listed in Table 13(c), and four elements (Si, Ni, Ge, and Au) were identified on a single criterion. Copper and silver thus show the greatest consistency in IMFP measurements by different groups. We recommend that Eq. (24) be used to represent the IMFP measurements for these two metals with the parameters given in Table 11 for the indicated electron energy ranges. If needed, Eq. (24) could be similarly used to represent the measured IMFPs for Si, Ni, Ge, and Au although the consistency of the measured IMFPs for these elements is less than that for Cu and Ag.

*(d) Comparison of measured and calculated IMFPs (Sec. 3.4.1.).* Table 12 shows that four elements (Ni, Cu, Ag, and Au) had values of  $RMS$  from Eq. (30) for the root-mean-square deviation of the measured IMFPs from the function fitted to the calculated IMFPs (Table 9) for each element which were less than the average value of  $RMS$  for the seven

elements. These elements are indicated with a + symbol in Table 13(d).

Three elements (Cu, Ag, and Au) in Table 12 have values of  $R$  from Eq. (31) (for the mean percentage deviation of the measured IMFPs from the function fitted to the calculated IMFPs for each element) less than the average value of  $R$  for the seven elements. These elements are identified in Table 13(d).

The average values of  $RMS$  and  $R$  in Table 12 are 4.56 Å and 17.4%, respectively. These values illustrate the current degree of consistency in measured and calculated IMFPs for the seven elements.

Three elements (Cu, Ag, and Au) were highlighted on both criteria in Table 13(d). These three elements thus show the greatest consistency in comparison of IMFP measurements and calculations.

Figures 27 and 28 show values of  $RMS$  and  $R$ , respectively, for each element from Tables 10, 11, and 12. The solid symbols indicate elements that have values of  $RMS$  and  $R$  less than the corresponding average values of  $RMS$  and  $R$  in Tables 10, 11, and 12. As expected from the previous discussion, Ni, Cu, Ag, and Au have the largest number of solid symbols in Figs. 27 and 28. It is also clear that copper shows the best overall consistency in the comparisons of

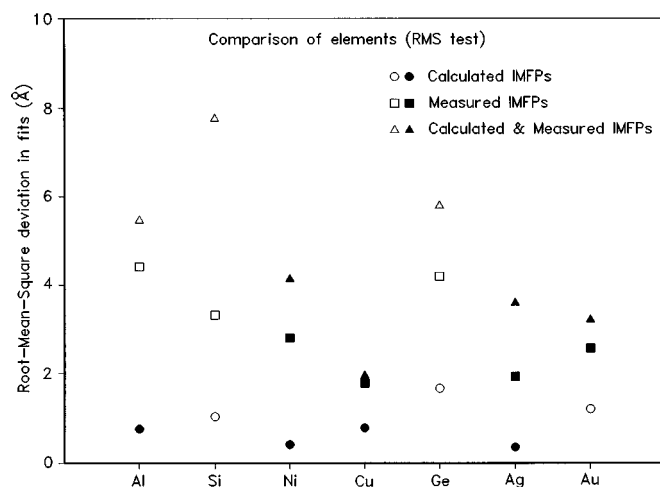


FIG. 27. Values of  $RMS$  for Al, Si, Ni, Cu, Ge, Ag, and Au from Tables 10, 11, and 12. The solid symbols denote elements for which the  $RMS$  values were less than half of the corresponding average values of  $RMS$  shown in Tables 10, 11, and 12. The open symbols indicate the other elements.

calculated IMFPs, of measured IMFPs, and of calculated and measured IMFPs.

For simplicity, we have assumed unit weight to the criteria in Table 13 and give the totals of the + entries for each element on the last line. We see a clear separation of the seven elements into two groups. One contains four elements (Ni, Cu, Ag, and Au) which have scores between 6 and 8 while the other group contains three elements (Al, Si, and Ge) which have scores between 1 and 3. We therefore give an overall recommendation for Ni, Cu, Ag, and Au as the elements that have adequate data [Table 13(a)], that show a high degree of consistency in their calculated IMFPs [Table 13(b)], that show adequate or high consistency in their measured IMFPs [Table 13(c)], and that show adequate or high consistency between their measured and calculated IMFPs [Table 13(d)]. On the basis of these results, we recommend these four elements as reference materials for the measurement of IMFPs by elastic-peak electron spectroscopy. For this and other purposes, IMFPs can be computed from Eq. (7) with  $n=2$  and the parameters in Table 10 for electron energies between 50 and  $10^4$  eV; we recommend this approach because the consistency of the calculated IMFPs (Table 10) is much better than the consistency of the measured IMFPs (Table 11).

Two of the remaining three elements (Al and Si) show reasonable consistency in their calculated IMFPs (Table 10), but the agreement between their measured IMFPs (Table 11) and between their measured and calculated IMFPs (Table 12) is generally inferior to that found for Ni, Cu, Ag, and Au. We therefore recommend that IMFPs for Al and Si be calculated from Eq. (7) with  $n=2$  and the parameters in Table 10 for electron energies between 50 and  $10^4$  eV.

In Secs. 3.2.1. and 3.4.1., we discussed the differences between two sets of calculated IMFPs for Ge and concluded that the IMFPs of Tanuma *et al.*<sup>47</sup> (which are consistent with the measured IMFPs for Ge) are to be preferred. We there-

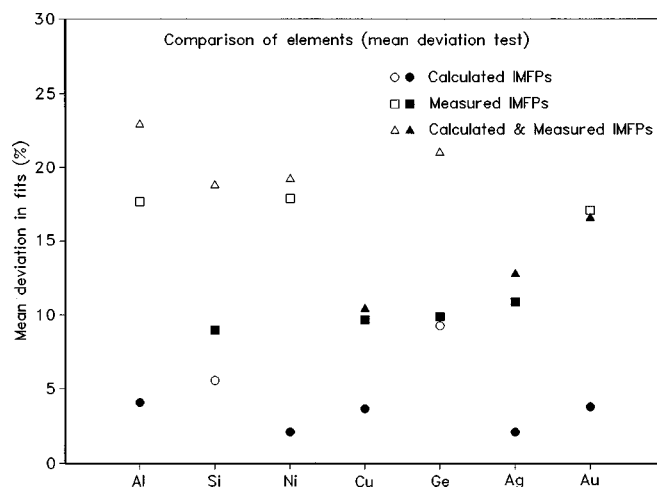


FIG. 28. Values of  $R$  for Al, Si, Ni, Cu, Ge, Ag, and Au from Tables 10, 11, and 12. The solid symbols denote elements for which the  $R$  values were less than half of the corresponding average values of  $R$  shown in Tables 10, 11, and 12. The open symbols indicate the other elements.

fore recommend that IMFPs for Ge be calculated from Eq. (6) using the following parameter values for Ge:<sup>47</sup>  $E_p = 15.6$  eV,  $\beta = 0.0484$  eV<sup>-1</sup> Å<sup>-1</sup>,  $\gamma = 0.0540$  eV<sup>-1</sup>,  $C = 0.175$  Å<sup>-1</sup>, and  $D = 17.8$  eV Å<sup>-1</sup>.

## 4. Conclusions

We have presented an evaluation of calculated and measured electron IMFPs near solid surfaces for electron energies between 50 and  $10^4$  eV. Information has been given on the methods used for calculating and measuring IMFPs, and on the various sources of uncertainty in the calculated and measured IMFPs. Most attention has been given to IMFPs calculated from experimental optical data and to IMFPs measured by EPES because these approaches currently seem to be the most reliable.

We have analyzed the degree of consistency of calculated and measured IMFPs for seven elemental solids: Al, Si, Ni, Cu, Ge, Ag, and Au. Specifically, we examined the degree of consistency of IMFPs calculated for each of these elements by different groups, the degree of consistency of IMFPs measured for each of the elements by different laboratories, and of the degree of consistency of measured and calculated IMFPs for each element. We also compared calculated and measured IMFPs for four additional elemental solids (Fe, Mo, W, and Pt) and calculated IMFPs for six compounds [Al<sub>2</sub>O<sub>3</sub>, SiO<sub>2</sub>, KCl, poly(butene-1-sulfone), polyethylene, and polystyrene)]. Our principal conclusions are as follows.

(1) The calculated IMFPs for Al, Ni, Cu, Ag, and Au from different groups showed a high degree of consistency [Tables 10 and 13(b)]. For the group of seven elements, the average value of the root-mean-square deviations of the calculated IMFPs from the function fitted to all of the calculated IMFPs for each element was  $0.89$  Å, and the average mean percentage deviation was 4.4%.

(2) The measured IMFPs for Cu and Ag from different laboratories showed reasonable consistency [Tables 11 and 13(c)]. For the group of seven elements, the average value of the root-mean-square deviations of the measured IMFPs from the function fitted to all of the measured IMFPs for each element was 3.00 Å, and the average mean percentage deviation was 13.2%.

(3) The measured IMFPs for Ni, Cu, Ag, and Au showed good consistency with the corresponding calculated IMFPs [Tables 12 and 13(d)]. For the group of seven elements, the average value of the root-mean-square deviations of the measured IMFPs from the function fitted to all of the calculated IMFPs for each element was 4.56 Å, and the average mean percentage deviation was 17.4%.

(4) The same four elements (Ni, Cu, Ag, and Au) showed the greatest overall consistency in their calculated IMFPs, in their measured IMFPs, and between their measured and calculated IMFPs (Table 13). IMFPs for these materials, determined for electron energies between 50 and 10<sup>4</sup> eV from Eq. (7) with  $n=2$  and the parameters in Table 10, can be used as reference IMFP data. Nickel, copper, silver, and gold are also recommended as reference materials in future IMFP measurements by EPES. We give recommendations in Sec. 3.5. for determining IMFPs for Al, Si, and Ge.

(5) It was not possible to identify experimentally the main sources of uncertainty in most of the IMFP calculations (the neglect of effects due to surface excitations and electron exchange that were discussed in Sec. 2.1.4.) because of the relatively large scatter in the measured IMFPs from different laboratories. It is hoped that the uncertainties in IMFP measurements (Sec. 2.2.4.) can be reduced in the future so that more detailed comparisons can be made of IMFP calculations and measurements (Sec. 3.4.1.). The effect of varying surface roughness on IMFPs measured by EPES needs to be determined.

(6) The measured IMFPs for Fe and Mo were consistent with the corresponding calculated IMFPs (Sec. 3.4.2.). There was poorer agreement in the measured and calculated IMFPs for W and Pt, but the differences here were similar to those found in the comparison of measured and calculated IMFPs for the seven elements (Sec. 3.4.1.).

(7) The calculated IMFPs for the six compounds shown in Figs. 12–17 [Al<sub>2</sub>O<sub>3</sub>, SiO<sub>2</sub>, KCl, poly(butene-1-sulfone), polyethylene, and polystyrene] showed a similar level of consistency as that found with the calculated IMFPs for the seven elements in Fig. 9.

(8) Although EPES is a new technique and there is a limited number of IMFP measurements that have been made using it (Tables 4 and 5), it has been shown to be superior to the widely used overlayer-film method (Secs. 2.2.1., 3.3., and 3.4.). It should be emphasized that, except for a very recent experiment,<sup>139</sup> an effective attenuation length is measured with the overlayer-film method rather than an IMFP. In addition, the effective attenuation length is not a well-defined material parameter but depends on the measurement conditions (Sec. 2.2.1.).

(9) IMFP measurements by EPES are expected to be most

reliable if the measurements are performed with normal incidence of the electron beam, with incident electron energies of at least 200 eV, and with emission angles between 25° and 45° (Sec. 2.2.4.).

## 5. Acknowledgments

The authors wish to thank Drs. T. Boutboul, Y. F. Chen, Z.-J. Ding, K.-H. Gaukler, G. Gergely, S. Mroz and W. S. M. Werner for providing numerical IMFP values and useful information and Drs. J. C. Ashley and D. R. Penn for helpful discussions. They are grateful to Drs. Y. F. Chen, Z.-J. Ding, G. Gergely, S. Mroz, S. W. Robey, D. R. Penn, W. S. M. Werner, and R. A. Velapoldi for their constructive comments on a previous draft of this paper. One of the authors (A.J.) wishes to acknowledge partial support by European Union Contract No. ERBIC15CT960800 and the other author (C.J.P.) wishes to acknowledge partial support by the NIST Standard Reference Data Program.

## 6. References

- D. P. Woodruff and T. A. Delchar, *Modern Techniques of Surface Science*, 2nd ed. (Cambridge University Press, Cambridge, 1994).
- C. J. Powell, A. Jablonski, I. Tilinin, S. Tanuma, and D. R. Penn, *J. Electron Spectrosc. Relat. Phenom.* (in press).
- C. J. Powell, in *Quantitative Surface Analysis of Materials*, edited by N. S. McIntyre, ASTM Special Technical Publication 643 (American Society for Testing and Materials, Philadelphia, PA, 1978), p. 5.
- C. J. Powell and M. P. Seah, *J. Vac. Sci. Technol. A* **8**, 735 (1990).
- M. P. Seah, in *Practical Surface Analysis*, 2nd ed., edited by D. Briggs and M. P. Seah, Auger and X-Ray Photoelectron Spectroscopy, Vol. I (Wiley, New York, 1990), p. 201.
- A. Jablonski and C. J. Powell, *Surf. Interface Anal.* **20**, 771 (1993).
- For example: A. Jablonski, I. S. Tilinin, and C. J. Powell, *Phys. Rev. B* **54**, 10927 (1996); A. Jablonski and C. J. Powell, *J. Vac. Sci. Technol. A* **15**, 2095 (1997); I. S. Tilinin, A. Jablonski, and W. S. M. Werner, *Prog. Surf. Sci.* **52**, 193 (1996); W. S. M. Werner, *Phys. Rev. B* **52**, 2964 (1995); R. Shimizu and Z.-J. Ding, *Rep. Prog. Phys.* **55**, 487 (1992); S. Tougaard, *J. Vac. Sci. Technol. A* **14**, 1415 (1996); I. S. Tilinin, A. Jablonski, and S. Tougaard, *Surf. Interface Anal.* **25**, 119 (1997); S. Tougaard and A. Jablonski, *ibid.* **25**, 404 (1997); J. Ferron and E. C. Goldberg, *Surf. Sci.* **275**, 114 (1992); Y. F. Chen, *ibid.* **345**, 213 (1996); Y. F. Chen and Y. T. Chen, *Phys. Rev. B* **53**, 4980 (1996); Y. F. Chen and C. M. Kwei, *Surf. Sci.* **364**, 131 (1996).
- Annual Book of ASTM Standards* (American Society for Testing and Materials, West Conshohocken, PA, 1997), Standard E 673, Vol. 3.06.
- F. Yubero and S. Tougaard, *Phys. Rev. B* **46**, 2486 (1992); F. Yubero, J. M. Sanz, B. Ramskov, and S. Tougaard, *ibid.* **53**, 9719 (1996); F. Yubero, D. Fujita, B. Ramskov, and S. Tougaard, *ibid.* **53**, 9728 (1996).
- Y. F. Chen, *J. Vac. Sci. Technol. A* **13**, 2665 (1995).
- J. Hubbard, *Proc. Phys. Soc. London, Sect. A* **68**, 441 (1955).
- H. Frohlich and H. Pelzer, *Proc. Phys. Soc. London, Sect. A* **68**, 525 (1955).
- D. Pines, *Elementary Excitations in Solids* (Benjamin, New York, 1963).
- K. D. Sevier, *Low Energy Electron Spectrometry* (Wiley-Interscience, New York, 1972).
- S. E. Schnatterly, in *Solid State Physics*, edited by F. Seitz and D. Turnbull (Academic, New York, 1979), Vol. 34, p. 275.
- H. Raether, *Springer Tracts Mod. Phys.* **88**, 1 (1980).
- C. J. Powell, *Surf. Sci.* **299/300**, 34 (1994).
- R. H. Ritchie, *Phys. Rev.* **106**, 874 (1957).
- S. Tanuma, C. J. Powell, and D. R. Penn, *Surf. Interface Anal.* **25**, 25 (1997).
- J. J. Quinn, *Phys. Rev.* **126**, 1453 (1962).
- B. I. Lundqvist, *Phys. Status Solidi* **32**, 273 (1969).

- <sup>22</sup>R. H. Ritchie, F. W. Garber, M. Y. Nakai, and R. D. Birkhoff, in *Advances in Radiation Biology*, edited by L. G. Augenstein, R. Mason, and M. Zelle (Academic, New York, 1969), Vol. 3, p. 1.
- <sup>23</sup>L. Kleinman, *Phys. Rev. B* **3**, 2982 (1971).
- <sup>24</sup>J. C. Shelton, *Surf. Sci.* **44**, 305 (1974).
- <sup>25</sup>D. R. Penn, *Phys. Rev. B* **13**, 5248 (1976); *J. Electron Spectrosc. Relat. Phenom.* **9**, 29 (1976).
- <sup>26</sup>C. J. Powell, *Surf. Sci.* **44**, 29 (1974).
- <sup>27</sup>S. Tanuma, C. J. Powell, and D. R. Penn, *J. Electron Spectrosc. Relat. Phenom.* **62**, 95 (1993).
- <sup>28</sup>H. Bethe, *Ann. Physik* **5**, 325 (1930).
- <sup>29</sup>E. Shiles, T. Sasaki, M. Inokuti, and D. Y. Smith, *Phys. Rev. B* **22**, 1612 (1980).
- <sup>30</sup>S. Tanuma, C. J. Powell, and D. R. Penn, *Surf. Interface Anal.* **11**, 577 (1988).
- <sup>31</sup>J. C. Ashley, C. J. Tung, and R. H. Ritchie, *Surf. Sci.* **81**, 409 (1979).
- <sup>32</sup>C. J. Tung, J. C. Ashley, and R. H. Ritchie, *Surf. Sci.* **81**, 427 (1979).
- <sup>33</sup>(a) C. J. Tung, J. C. Ashley, R. D. Birkhoff, R. H. Ritchie, L. C. Emerson, and V. E. Anderson, *Phys. Rev. B* **16**, 3049 (1977); (b) J. C. Ashley, C. J. Tung, and R. H. Ritchie, *IEEE Trans. Nucl. Science NS-25*, 1566 (1978); (c) L. R. Painter, E. T. Arakawa, M. W. Williams, and J. C. Ashley, *Radiat. Res.* **83**, 1 (1980); (d) J. C. Ashley and V. E. Anderson, *J. Electron Spectrosc. Relat. Phenom.* **24**, 127 (1981); (e) J. C. Ashley, *ibid.* **28**, 177 (1982); (f) *J. Appl. Phys.* **63**, 4620 (1988).
- <sup>34</sup>J. C. Ashley, *J. Electron Spectrosc. Relat. Phenom.* **46**, 199 (1988).
- <sup>35</sup>J. C. Ashley, *J. Electron Spectrosc. Relat. Phenom.* **50**, 323 (1990); J. C. Ashley (private communication).
- <sup>36</sup>J. Lindhard, *Kgl. Danske Videnskab. Selskab., Mat.-Fys. Medd.* **28**, No. 8 (1954).
- <sup>37</sup>J. Lindhard and M. Scharff, *Kgl. Danske Videnskab. Selskab., Mat.-Fys. Medd.* **27**, No. 15 (1953); J. Lindhard, M. Scharff, and H. E. Schiott, *ibid.* **33**, No. 14 (1963).
- <sup>38</sup>J. C. Ashley, C. J. Tung, R. H. Ritchie, and V. E. Anderson, *IEEE Trans. Nucl. Sci.* **NS-23**, 1833 (1976).
- <sup>39</sup>C. J. Tung, J. C. Ashley, V. E. Anderson, and R. H. Ritchie, Inverse Mean Free Path, Stopping Power, CSDA Range, and Straggling in Silicon and Silicon Dioxide for Electrons of Energy  $\leq 10$  keV, US Air Force Report RADC-TR-76-125 (April, 1976). Available from National Technical Information Service, US Department of Commerce, Springfield, VA 22161 as Report AD-A025 488.
- <sup>40</sup>J. C. Ashley, C. J. Tung, R. H. Ritchie, and V. E. Anderson, Inverse Mean Free Path, Stopping Power, CSDA Range, and Straggling in Ge and GaAs for Electrons of Energy  $\leq 10$  keV, US Air Force Report RADC-TR-76-350 (November, 1976). Available from National Technical Information Service, US Department of Commerce, Springfield, VA 22161 as Report AD-A035 511.
- <sup>41</sup>A. Howie and R. M. Stern, *Z. Naturforsch.* **27a**, 382 (1972).
- <sup>42</sup>J. Szajman and R. C. G. Leckey, *J. Electron Spectrosc. Relat. Phenom.* **23**, 83 (1981).
- <sup>43</sup>C. J. Powell, *Surf. Interface Anal.* **7**, 263 (1985).
- <sup>44</sup>D. R. Penn, *Phys. Rev. B* **35**, 482 (1987).
- <sup>45</sup>N. Swanson and C. J. Powell, *Phys. Rev.* **145**, 195 (1966).
- <sup>46</sup>D. R. Penn, C. W. Clark, C. J. Powell, T. Fulop, and S. Tanuma, *Ultramicroscopy* **69**, 69 (1997).
- <sup>47</sup>S. Tanuma, C. J. Powell, and D. R. Penn, *Surf. Interface Anal.* **17**, 911 (1991); (to be published).
- <sup>48</sup>S. Tanuma, C. J. Powell, and D. R. Penn, *Surf. Interface Anal.* **17**, 927 (1991).
- <sup>49</sup>S. Tanuma, C. J. Powell, and D. R. Penn, *Surf. Interface Anal.* **20**, 77 (1993).
- <sup>50</sup>S. Tanuma, C. J. Powell, and D. R. Penn, *Surf. Interface Anal.* **21**, 165 (1994).
- <sup>51</sup>C. M. Kwei, Y. F. Chen, C. J. Tung, and J. P. Wang, *Surf. Sci.* **293**, 202 (1993); Y. F. Chen (private communication).
- <sup>52</sup>Z.-J. Ding and R. Shimizu, *Scanning* **18**, 92 (1996); Z.-J. Ding (private communication).
- <sup>53</sup>T. Boutboul, A. Akkerman, A. Breskin, and R. Chechik, *J. Appl. Phys.* **79**, 6714 (1996); T. Boutboul (private communication).
- <sup>54</sup>A. Akkerman, T. Boutboul, A. Breskin, R. Chechik, A. Gibrekhterman, and Y. Lifshitz, *Phys. Status Solidi B* **198**, 769 (1996); T. Boutboul (private communication).
- <sup>55</sup>R. H. Ritchie and A. Howie, *Philos. Mag.* **36**, 463 (1977).
- <sup>56</sup>M. Inokuti, *Rev. Mod. Phys.* **43**, 297 (1971).
- <sup>57</sup>J. C. Ashley and C. J. Tung, *Surf. Interface Anal.* **4**, 52 (1982).
- <sup>58</sup>M. P. Seah and W. A. Dench, *Surf. Interface Anal.* **1**, 2 (1979).
- <sup>59</sup>R. W. Rendell and D. R. Penn, *Phys. Rev. Lett.* **45**, 2057 (1980).
- <sup>60</sup>*Handbook of Optical Constants of Solids*, edited by E. D. Palik (Academic, New York, 1985); *Handbook of Optical Constants of Solids II*, edited by E. D. Palik (Academic, New York, 1991).
- <sup>61</sup>H.-J. Hagemann, W. Gudat, and C. Kunz, *Optical Constants from the Far Infrared to the X-Ray Region: Mg, Al, Cu, Ag, Au, Bi, C, and Al<sub>2</sub>O<sub>3</sub>* (Deutsches Elektronen-Synchrotron, Hamburg, 1974); R.-P. Haelbich, M. Iwan, and E. E. Koch, *Optical Properties of Some Insulators in the Vacuum Ultraviolet Region*, Physics Data No. 8-1 (Zentralstelle fuer Atomkernenergie-Dokumentation, Eggenstein-Leopoldshafen, 1977); J. H. Weaver, C. Krafka, D. W. Lynch, and E. E. Koch, *Optical Properties of Metals*, Physics Data Nos. 18-1 and 18-2 (Fachinformationzentrum, Karlsruhe, 1981).
- <sup>62</sup>B. L. Henke, P. Lee, T. J. Tanaka, R. L. Shimabukuro, and B. K. Fujikawa, *At. Data Nucl. Data Tables* **27**, 1 (1982); E. B. Saloman, J. H. Hubbell, and J. H. Scofield, *ibid.* **38**, 1 (1988); B. L. Henke, J. C. Davis, E. M. Gullikson, and R. C. C. Perera, A Preliminary Report on X-Ray Photoabsorption Coefficients and Atomic Scattering Factors for 92 Elements in the 10–10 000 eV Region, Lawrence Berkeley Laboratory Report LBL-26259 (1988).
- <sup>63</sup>(a) P. J. Feibelman, *Surf. Sci.* **36**, 558 (1973); (b) C. J. Powell, *Phys. Rev.* **175**, 972 (1968).
- <sup>64</sup>Z.-J. Ding, *J. Phys: Condens. Matter* **10**, 1733 (1998); **10**, 1753 (1998).
- <sup>65</sup>Y. F. Chen, *Surf. Sci.* **407**, 73 (1998); C. M. Kwei, C. Y. Wang, and C. J. Tung, *Surf. Interface Anal.* **26**, 682 (1998).
- <sup>66</sup>W. Dolinski, S. Mroz, and M. Zagorski, *Surf. Sci.* **200**, 361 (1988).
- <sup>67</sup>Z.-J. Ding (to be published); Z.-J. Ding (private communication).
- <sup>68</sup>K. Siegbahn, C. Nordling, A. Fahlman, R. Nordberg, K. Hamrin, J. Hedman, G. Johansson, T. Bergmark, S.-E. Karlsson, L. Lindgren, and B. Lindberg, *ESCA. Atomic, Molecular and Solid State Structure Studied by Means of Electron Spectroscopy* (Almqvist and Wiksells, Uppsala, 1967), Chap. 5; P. W. Palmberg and T. N. Rhodin, *J. Appl. Phys.* **39**, 2425 (1968).
- <sup>69</sup>C. J. Powell, in *Scanning Electron Microscopy/1984*, edited by O. Johari (SEM, AMF O'Hare, IL, 1984), p. 1649.
- <sup>70</sup>(a) A. Barbier, *Surf. Sci.* **406**, 69 (1998); (b) C. J. Powell, *J. Electron Spectrosc. Relat. Phenom.* **47**, 197 (1988).
- <sup>71</sup>O. A. Baschenko, G. V. Machavariani, and V. I. Nefedov, *J. Electron Spectrosc. Relat. Phenom.* **34**, 305 (1984); A. Jablonski, *Surf. Sci.* **188**, 164 (1987); *Surf. Interface Anal.* **15**, 559 (1990); I. S. Tilinin, A. Jablonski, and W. S. M. Werner, *Prog. Surf. Sci.* **52**, 193 (1996).
- <sup>72</sup>A. Jablonski and H. Ebel, *Surf. Interface Anal.* **11**, 627 (1988).
- <sup>73</sup>A. Jablonski and S. Tougaard, *J. Vac. Sci. Technol. A* **8**, 106 (1990).
- <sup>74</sup>M. Klasson, A. Berndtsson, J. Hedman, R. Nilsson, R. Nyholm, and C. Nordling, *J. Electron. Spectrosc. Relat. Phenom.* **3**, 427 (1974).
- <sup>75</sup>M. Flitsch and S. I. Raider, *J. Vac. Sci. Technol.* **12**, 305 (1975).
- <sup>76</sup>J. M. Hill, D. G. Royce, C. S. Fadley, L. F. Wagner, and F. J. Grunthaner, *Chem. Phys. Lett.* **44**, 225 (1976).
- <sup>77</sup>P. Cadman, G. Gossedge, and J. D. Scott, *J. Electron. Spectrosc. Relat. Phenom.* **13**, 1 (1978).
- <sup>78</sup>A. Ishizaka, S. Iwata, and J. Kamigaki, *Surf. Sci.* **84**, 355 (1979).
- <sup>79</sup>M. F. Ebel and W. Lieble, *J. Electron. Spectrosc. Relat. Phenom.* **16**, 463 (1979).
- <sup>80</sup>T. Hattori and T. Suzuki, *Appl. Phys. Lett.* **43**, 470 (1983).
- <sup>81</sup>M. F. Hochella and A. H. Carim, *Surf. Sci.* **197**, L260 (1988).
- <sup>82</sup>G. Leonhardt and H. J. Bilz, *Krist. Tech.* **10**, K35 (1975).
- <sup>83</sup>T. Hattori and T. Nishina, *Surf. Sci.* **86**, 555 (1979).
- <sup>84</sup>R. P. Vasquez and F. J. Grunthaner, *Surf. Sci.* **99**, 681 (1980).
- <sup>85</sup>(a) M. F. Ebel, H. Ebel, A. Hoffman, and R. Svagera, *Surf. Interface Anal.* **22**, 51 (1994); (b) F. Yano, A. Hiraoka, T. Itoga, H. Kojima, K. Kanehori, and Y. Mitsui, *J. Vac. Sci. Technol. A* **13**, 2671 (1995); (c) Z. H. Lu, J. P. McCaffrey, B. Brar, G. D. Wilk, R. M. Wallace, L. C. Feldman, and S. P. Tay, *Appl. Phys. Lett.* **71**, 2764 (1997); (d) J. E. Fulghum, R. Stokell, G. E. McGuire, B. Patnaik, N. Yu, Y. J. Zhao, and N. Parikh, *J. Electron Spectrosc. Relat. Phenom.* **60**, 117 (1992).
- <sup>86</sup>J. S. Schilling and M. B. Webb, *Phys. Rev. B* **2**, 1665 (1970).
- <sup>87</sup>G. Gergely, *Surf. Interface Anal.* **3**, 201 (1981).
- <sup>88</sup>R. Schmid, Ph.D. thesis, Eberhard-Karls University, Tübingen, Germany, 1982.

- <sup>89</sup>R. Schmid, K. H. Gaukler, and H. Seiler, in *Scanning Electron Microscopy/1983*, edited by O. Johari (SEM, AMF O'Hare, IL, 1983), p. 501.
- <sup>90</sup>V. M. Dwyer and J. M. Richards, *Surf. Interface Anal.* **18**, 555 (1992).
- <sup>91</sup>A. Jablonski, P. Mrozek, G. Gergely, M. Menyhard, and A. Sulyok, *Surf. Interface Anal.* **6**, 291 (1984).
- <sup>92</sup>A. Jablonski, *Surf. Sci.* **151**, 166 (1985).
- <sup>93</sup>V. M. Dwyer, *J. Vac. Sci. Technol. A* **12**, 2680 (1994).
- <sup>94</sup>S. Ichimura, M. Aratama, and R. Shimizu, *J. Appl. Phys.* **51**, 2853 (1980).
- <sup>95</sup>A. Jablonski, *Surf. Sci.* **188**, 164 (1987).
- <sup>96</sup>A. Jablonski, J. Gryko, J. Kraaer, and S. Tougaard, *Phys. Rev. B* **39**, 61 (1989).
- <sup>97</sup>W. Dolinski, H. Nowicki, and S. Mroz, *Surf. Interface Anal.* **11**, 229 (1988).
- <sup>98</sup>W. Dolinski, S. Mroz, and M. Zagorski, *Surf. Sci.* **200**, 361 (1988).
- <sup>99</sup>B. Lesiak, A. Jablonski, Z. Prussak, and P. Mrozek, *Surf. Sci.* **223**, 213 (1989).
- <sup>100</sup>A. Jablonski, B. Lesiak, and G. Gergely, *Phys. Scr.* **39**, 363 (1989).
- <sup>101</sup>W. S. M. Werner, I. S. Tilinin, and M. Hayek, *Phys. Rev. B* **50**, 4819 (1994).
- <sup>102</sup>H. Beilschmidt, I. S. Tilinin, and W. S. M. Werner, *Surf. Interface Anal.* **22**, 120 (1994).
- <sup>103</sup>I. S. Tilinin, A. Jablonski, and S. Tougaard, *Phys. Rev. B* **52**, 5935 (1995).
- <sup>104</sup>A. Jablonski, I. S. Tilinin, and C. J. Powell, *Phys. Rev. B* **54**, 10927 (1996).
- <sup>105</sup>P. Mrozek, A. Jablonski, and A. Sulyok, *Surf. Interface Anal.* **11**, 499 (1988).
- <sup>106</sup>P. Mrozek, B. Lesiak, and A. Jablonski, *Surf. Interface Anal.* **18**, 403 (1992).
- <sup>107</sup>M. Krawczyk, L. Zommer, B. Lesiak, and A. Jablonski, *Surf. Interface Anal.* **25**, 256 (1997).
- <sup>108</sup>(a) G. Gergely *et al.*, *ECASIA 97, Proceedings of the 7th European Conference on Applications of Surface and Interface Analysis*, edited by I. Olefjord, L. Nyborg, and D. Briggs (Wiley, Chichester, 1997), p. 836; (b) L. Zommer, B. Lesiak, A. Jablonski, G. Gergely, M. Menyhard, A. Sulyok, and S. Gurban, *J. Electron Spectrosc.* **87**, 177 (1998); (c) M. Krawczyk, A. Jablonski, S. Tougaard, J. Toth, D. Varga, and G. Gergely, *Surf. Sci.* **402–404**, 491 (1998); (d) G. Gergely, M. Menyhard, J. Toth, D. Varga, A. Jablonski, M. Krawczyk, B. Gruzza, L. Bideux, and C. Robert (to be published); (e) B. Lesiak, A. Kosinski, M. Krawczyk, L. Zommer, A. Jablonski, J. Toth, and J. Cserny (to be published).
- <sup>109</sup>B. Lesiak, A. Jablonski, J. Zemek, and P. Jiricek, *Surface Interface Anal.* **26**, 400 (1998).
- <sup>110</sup>G. Gergely, M. Menyhard, K. Pentek, A. Sulyok, A. Jablonski, B. Lesiak, and Cs. Daroczi, *Surf. Sci.* **331–333**, 1203 (1995).
- <sup>111</sup>G. Gergely, A. Konkol, M. Menyhard, B. Lesiak, A. Jablonski, D. Varga, and J. Toth, *Vacuum* **48**, 621 (1997).
- <sup>112</sup>B. Lesiak, A. Jablonski, L. Zommer, A. Kosinski, G. Gergely, A. Konkol, A. Sulyok, Cs. S. Daroczi, and P. Nagy, in *Proceedings of the 6th European Conference on Applications of Surface and Interface Analysis: ECASIA95*, Montreux, 1995, edited by H. J. Mathieu, B. Reihl, and D. Briggs (Wiley, Chichester, 1996), p. 619.
- <sup>113</sup>W. Dolinski, S. Mroz, J. Palczynski, B. Gruzza, P. Bondot, and A. Porte, *Acta Physica Polon.* **A81**, 193 (1992).
- <sup>114</sup>G. Gergely, M. Menyhard, K. Pentek, A. Sulyok, A. Jablonski, and B. Lesiak, *Vacuum* **46**, 591 (1995).
- <sup>115</sup>A. Koch, Ph.D. thesis, Physics Department, Eberhard-Karls-Universität, Tübingen, Germany, 1996.
- <sup>116</sup>D. Zeze, L. Bideux, B. Gruzza, F. Golek, D. Danko, and S. Mroz, *Vacuum* **48**, 399 (1997).
- <sup>117</sup>B. Lesiak, A. Jablonski, and G. Gergely, *Vacuum* **40**, 67 (1990).
- <sup>118</sup>F. Golek and W. Dolinski, *Phys. Status Solidi A* **151**, K37 (1995).
- <sup>119</sup>A. Jablonski, *Phys. Rev. B* **43**, 7546 (1991).
- <sup>120</sup>A. Jablonski, H. S. Hansen, C. Jansson, and S. Tougaard, *Phys. Rev. B* **45**, 3694 (1992).
- <sup>121</sup>A. Jablonski, C. Jansson, and S. Tougaard, *Phys. Rev. B* **47**, 7420 (1993).
- <sup>122</sup>L. Zommer, B. Lesiak, and A. Jablonski, *Phys. Rev. B* **47**, 13759 (1993).
- <sup>123</sup>A. Jablonski and P. Jiricek, *Surf. Interface Anal.* **24**, 781 (1996).
- <sup>124</sup>A. Jablonski and J. Zemek, *Surf. Sci.* **347**, 207 (1996).
- <sup>125</sup>Z. Czyzewski, D. O. MacCallum, A. Romig, and D. C. Joy, *J. Appl. Phys.* **68**, 3066 (1990).
- <sup>126</sup>A. Jablonski, *Physica A* **183**, 361 (1992).
- <sup>127</sup>NIST Elastic-Electron-Scattering Cross-Section Database, Standard Reference Data Program Database 64, National Institute of Standards and Technology, Gaithersburg, MD (1996).
- <sup>128</sup>M. J. Berger, S. M. Seltzer, R. Wang, and A. Schecter, *Elastic Scattering of Electrons and Positrons by Atoms: Database ELAST*, NIST Internal Report NISTIR 5188, National Institute of Standards and Technology, Gaithersburg, MD (1993).
- <sup>129</sup>A. Jablonski and P. Jiricek, *Surf. Sci.* **413**, 42 (1998).
- <sup>130</sup>J. B. Malherbe, *Crit. Rev. Solid State Mater. Sci.* **19**, 129 (1994).
- <sup>131</sup>L. S. Dake, D. E. King, J. R. Pitts, and A. W. Czanderna, in *Beam Effects, Surface Topography, and Depth Profiling in Surface and Near-Surface Analysis*, edited by A. W. Czanderna, T. E. Madey, and C. J. Powell, *Methods of Surface Characterization*, Vol. 5 (Plenum, New York, 1998), Chap. 3.
- <sup>132</sup>C. Robert, B. Gruzza, L. Bideux, and P. Bondot, *Math. Comput. Simulation* **47**, 419 (1998).
- <sup>133</sup>W. F. Egelhoff, *Crit. Rev. Solid State Mater. Sci.* **16**, 213 (1990); S. A. Chambers, *Adv. Phys.* **40**, 357 (1991); *Surf. Sci. Rep.* **16**, 261 (1992); S. Mroz, *Prog. Surf. Sci.* **48**, 157 (1995); C. S. Fadley, *ibid.* **54**, 341 (1997).
- <sup>134</sup>H. E. Bishop, B. Chornik, C. Le Gressus, and A. LeMoel, *Surf. Interface Anal.* **6**, 116 (1984); F. E. Doern, L. Kover, and N. S. McIntyre, *ibid.* **6**, 282 (1984); P. Morin, *Surf. Sci.* **164**, 127 (1985); H. E. Bishop, *Surf. Interface Anal.* **15**, 27 (1990).
- <sup>135</sup>S. Tanuma, S. Ichimura, and K. Goto, *J. Surf. Anal.* (in press).
- <sup>136</sup>G. Gergely, A. Barna, A. Sulyok, C. Jardin, J. Toth, D. Varga, B. Gruzza, L. Bideux, and C. Robert (to be published).
- <sup>137</sup>C. J. Powell, *Surf. Interface Anal.* **7**, 256 (1985).
- <sup>138</sup>S. Tougaard, *Surf. Interface Anal.* **25**, 137 (1997).
- <sup>139</sup>C. J. Powell, W. F. Egelhoff, P.-J. Chen, and S. Tougaard (to be published).